

Durham E-Theses

The chemistry of some dithiadiazolyls and their platinum complexes

Dawe, Owen Gerard

How to cite:

Dawe, Owen Gerard (1995) *The chemistry of some dithiadiazolyls and their platinum complexes*, Durham theses, Durham University. Available at Durham E-Theses Online:
<http://etheses.dur.ac.uk/5148/>

Use policy

The full-text may be used and/or reproduced, and given to third parties in any format or medium, without prior permission or charge, for personal research or study, educational, or not-for-profit purposes provided that:

- a full bibliographic reference is made to the original source
- a [link](#) is made to the metadata record in Durham E-Theses
- the full-text is not changed in any way

The full-text must not be sold in any format or medium without the formal permission of the copyright holders.

Please consult the [full Durham E-Theses policy](#) for further details.

**THE CHEMISTRY OF SOME DITHIADIAZOLYLS
AND THEIR
PLATINUM COMPLEXES**

Owen Gerard Dawe B.Sc.(Q.U.B.)
St. Aidans College

The copyright of this thesis rests with the author.
No quotation from it should be published without
his prior written consent and information derived
from it should be acknowledged.

A thesis Submitted in fulfillment for the degree of Master of Science
at the University of Durham.

September 1995.



- 8 JAN 1996

To
My Parents
and
Family.

Acknowledgements

I would very much like to thank my supervisor Dr.A.J. Banister, for all his help and guidance throughout the year, and for getting me started here in the first place.

There are numerous people that I would very much like to thank. Thanks to Dr.J.M. Rawson for carrying out e.s.r. experiments for me in Edinburgh and with help, along with Dr.A. Batsanov, in solving my crystal structures. To Dr.N. Bricklebank for his time in reading my earlier work and results.

To the Celtic members of lab.100, Iain May and Colin Campbell, for their friendship, advice and for putting up with me throughout the year.

To all the technical staff at Durham University. The glassblowers Ray and Gordon for their friendly and efficient service. To Jaraka Dostal, Judith Magee and Bob Coult for elemental analysis and Dr.A. Royston for computing assistance.

To Iain May for his help in NMR and U.V/Vis. spectroscopy.

Memorandum

The work described in this thesis was carried out by me, in the department of Chemistry at the University of Durham between October 1994 and October 1995. I declare that this work has not been submitted previously for a degree at this or any other University. This thesis is a summary of my own original work, except where acknowledged by reference. The copyright of this thesis rests with the author. No quotation should be published without written consent, and information derived from it should be acknowledged.

Abstract

The work outlined in this thesis is mainly concerned with the preparation and reactions of dithiadiazolylium salts, dithiadiazolyls and their Pt complexes.

Chapter one outlines the chemistry, the synthesis and properties of dithiadiazolylium salts and dithiadiazolyls.

Chapter two is concerned with the preparation and characterisation of some dithiadiazolyls and their platinum complexes, and comprehensive DSC and Ultraviolet/visible spectroscopic studies of these complexes, highlights some of their properties.

Chapter three outlines the preparation and characterisation of some fluorine substituted dithiadiazolyls and their platinum complexes. It also discusses the crystal structures of the complex $\text{Pt}_3[\text{PPh}_3]_4[3,4\text{-F}_2\text{.C}_6\text{H}_3\text{.CNSSN}]_2$ and the fluorine substituted dithiadiazolyls $(2,3\text{-F}_2\text{.C}_6\text{H}_3\text{.CNSSN})_2$ and $(2,5\text{-F}_2\text{.C}_6\text{H}_3\text{.CNSSN})$.

Chapter four outlines the main experimental techniques which were employed throughout my research.

Appendix I contains additional crystallographic data, for the crystal structures mentioned previously, while Appendix II lists all the colloquia, lectures and seminars attended by the author.

Abbreviations

R	organic substituent
Pr	iso-propyl
Bu ^t	tert-butyl
C ₆ H ₅	phenyl
CNSSN	the 1,2,3,5-dithiadiazoly/ium ring system
CNSNS	the 1,3,2,4-dithiadiazoly/ium ring system
MO	molecular orbital
HOMO	highest occupied molecular orbital
LUMO	lowest unoccupied molecular orbital
SOMO	singly occupied molecular orbital
C.I.	chemical ionisation
E.I.	electron ionisation
U.V.	ultraviolet
DSC	differential scanning calorimetry
e.s.r.	electron spin resonance
NMR	nuclear magnetic resonance
THF	tetrahydrofuran

Table of Contents

Chapter One

Chemistry of Some Dithiadiazolium/zoyl Compounds

1.1 Introduction	2
1.2 Theoretical Studies of 1,2,3,5 Dithiadiazolium/zoyl Rings	3
1.3 Synthesis of Dithiadiazolium Species	5
1.3.1 Synthesis of 1,2,3,5 Dithiadiazolium Salts	5
1.3.2 Synthesis of 1,3,2,4 Dithiadiazolium Salts	7
1.3.3 Preparation of Mixed 1,3,2,4/1,2,3,5 Dithiadiazolium Salts	8
1.4 Reactions of Dithiadiazolium salts	9
1.5 Preparation of 1,2,3,5 Dithiadiazolyls and the Mixed Dication	10
1.6 Reactions of 1,2,3,5 Dithiadiazolyls	11
1.6.1 Insertion of N into the S-S bond	11
1.6.2 Complexation	11
1.6.3 Oxidation	13
1.6.4 Radical Coupling Reactions	13
1.7 Physical Properties of the 1,2,3,5 Dithiadiazolyls	14
1.8 Structural Properties of the Dithiadiazolyls	16
1.9 References	18

Chapter Two

Preparation and Characterisation of Some Dithiadiazolyls and their Platinum Complexes

2.1 Introduction	22
2.1.1 Synthesis of Metal Dithiadiazolyl Complexes	23
2.1.2 Structural Studies of Monometallic Dithiadiazolyl Complexes	24
2.1.3 Structural Studies of Dimetallic Complexes	25
2.1.4 Structural Studies of Trimetallic Complexes	26
2.1.5 Comparison of some Metal Dithiadiazolyl Complexes	27
2.1.6 Biological Properties	28
2.2 Experimental	
2.2.1 Preparation of (C ₆ H ₅ .CNSSN) ₂	30
2.2.2 Preparation of (<i>para</i> -Br.C ₆ H ₄ .CNSSN) ₂	31
2.2.3 Preparation of (<i>para</i> -Cl.C ₆ H ₄ .CNSSN) ₂	31
2.2.4 Preparation of (<i>para</i> -Me.C ₆ H ₄ .CNSSN) ₂	32
2.2.5 Attempted Preparation of (<i>para</i> -Me ₂ N.C ₆ H ₄ .CNSSN) ₂	32
2.2.6 Attempted Preparation of 2,4-Dimethoxydithiadiazolium Chloride	33
2.2.7 Preparation of Tetrakis (triphenylenephosphine)platinum(0)	33
2.2.8 Preparation of Pt(dppe) ₂	34

2.3 Results and Discussion	35
2.3.1 Preparation of $(C_6H_5.CNSSN)_2$	35
2.3.2 Preparation of $(para-Br.C_6H_4.CNSSN)_2$	36
2.3.3 Preparation of $(para-Cl.C_6H_4.CNSSN)_2$	37
2.3.4 Preparation of $(para-Me.C_6H_4.CNSSN)_2$	38
2.3.5 Reaction of $Pt(PPh_3)_4$ with $(para-Br.C_6H_4.CNSSN)_2$	39
2.3.6 Reaction of $Pt(PPh_3)_4$ with $(para-Cl.C_6H_4.CNSSN)_2$	40
2.3.7 Reaction of $Pt(dppe)_2$ with $(para-Cl.C_6H_4.CNSSN)_2$	41
2.3.8 Reaction of $Pt(PPh_3)_4$ with $(para-Me.C_6H_4.CNSSN)_2$	42
2.4 Differential Scanning Calorimetry Studies	43
2.5 Ultraviolet/vis. Studies on Some Metal Dithiadiazolyls Complexes	46
2.6 References	48

Chapter Three

Preparation and Characterisation of Some Fluorine Substituted Dithiadiazolyls and their Platinum Complexes

3.1 Introduction	51
3.1.1 Structural studies of Fluorine Substituted Dithiadiazolyls	52
3.1.2 Bonding in Fluorine Substituted Dithiadiazolyls	55
3.1.3 Conclusion	56
3.2 Experimental	
3.2.1 Preparation of $(2,6-F_2.C_6H_3.CNSSN)_2$	57
3.2.2 Preparation of $(3,4-F_2.C_6H_3.CNSSN)_2$	58
3.2.3 Preparation of $(2,3-F_2.C_6H_3.CNSSN)_2$	58
3.2.4 Preparation of $(C_6F_5.CNSSN)_2$	59
3.2.5 Preparation of $(3,5-F_2.C_6H_3.CNSSN)_2$	59
3.2.6 Preparation of $(2,5-F_2.C_6H_3.CNSSN)_2$	60
3.2.7 Attempted Preparation of $[H_2N-C_6F_4.CNSSN]^+Cl^-$	60
3.2.8 Attempted Crystal Growth of $[Pt(PPh_3)_2(3,4-F_2.C_6H_3.CNSSN)]_2$	61
3.3 Solid State Structures	62
3.3.1 The Crystal Structure of $Pt_3[PPh_3]_4[3,4-F_2.C_6H_3.CNSSN]_2$	63
3.3.2 The Crystal Structure of $(2,3-F_2.C_6H_3.CNSSN)_2$	70
3.3.3 The Crystal Structure of $(2,5-F_2.C_6H_3.CNSSN)_2$	77
3.4 Electron Spin Resonance of Some Fluorine Substituted Dithiadiazolyls	84
3.4.1 Introduction	84
3.4.2 Results and Discussion	85
3.5 NMR (^{31}P) of $Pt_3[PPh_3]_4[3,4-F_2.C_6H_3.CNSSN]_2$	88

3.6 Results and Discussion	91
3.6.1 Preparation of (2,6-F ₂ .C ₆ H ₃ .CNSSN) ₂	91
3.6.2 Preparation of (3,4-F ₂ .C ₆ H ₃ .CNSSN) ₂	92
3.6.3 Preparation of (2,3-F ₂ .C ₆ H ₃ .CNSSN) ₂	93
3.6.4 Preparation of (3,5-F ₂ .C ₆ H ₃ .CNSSN) ₂	94
3.6.5 Preparation of (2,5-F ₂ .C ₆ H ₃ .CNSSN)	95
3.6.6 Reaction of Pt(PPh ₃) ₄ with (3,4-F ₂ .C ₆ H ₃ .CNSSN) ₂	96
3.6.7 Reaction of Pt(dppe) ₂ with (3,4-F ₂ .C ₆ H ₃ .CNSSN) ₂	97
3.8 References	98

Chapter Four Experimental Techniques

4.1 General Techniques	102
4.2 Specialised Techniques	102
4.2.1 The Closed Extractor	102
4.2.2 The "Dog"	102
4.3 Temperature Control	105
4.4 Analytical Techniques	105
4.4.1 Infrared Spectroscopy	105
4.4.2 Differential Scanning Calorimetry	105
4.4.3 Elemental Analysis	105
4.4.4 Ultraviolet	105
4.4.5 Electron Spin Resonance	105
4.4.6 Mass Spectroscopy	105
4.4.7 Nuclear Magnetic Resonance Spectroscopy	106
4.5 Chemicals and Solvents	106
4.5.1 Purification of Solvents	106
4.6 Single Crystal X-Ray Structure Determination	106
4.7 References	106
Appendix I	107
Additional Crystallographic Data	
Appendix II	113
Lecturers, Colloquia and Seminars attended.	

CHAPTER 1

THE CHEMISTRY OF SOME DITHIADIAZOLYLIUM/ZOLYL COMPOUNDS.



1.1 Introduction.

The first cyclic sulfur nitrogen free radical species, $S_3N_2^+$, as found in S_3N_2Cl was synthesised in 1880.¹ It was prepared as a deep green powder with a metallic lustre. Electron Spin Resonance studies indicated that in solution it existed as a monomeric radical.

It was in 1984,² when comprehensive X-Ray studies on an $S_3N_2^+$ salt revealed an unusual dimeric structure in the solid state. Two $S_3N_2^+$ rings dimerise through the overlap of the singly occupied molecular orbitals (SOMO) of the sulfur atoms forming the $[S_6N_4]^{2+}$ cation as shown in Figure 1.1. The trans like configuration as illustrated in Figure 1.1, avoids the repulsion between the π clouds present in the cis configuration and it minimises the $Cl\delta^- \cdots S\delta^+$ attractions present.

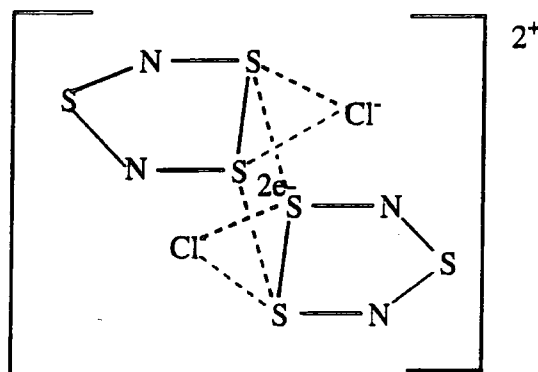


Figure 1.1 The structure of $[S_6N_4]Cl_2$.

It was hoped that by changing one of the S^+ atoms with a isoelectronic carbon, as in the $>R-C$ unit, that a new family of heterocycles could be synthesised. These 7π e^- systems are called dithiadiazolyls, and can exist in four possible isomeric forms, however only the 1,2,3,5 and 1,3,2,4 dithiadiazolyls have been isolated, see Figure 1.2. By simply changing the R group the chemical and physical properties of these new heterocycles can be modified.

Figure 1.2 below highlights the two known structures for the dithiadiazoly ring, viz the 1,2,3,5 and 1,3,2,4 isomers.

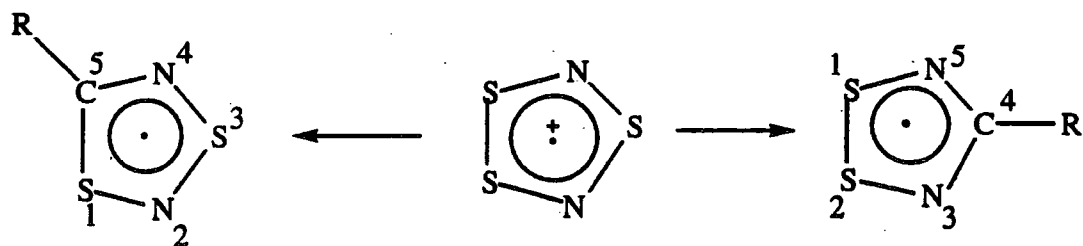


Figure 1.2. shows the two possible isomers, 1,2,3,5 and 1,3,2,4 dithiadiazoly.

Recently more extensive research has been carried out on the physical properties of these dithiadiazolyls, with particular interest in their potential use as organic metals. For example, it has recently been shown that one form of the $p\text{-NC}_6\text{F}_4$ derivative, $p\text{-NCC}_6\text{F}_4\text{.CNSSN}$.³³ is weakly ferromagnetic below 36K.

1.2 Theoretical Studies of 1,2,3,5 Dithiadiazolylium/zolyl Rings.

The unusual configuration of the cation in $[S_6N_4]Cl_2$ is due to secondary S---S bonding interactions between the two $S_3N_2^+$ rings.³ The overlap of these two rings is accomplished by two π electrons, one from each singly occupied molecular orbital. This arrangement minimises any cation-cation and anion-anion repulsions present as illustrated in Figure 1.1, with each of the $S_3N_2^+$ rings providing $1e^-$ for a $\pi^*-\pi^*$ interaction.

Theoretical studies have been carried out by a number of groups.¹¹ They found that examining the frontier molecular orbitals (HOMO, SOMO and LUMO) assisted in rationalising the bonding and the appearance of ultraviolet/visible spectra.

Molecular Orbital calculations (MNDO) which were carried out by Mews *et al.*, have examined the energy difference between the cis, trans and staggered configurations. These calculations have shown that the energy difference between the cis and trans configuration is only $5KJ/mol^{-1}$. Modification of the molecular orbitals, which will alter the HOMO-SOMO energy gap, can occur by simply changing the substituent R group. If this new R group contains lone pairs (e.g. H_2N or Cl) this will change the charge distribution around the heterocyclic ring which will change the lowest possible energy electronic transitions. The effects of the new R group will be manifested through the colour of these materials in solution. The dimer configurations adopted depend upon the R substituent because this influences the type of bonding and packing.

Molecular Orbital calculations on the 1,2,3,5 dithiadiazolylium cation show that a nodal plane is present between the nitrogen and the sulfur atoms (Figure 1.2) of the heterocyclic ring i.e. the orbitals of $2b_1$ and $6a_1$ symmetry. Such a nodal plane prevents through-bond interactions between the heterocyclic ring and the aryl substituent.

Whenever e^- donation occurs from a π donor anion e.g. $S_3N_3^-$ into the $2b_1$ symmetry π based HOMO on the carbon atom an increase in S-S bond length is observed and a strong out-of-plane interaction takes place. However if charge transfer occurs from a soft anion e.g. Cl^- to the S^+ on the $RCN_2S_2^+$, then a decrease in the S-S bond length is observed, as a 3 centre, $2e^-$ bond is created.

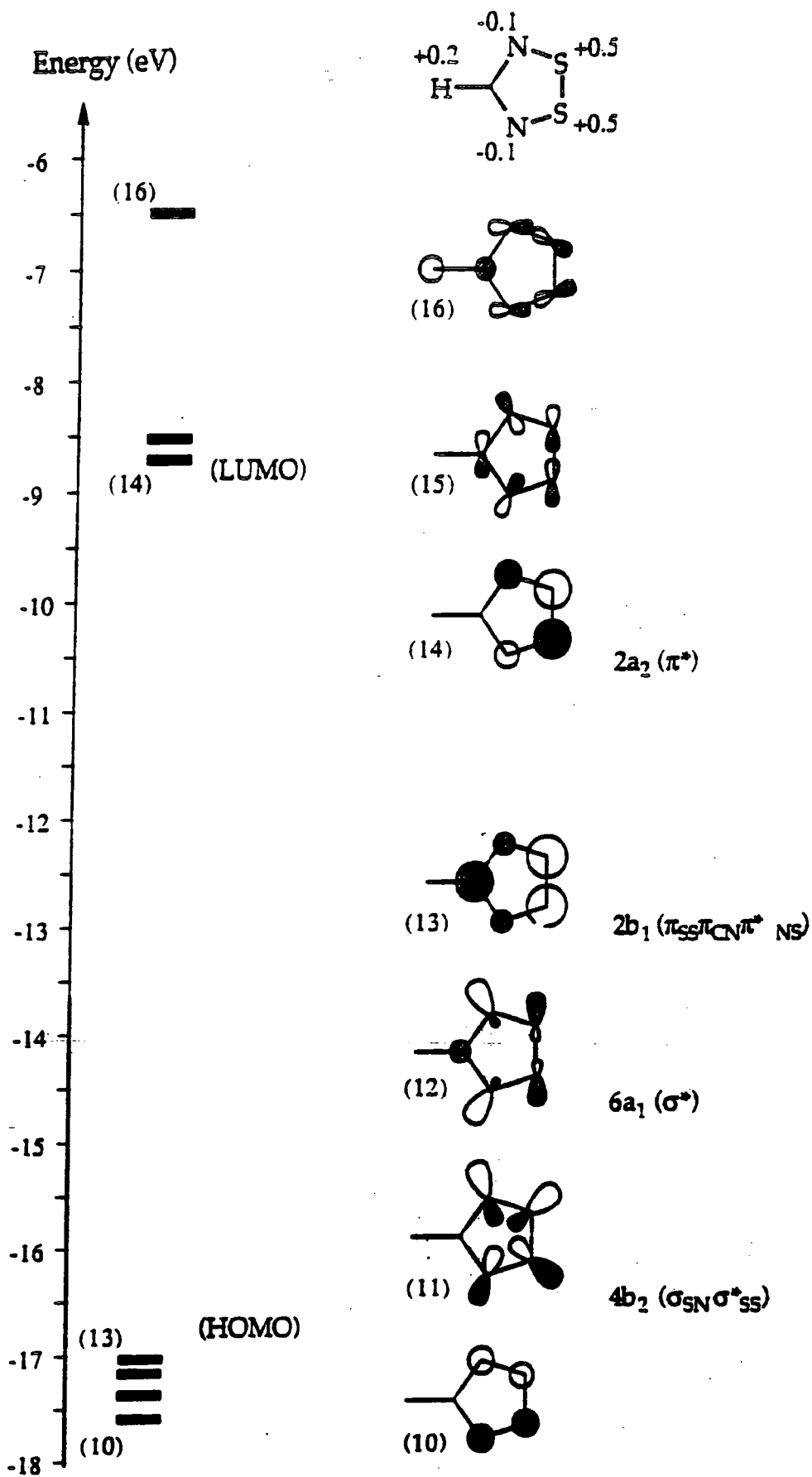
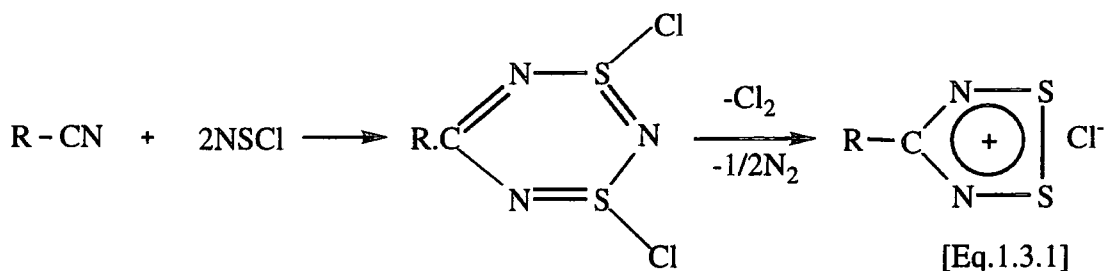


Figure 1.2 MO diagram for the 1,2,3,5 dithiadiazolylium cation [H.CNSSN]⁺

1.3 The Synthesis of Dithiadiazolylium Species.

1.3.1 Synthesis of 1,2,3,5 Dithiadiazolylium Salts

There are several methods available for synthesising the dithiadiazolylium ring.⁴ The first synthesis of a 1,2,3,5 dithiadiazolylium salt [Eq.1.3.1], shows how thiazyl chloride is reacted with an organic nitrile, under refluxing conditions; (the best results are achieved after prolonged heating).

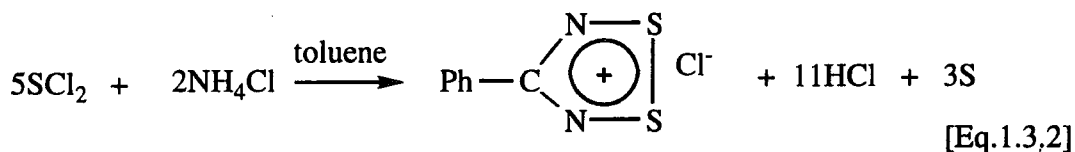


The chlorine and nitrogen arise from the decomposition of the intermediate. The yields (up to 50% recoverable yield) are dependent upon the, temperature, solvent and nature of the R group.

Other possible routes include.

(a) From Nitriles^{4,5}

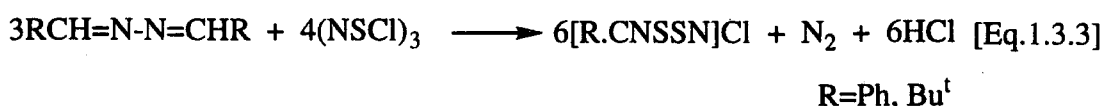
When a mixture of sulfur dichloride and ammonium chloride, [Eq.1.3.2], are refluxed in toluene a small amount (3%) of phenyl dithiadiazolylium chloride is formed.



The formation of $\text{S}_3\text{N}_2\text{Cl}_2$ side product is avoided by continually flushing the reaction mixture with dry Cl_2 gas which converts $\text{S}_3\text{N}_2\text{Cl}_2$ into $(\text{NSCl})_3$.

(a) From Aldazines and $(\text{NSCl})_3$ ³

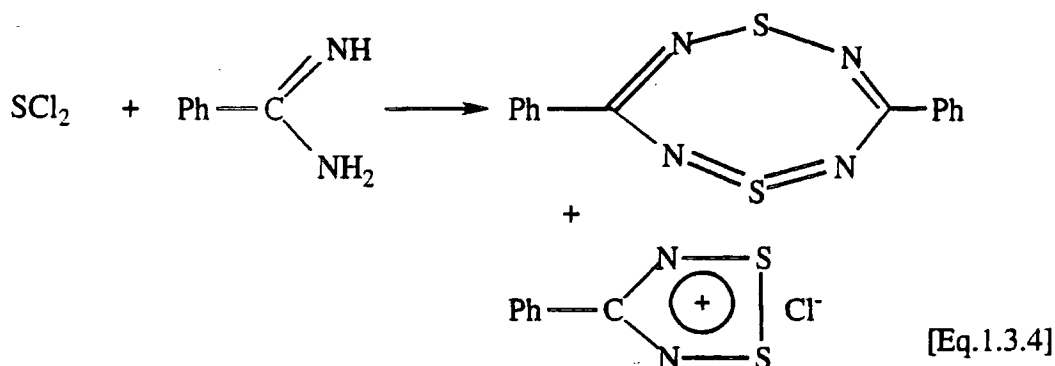
Work carried out by Roesky *et al* has shown that the reaction of $(\text{NSCl})_3$ with several aldazines, RC(H)=N-N=C(H)R , where $\text{R}=\text{Ph}$ or Bu^t , provides a clean route to $[\text{RCNSSN}]\text{Cl}$. [Eq.1.3.3]



The yield is largely dependent upon the nature of the substituent.

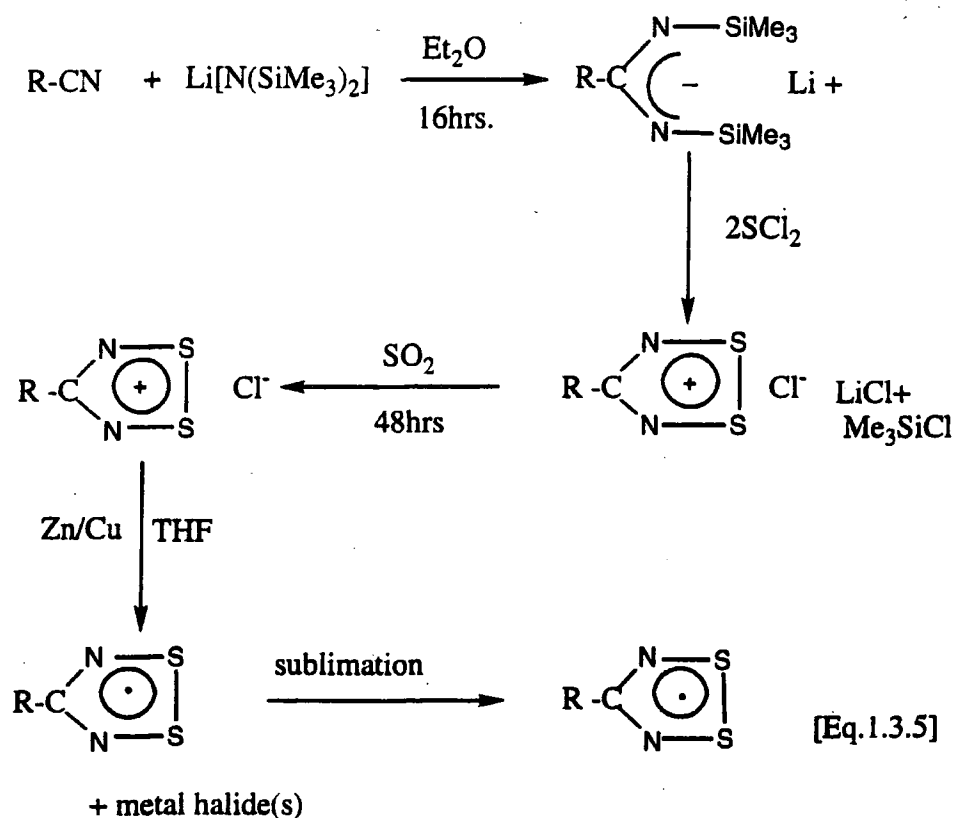
(c) Reaction of SCl_2 or S_2Cl_2 on Amidines¹

Here the yields can be improved by simply adding a tertiary base such as DBU (1,8-diazobicyclo-[5,4,0]-undec-7-ene), [Eq.1.3.4], which removes HCl formed.



(d) Silyl Route⁶

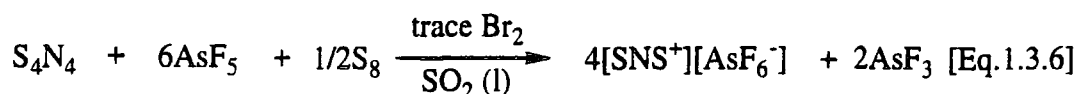
This route produces 1,2,3,5 dithiadiazolyls; it can also be used to prepare the selenium analogues. This pathway was used extensively throughout my research. Yields of up to 70% are obtainable. The pathway is shown below [Eq.1.3.5].



Purification by $\text{SO}_2(\text{l})$ extraction using a sealed Soxhlet extractor, produces the respective chloride salt, which is then reduced by Zn/Cu couple in THF. The pure radical or dimer was obtained by sublimation *in vacuo*.

1.3.2 Synthesis of 1,3,2,4 Dithiadiazolylium Salts

Preparation of the mono-1,3,2,4 dithiadiazolylium salts, [Eq.1.3.6] can be carried out several ways, using dithianitronium salts. The SNS⁺ cation is prepared as the AsF₆⁻ salt. The trace of bromine present helps to catalyse the reaction by increasing the solubility of the S₈. The reaction is carried out under a pressure of 3-4 bars. (This is created by SO₂ (l) at room temperature).



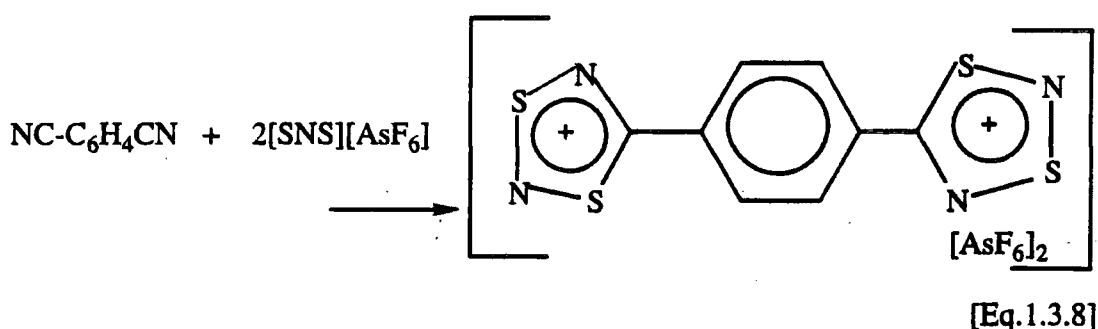
1.3(a) From Dithianitronium cation and a Nitrile

This hexafluoroarsenate route provides the cleanest method, with yields of approximately 95% obtainable, [Eq.1.3.7]. Kinetic studies by Passmore³⁶ *et al* have shown that the reaction proceeds via a "reverse electron demand" cycloaddition reaction; where the 2π nitrile donates electron density into the LUMO of the SNS⁺ (4π). This is the reverse of normal cycloaddition processes where electron drift occurs from the 4π diene to the 2π dienophile. Modification of the nitrile group changes the HOMO-LUMO energy gap which can alter the reactivity of the nitriles.



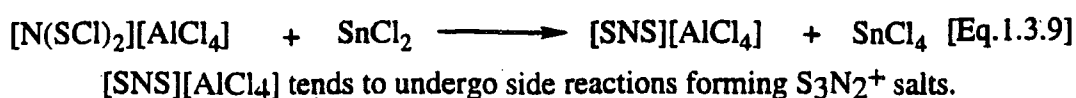
1.3(b) S₂N⁺ and with Multicyano Compounds⁴

Here the corresponding bis and tris dithiadiazolylium cations are formed, [Eq.1.3.8], with 90% yields possible.



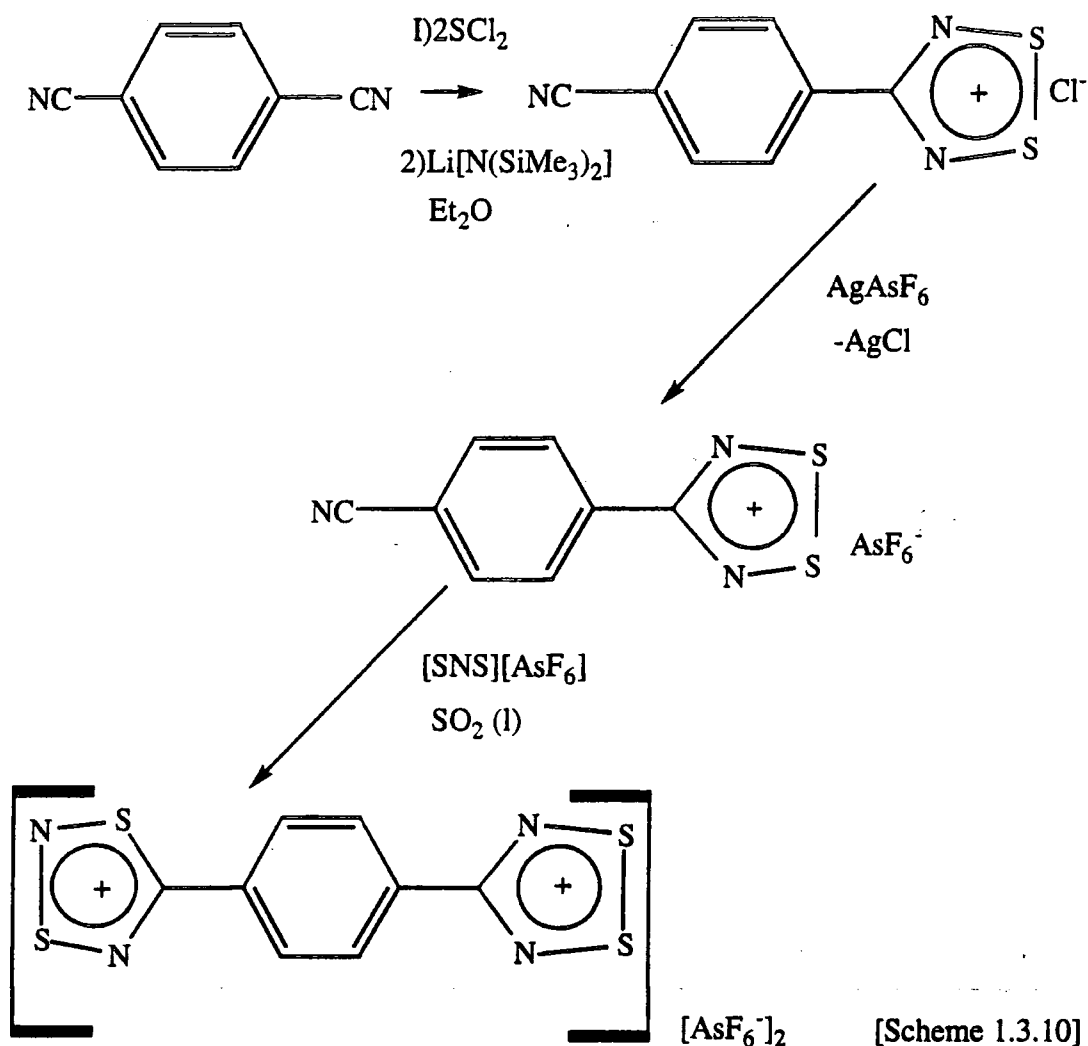
1.3(c) Reduction of N(SCl)₂⁺ Salts^{7,8} using SnCl₂

Other salts such as [SNS][CF₃SO₃] give yields in excess of 50%, [Eq.1.3.9]. However the reaction is slower than the equivalent AsF₆⁻ salt reaction.



1.3.3 Preparation of the Mixed 1,3,2,4-/1,2,3,5-Dithiadiazolylium Salt

This is carried out in three stages,^{9a} [Scheme 1.3.10]. The first step leads to the formation of the 1,2,3,5 dithiadiazolylium salt, the second involves the conversion into the AsF_6^- salt, which is achieved by metathesis with AgAsF_6 in MeCN. Finally the AsF_6^- salt reacts with $[\text{SNS}]\text{AsF}_6$ in liquid SO_2 and the mixed cation is precipitated as a pale yellow AsF_6^- salt.



The salt was prepared in 92% recoverable yield. The corresponding radicals of some of these mixed dithiadiazolylium salts form a polymeric array in the solid state, see section 1.8.

The route outlined above provides a convenient general synthesis of the mixed 1,3,2,4-/1,2,3,5-dithiadiazolylium salts. Passmore *et al.* had previously prepared the hexafluoroarsenate as the radical cation and dication with a 32% yield.^{9b}

1.4 Reactions of the Dithiadiazolylium salts.

For both 1,2,3,5 and 1,3,2,4 dithiadiazolylium salts, conversion to other salts is possible. The 1,2 dithiadiazolylium is most easily prepared as the chloride, while the 1,3 dithiadiazolylium is prepared as the AsF_6^- salt. The reactions of the 1,2 salt are more widely studied, than those of the 1,3 isomer.

The ionic nature of the dithiadiazolylium salts is shown in their addition and metathesis reactions.^{4,15}

1.4(a) Metathesis

Several reactions are known, which are highlighted below in Figure 1.4.1.

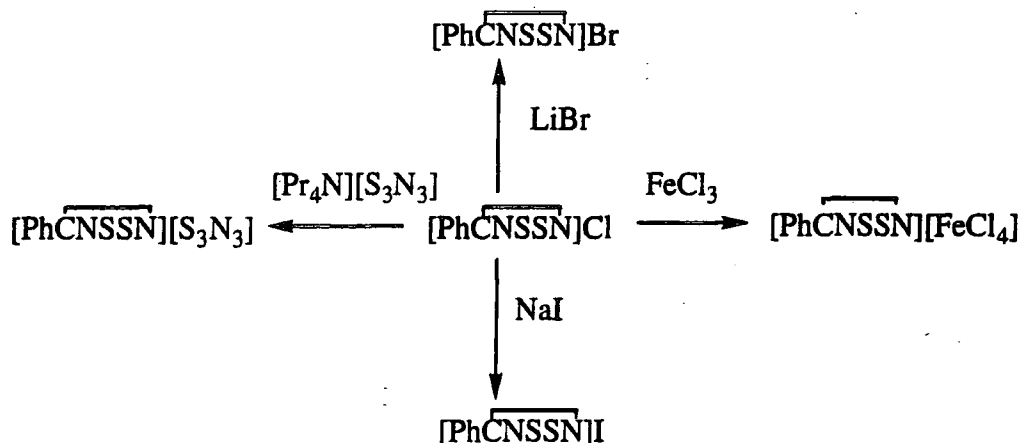
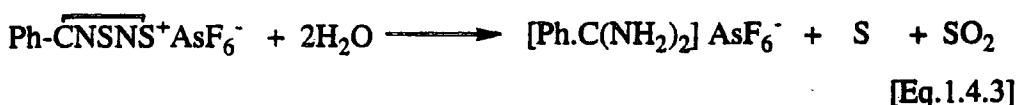
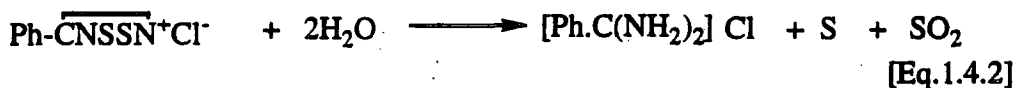


Figure 1.4.1 Metathesis reactions of the 1,2 dithiadiazolylium salts.

1.4(b) Hydrolysis

Both salts are susceptible to hydrolysis.⁴ Equations 1.4.2 and 1.4.3, highlight the ease with which hydrolysis can occur. This is influenced by the solid state structure and the counter-ion; salts containing 'hard' anions, e.g. AsF_6^- , are more susceptible to hydrolysis. In contrast, salts containing 'soft' anions e.g. Cl^- are more resistant to hydrolysis as a planar interaction occurs between the anion and cation, i.e. a high degree of charge transfer is present. This results in a stronger S-S bond in the layered heterocycle and a smaller δ^+ at S.



1.4(c) Act as Cationic Polymerisation Initiators

The $[\text{SNS}][\text{AsF}_6]$ and $[\text{S}_3\text{N}_2][\text{AsF}_6]$ salts have been shown to be cationic initiators for the polymerisation of THF; complex mechanisms are involved, with high molecular weight polymers being produced ($190,000\text{--}200,000 \text{ gmol}^{-1}$).

1.5 Preparation of 1,2,3,5 Dithiadiazolyls and a mixed Dication.

1.5(a) Chemical Reduction

Radicals are easily prepared by chemical reduction, using a variety of reagents³ e.g. Zn/Cu couple¹⁶ or Ph₃Sb¹⁷ in liquid SO₂ or THF. The dithiadiazolyll usually appears from solution as reddish purple flakes [Eq.1.5.1].



The radicals are purified by sublimation *in vacuo*, with yields of 15% obtainable. The corresponding 1,3 dithiadiazolyllium radical is more difficult to prepare as it tends to rearrange³ to the 1,2 isomer in solution or when heated.

1.5(b) Disproportionation of the 1,2,3,5 Dithiadiazolyll Salts

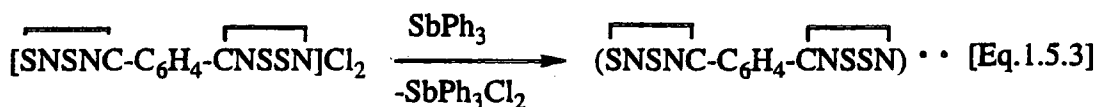
By simply heating or by dissolving certain dithiadiazolyllium salts, especially those containing soft (readily oxidisable) anions, e.g. NCS [Eq.1.5.2] the corresponding dithiadiazolylls can be released.



1.5(c) Preparation of the Mixed Free Radical p-(SNSNC-C₆H₄-CNSSN)••

The preparation of the mixed 1,3,2,4-1,2,3,5 dithiadiazolyllium dication¹⁸ as the AsF₆⁻ salt was outlined in section 1.3. The mixed diradical, [Eq.1.5.3] was prepared by chemical reduction.

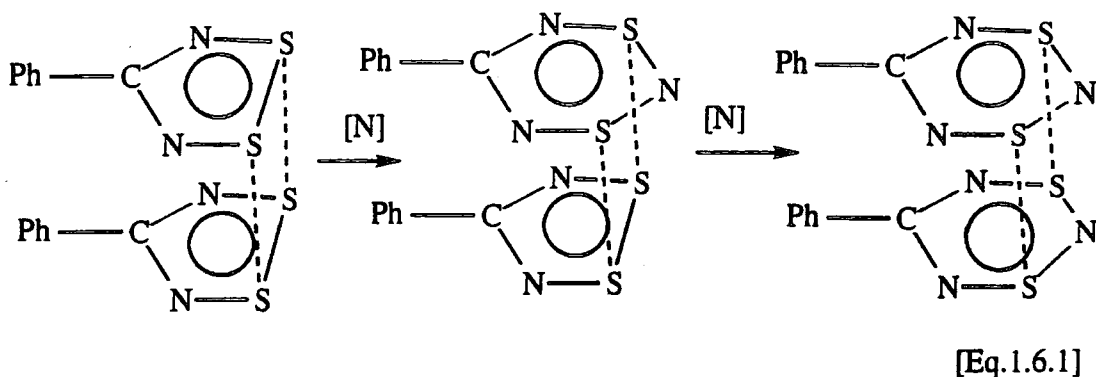
Metathesis of the AsF₆⁻ salts with NBu₄Cl in CH₂Cl₂, produces the chloride salt.^{9a} [Eq. 1.5.3] This was then reduced with triphenylstibine to provide the diradical (SNSNC-C₆H₄-CNSSN)••



1.6 Reactions of 1,2,3,5 Dithiadiazolyls.

1.6.1 Insertion of N atoms into S-S link

When $(\text{Ph.CNSSN})_2$ is treated with atomic nitrogen, generated in a cool, direct current plasma^{3,20} discharge, the N atoms are trapped and inserted into the S-S link, to give the corresponding dithiazine dimers [Eq.1.6.1].



The nitrogenation occurs for $(\text{RCNSSN})_2$ (where $\text{R}=\text{Ph}$, $p\text{-Cl.C}_6\text{H}_4$), however for $(\text{Me.CNSSN})_2$ a black polymeric material was formed.⁴

It is believed that this solid-state reaction may be diffusion controlled.²⁰ X-Ray studies on $(\text{PhCNSSN})_2$ indicate the presence of parallel channels running throughout the lattice with diameters in excess of 3.5\AA . The atomic radii of atomic nitrogen is only 1.3\AA , making it possible for N atoms to diffuse through the crystal structure to the reaction sites.

1.6.1 Metal Complexation

Reaction of the 1,2,3,5 dithiadiazolyl with a metal complex, e.g $\text{Pt}(\text{PPh}_3)_4$, results in the S-S bond of the dithiadiazolyl opening up and chelating the metal centre, as shown in Figure 1.6.1.

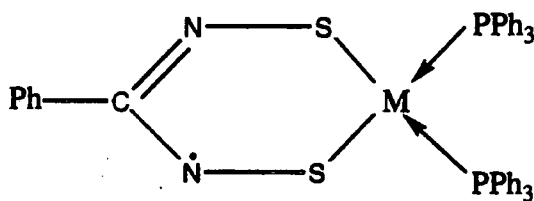
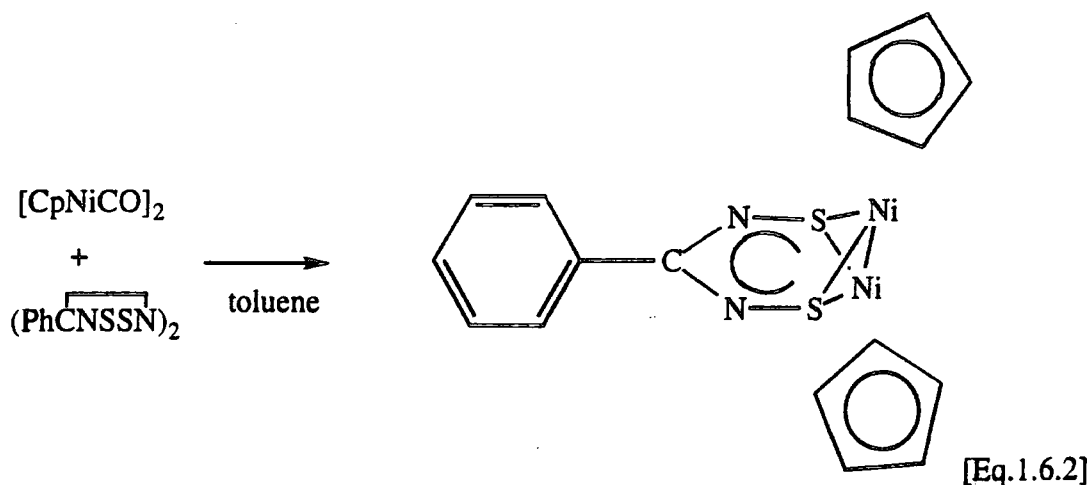


Figure 1.6.1 The monometallic complex $[\text{Pt}(\text{SNSPhNS-S,S})(\text{PPh}_3)_2]$

The dimetallic complex $[\text{Ni}_2(\text{Cp})_2(\text{PhCN}_2\text{S}_2)]^{3,31}$ [Eq.1.6.2] can be prepared by reacting $(\text{PhCNSSN})_2$ and $[\text{Ni}(\text{Cp})(\text{CO})_2]$ in toluene at room temperature. In this complex the S-S bond bridges across two metal centres, which give rise to μ_2 sulfur atoms.³²



The trimetallic species can be synthesised directly, [Eq.1.6.3] by reacting $3\text{Pt}(\text{PPh}_3)_2$ with $(\text{PhCNSSN})_2$ in toluene. Alternatively, by leaving the monometallic species standing in solution, it decomposes after a few days (as indicated by a change in colour), forming the trimetallic species, $[\text{Pt}_3(\mu\text{-SNCPHNS-S,S})_2(\text{PPh}_3)_4]$.

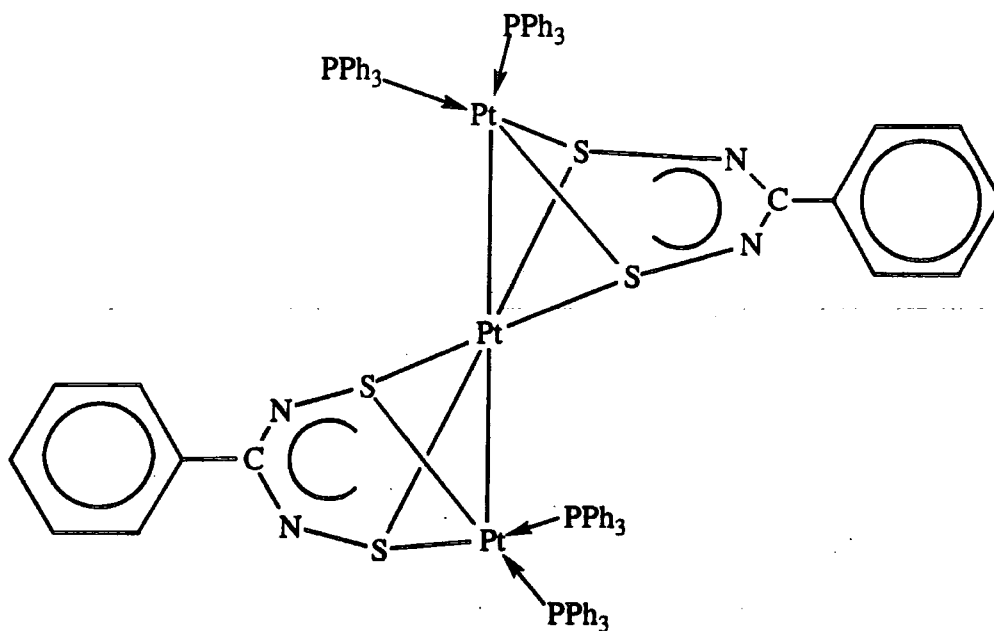
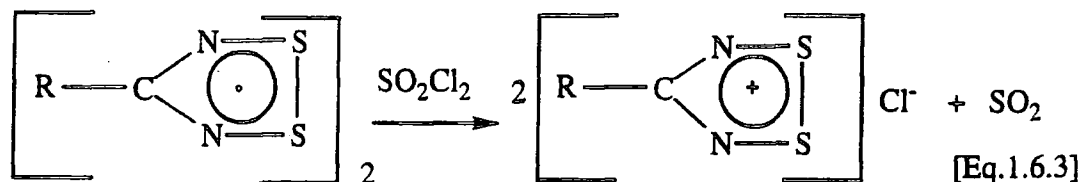


Figure 1.6.2 The trimetallic complex $[\text{Pt}_3(\mu\text{-SNCPHNS-S,S})_2(\text{PPh}_3)_4]$.

1.6.3 Oxidation

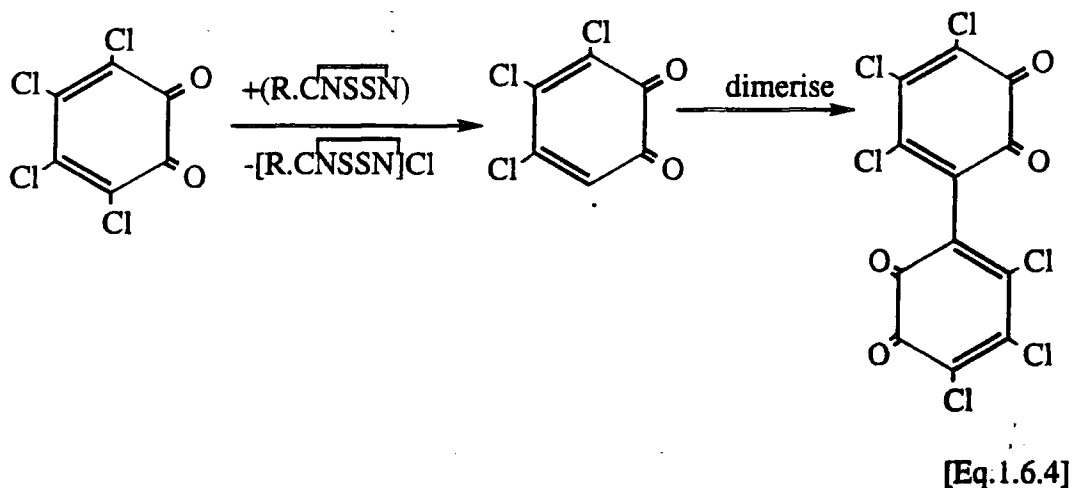
The radicals can be easily reoxidised⁴ to a corresponding dithiazolium salt. Chlorination is affected by SO_2Cl_2 or Cl_2 , [Eq. 1.6.3]. Bromine produces the bromide **16** while iodination produces a number of poly-iodides,^{4,16} depending upon the ratio of the reactants.



Oxidation can also be achieved by using high oxidation state Lewis acid halides, [Eq. 1.6.4] such as SbCl_5 .

1.6.4 Radical Coupling Reactions

$(\text{Ph.CNSSN})_2$ can function as a dehalogenating agent by attacking P-Cl, Si-Br and C-Cl bonds, forming new C-C and P-P bonds.



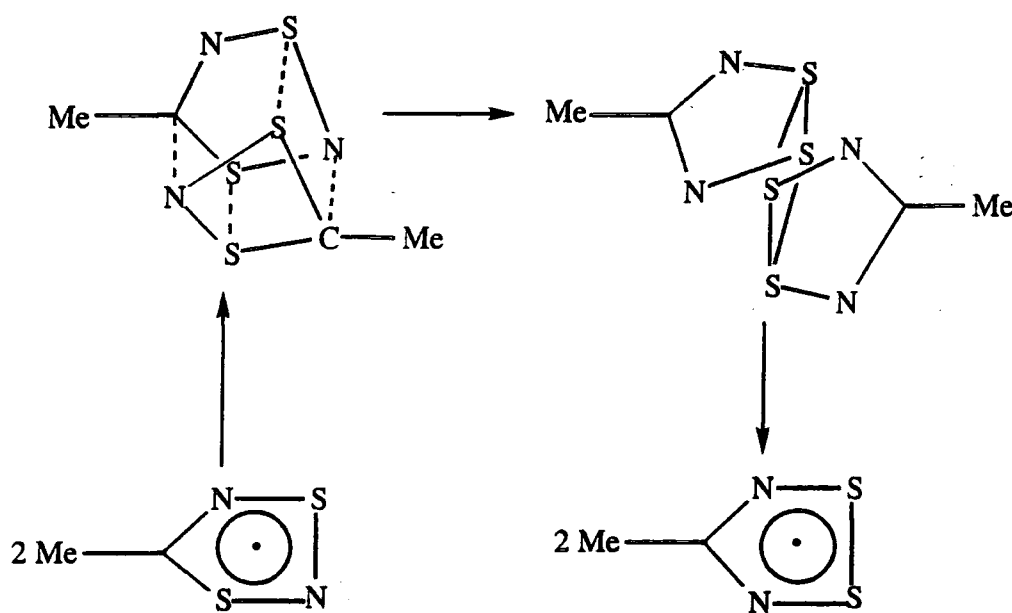
The postulated mechanism [Eq. 1.6.4] suggests that an intermediate radical is developed, whose reactivity can be altered by changing the substituent R group.

1.7 Physical properties of the 1,2,3,5 Dithiadiazolyls.

The presence of these radicals, both in solution and the solid state and hence their rearrangement from 1,3,2,4 to 1,2,3,5 dithiadiazolyl,²⁷ can be detected by e.s.r. spectroscopy²⁶ and cyclic voltammetry.

In the solid state the 1,2,3,5 dithiadiazolyls are associated through spin pairing of two heterocyclic rings, forming diamagnetic dimers. In solution the free radicals are detectable as they exist in an equilibrium between the monomeric and the dimeric form. Frozen solutions of the 1,2 isomer exhibit e.s.r. spectra similar to those observed in the solid state.⁴ This indicates that the energy of dimerisation is low; it is found to be approximately 5KJ/mol^{-1} .

The isomerisation process,²⁷ [scheme 1.7.1] proceeds through a variety of intermolecular C---N and S---S interactions to give the corresponding 1,2,3,5, dithiadiazolyl. The e.s.r. spectra¹ also provide evidence for the rearrangement process.



[Scheme 1.7.1]

The 1,3,2,4 isomer shows a 1:1:1 triplet as the unpaired electron is localised on the N atom which is furthest from the ring substituent. The solution e.s.r. spectra of the 1,2,3,5 isomer produces a 5 line quintet splitting pattern, arising from the interaction of the free radical with 2 equivalent ^{14}N nuclei. Coupling to S atoms is not observed as there is a low abundance of ^{33}S , and the nuclei have a (spin) $I=0$.

Changes in the splitting pattern on changing the substituent R group can be seen in studies carried out on $\text{CF}_3\cdot\text{CNSSN}$ and $\text{C}_6\text{H}_5\cdot\text{CNSSN}$.²⁹ This will be discussed further in chapter 3.

Figure 1.7.2 shows the changes in spectra which takes place when 5-phenyl-1,3,2,4-dithiadiazolyl rearranges to the 4-phenyl-1,2,3,5 dithiadiazolyl.

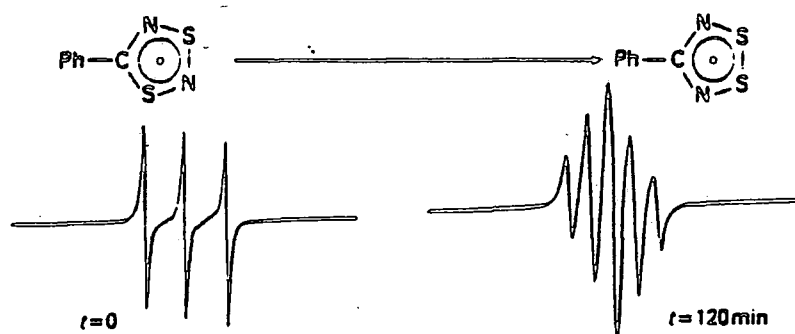


Fig.1.7.2 Rearrangement of 1,3,2,4 to 1,2,3,5 dithiadiazolyl observed by e.s.r.

Cyclic Voltammetry.

A recent electrochemical study³⁰ by C. Aherne *et al* on both 1,2,3,5 and 1,3,2,4 dithiadiazolylium derivatives as the hexafluorarsenate(v) salts, revealed reversible redox behaviour, giving the corresponding dithiadiazolyl radicals.

A linear free energy relationship between the half-wave reduction potential $E_{1/2}(\text{red})$ and the Hammett value (ρ) is observed for both dithiadiazolylium ring systems in the para-substituent derivatives.

Magnetic Behaviour.

Recently there has been a great deal of interest in the magnetic properties of organic free radicals^{31,32} and in their potential as semiconductors. Dithiadiazolyls are predominately diamagnetic, due to their association in the solid state, through weak S—S interactions.

However some residual paramagnetism is present, the extent of which depends upon the strength of the bonding between the monomers and the degree of crystallinity.⁴ The dimerisation process can inhibit any paramagnetism present. This association of monomers in the solid state can be controlled by heating, resulting in the snapping of the weak S—S interactions or by careful selection of the substituent group. The lone pairs present on the fluorine atoms give rise to repulsion between the two π clouds of the dithiadiazolyl. Alternatively by placing a cyano group CN on the *para* position, a more energy favourable one dimensional structure is observed; where the plane interactions can compete strongly with the out of plane S-S interactions.

A new crystalline phase of the dithiadiazolyl $p\text{-NC}_6\text{F}_4\text{CNSSN}\cdot$ has been shown,³³ to exhibit weak ferromagnetism at 36K. Until now the highest Curie temperature reported for organic ferromagnets was 1.4K, in $N'N'$ -dioxo-1,3,5,7-tetramethyl-2,6-diazaadamantane.³ This is clearly a major break-through for the future application of dithiadiazolyl as organic magnets.

1.8 Structural Studies of Dithiadiazolys.

The first X-Ray crystal structure of a 1,2, dithiadiazolyl¹⁹ was that of $(\text{PhCNSSN})_2$, shown in Figure 1.8.1.

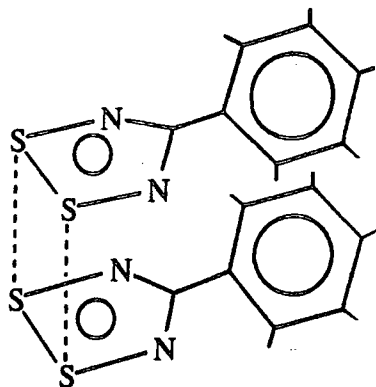


Figure 1.8.1 The structure of 1,2 dithiadiazolyl, indicating the overlap of p_z orbitals.

Since then other structures have been determined,^{20,21,22,23} as discussed in section 1.3. The majority of the phenyl derivatives reported, for example p-Cl, p-CN, p-MeO adopt a cis configuration with both rings lying approximately above one another. The dithiadiazolys are held together as dimer pairs³ through weak S---S interactions.

However in the case of $(\text{CF}_3.\text{CNSSN})_2$, $(\text{Me}.\text{CNSSN})_2$ and $(\text{Bu}^t.\text{CNSSN})_2$ a staggered conformation is favoured, where the two rings are held together through one S---S bond^{3,24} and are twisted at 90° with respect to one another, Figure 1.8.2. The loss of one S--S bond appears to be compensated by S--S and S--N interactions between the dimers.

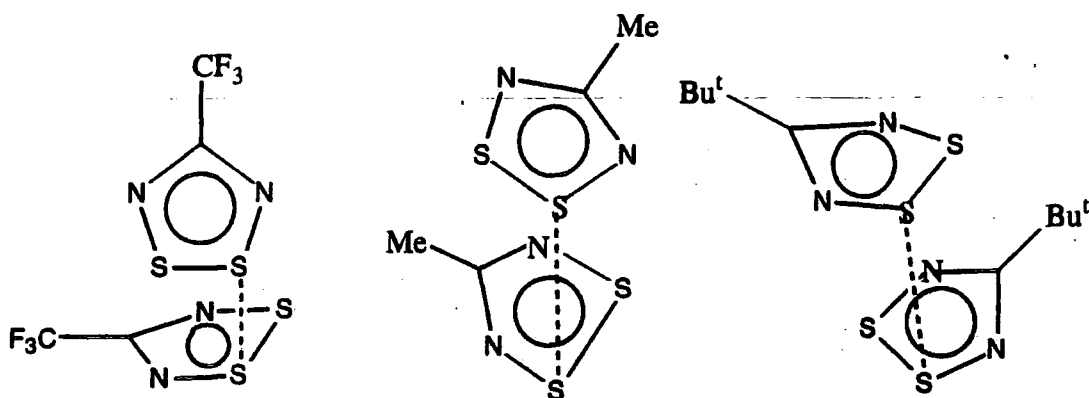


Figure 1.8.2 The conformation of $(\text{CF}_3.\text{CNSSN})_2$, $(\text{Me}.\text{CNSSN})_2$ and $(\text{Bu}^t.\text{CNSSN})_2$

The molecular arrangement adopted is dependant upon the R group which influences both the electronic effects and stereochemistry of the dithiadiazolyl.

Bulky substituents, for example tertiary butyl, will cause the rings to twist with respect to one another due to the steric hindrance of this large R group. This derivative is a paramagnetic liquid a room temperature.

The molecular arrangement of the $(\text{meta-CN.C}_6\text{H}_4.\text{CNSSN})_2$ and the more recently prepared $(\text{meta-CN.C}_6\text{F}_4.\text{CNSSN})_2$ is that of a trans configuration.

The structures of fluorinated dithiadiazolyls will be discussed in chapter 3.

The detection of 1,3 dithiadiazolyls has not been observed by e.s.r. spectroscopy²⁶ Since they are unstable with respect to isomerisation to the 1,2,3,5 dithiadiazolyl.

Altering the aryl substituent will significantly change the molecular packing.⁴ Such modification of the substituent group is crucial in developing polymeric material as observed in Figure 1.8.3. This shows the polymeric structure³ para-phenylenebis (1,3,2,4 dithiadiazolyl).

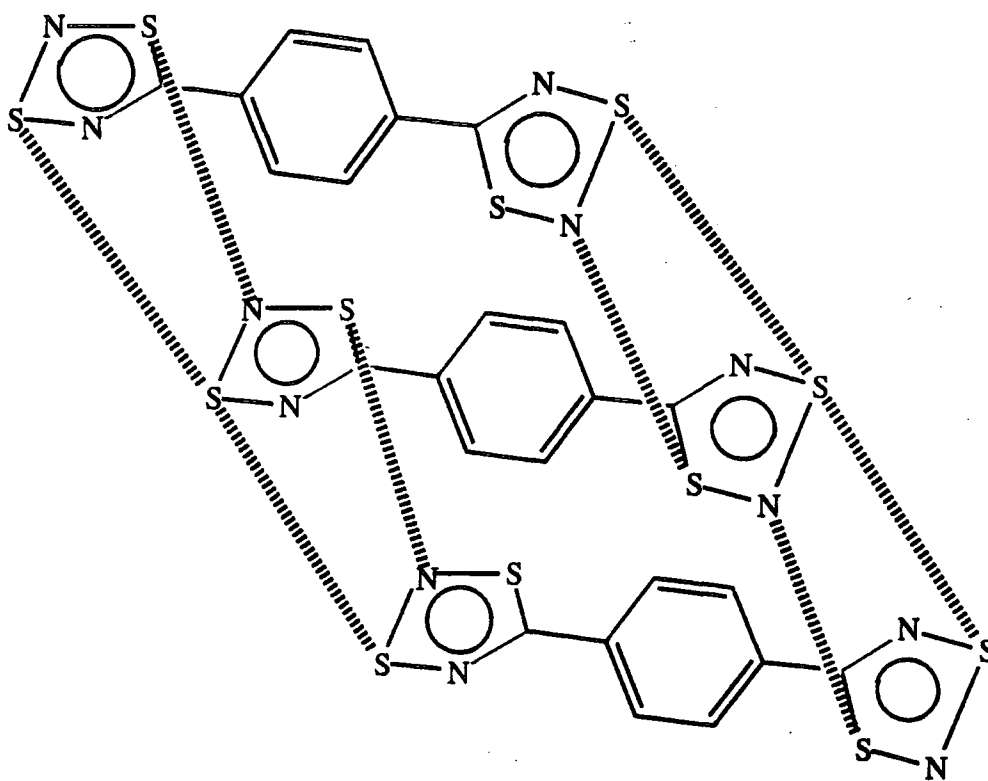


Figure 1.8.3 Structure of $(\text{SNSNC.C}_6\text{H}_4.\text{CSNSN})$

In this compound the $(\text{CNSNS})\cdot$ heterocycle is stabilised by the polymeric structure, where the radical centres have the possibility of electron pairing through N and S secondary interactions between the rings of different molecules.²⁷

These secondary interactions present produce a polymeric non-conductive array.

1.9 References.

1. A.J. Banister and J.M. Rawson, *Chem. Br.*, 1992, 148.
2. A.J. Banister et al, *Inorg. Nucl.Chem. Lett.*, 1974, **10**, 647; R.W.H. Small, A.J. Banister and Z.V. Hauptman, *J. Chem. Soc., Dalton Trans.*, 1984, 1377.
3. A.J. Banister and J.M. Rawson, *The Chemistry of Inorganic Ring systems*, ed. R. Steudal, Elsevier, Amsterdam, 1992, p.323.
4. J.M. Rawson, A.J. Banister and I. Lavender, *Adv. Heterocycl. Chem.*, 1995, **62**, p. 137-247.
5. A.J. Banister, N.R.M. Smith and R.G. Hey, *J Chem. Soc., Perkin Trans.*, 1983, 1181.
6. A.W. Cordes, R.C. Haddon, R.T. Oakley, L.F. Schneemeyer, J.V. Wasczak, K.M. Young and N.M. Zimmerman, *J.Am.Chem.Soc.*, 1991, **113**, 582.
7. B. Ayres, A.J. Banister, P.D. Coates, M.I. Hansford, J.M. Rawson, C.E.F. Richard, M.B. Hursthouse, K.M.A. Malik and M. Motevalli, *J. Chem. Soc. Dalton Trans.*, 1992, 3097.
8. A.J. Banister and J.M. Rawson, *J. Chem. Soc., Dalton Trans.*, 1990, 1517.
- 9a. A.J. Banister, I. Lavender, J.M. Rawson and R.J. Whitehead, *J.Chem.Soc.Dalton.Trans.*, 1992, 1449.
- 9b. S. Parsons, J. Passmore, M.J. Schriver and P.S. White, *J.Chem. Soc., Chem. Commun.*, 1991, 369.
10. S.A. Fairhurst, K.M. Johnson, L.H. Sutcliffe, K.F. Preston, A.J. Banister, Z.V. Hauptman and J. Passmore, *J.Chem.Soc., Dalton Trans.*, 1986, 1465.
11. S.E. Lawrence, Ph.D. Thesis, University of Durham, 1995.
12. A.J. Banister, M.I. Hansford, Z.V. Hauptman, A.W. Luke, S.T. Wait, W. Clegg and K.A. Jørgensen, *J.Chem.Soc., Dalton Trans.*, 1990, 2793.
13. A.C. Hazell and R.G. Hazell, *Acta. Crystallagr., Sect C*, 1988, 1807.
14. U. Scholz, H.W. Roesky, J. Schimkowiak and M. Nolteme, *Chem. Ber.*, 1989, **22**, 1067.
15. S. Parsons and J. Passmore, *J. Am. Soc.*, 1994, 101.
16. A.J. Banister, N.R.M. Smith and R.G. Hey, *J.Chem.Soc., Perkin Trans.*, 1983, 1181.
17. G.G. Alange, A.J. Banister and P.J. Dainty, *Inorg. Nucl.Chem.Lett.*, 1979, **15**,175.

18. A.J. Banister, I. Lavender, J.M. Rawson and R.J. Whitehead, *J.Chem.Soc., Dalton Trans.*, 1992, 1449.
19. A. Vegas, A. P. Salazar, A.J. Banister and R.G. Hey, *J.Chem. Soc., Dalton Trans.*, 1980, 1812.
20. A.J. Banister, M.I. Hansford, Z.V. Hauptman, S.T. Wait and W. Clegg, *J.Chem.Soc., Dalton Trans.*, 1989, 1705.
21. H.W. Roesky and T. Muller, *Chem.Ber.*, 1978, **111**, 2960.
22. A.W. Cordes, R.C. Haddon, R.T. Oakley, L.F. Schneemeyer, J.V. Wasczak, K.M. Young and N.M. Zimmerman, *J.Am. Chem. Soc.*, 1191, **113**, 582.
23. M.P. Andrews, A.W. Cordes, D.C. Douglass, R.M. Fleming, S.H.G. Iarum, R.C. Haddon, P. Marsh, R.T. Oakley, T.T.M. Palstra, L.F. Schneemeyer, G.W. Trucks, R. Tycko, J.V. Wasczak, K.M. Young and M. Zimmerman, *J.Chem.Soc.*, 1991, **113**, 3559.
24. A.W. Cordes, J.O. Goddard, R.T. Oakley and N.P.C. Westwood, *J.Am.Chem. Soc.*, 1989, **111**, 6147.
25. H.U. Höfs, J.W. Bats, R. Gleiter, G. Hartmann, R. Mews, M.E. Maksic, H. Oberhammer, G.M. Sheldrick, *Chem.Ber.*, 1985, **118**, 3781.
- 26a. N. Burford, J. Passmore and M.J. Schriver, *J.Chem., Chem.Comm.*, 1986, 140.
- 26b. W.V.F Brooks, N.Burford, J. Passmore, M.J. Schriver and L.H. Sutcliffe *J.Chem. Soc., Chem.Comm.*, 1987, 69,
- 26c. K.F. Preston and L.H. Sutcliffe, *Magn.Reson.Chem* , 1990, **28**, 189.
27. C. Aherne, A.J. Banister, A.W. Luke, J.M. Rawson and R.J. Whitehead, *J.Chem.Soc., Dalton Trans.*, 1992, 1277.
28. R.B. Woodward and R. Hoffman, Conservation of Orbital Symmetry, *Acad.Press*, 1970.
29. S.A. Fairhurst, L.H. Sutcliffe, K.F. Preston, A.J. Banister, A.S. Partington, J.M. Rawson, J. Passmore and M.J. Schriver. *Magn.Reson.Chem.*, 1993, **131**, 1027.
30. C. Aherne, A.J. Banister, I.B. Gorrell, M.I. Hansford, Z.V. Hauptman, A.W. Luke and J.M. Rawson, *J.Chem.Soc., Dalton Trans.*, 1993, 967.
31. D.A. Dougherty, in Research Frontiers in Magnetochemistry (ed. C.J. O'Conner), *World Scientific*, Singapore, 1993, 327-350.
32. P. Day, *Nature*, 1993, **363**, 147-149.

33. A.J. Banister, N. Bricklebank, I. Lavender, J.M. Rawson, I. Gregory, B.K. Tanner, W. Clegg, M.R.J. Elsewood and F. Palacio, unpublished results.
34. A.J. Banister, I.B. Gorrell, W. Clegg and K.A. Jørgensen. *J.Chem.Soc., Dalton Trans.*, 1991, 1105.
35. A.J. Banister, I.B. Gorrell, S.E. Lawrence, C.E. Lehman, I. May, G. Tate, A.J. Blake and J.M. Rawson. *J.Chem.Soc., Chem. Commun.*, 1994, 1779.
36. N. Burford, J.P. Johnson, J. Passmore, M.J. Schriver and P.S. White, *J.Chem.Soc., Chem.Commun.*, 1986, 966

CHAPTER 2

PREPARATION AND CHARACTERISATION OF SOME DITHIADIAZOLYLS AND THEIR PLATINUM COMPLEXES.

2.1 Introduction.

Group VIII transition metals, Ni, Pt, and Pd are known to form stable square planar complexes¹ in the 2+ oxidation state. Those involving sulfur and nitrogen ligands have been known since the early 1900's.^{2,3}

The only dithiadiazolylium metal complex reported is with the 1,3,2,4 complex $[\text{Hg}(\text{CNSNS})_2][\text{AsF}_6]_2$.⁴ Here the dithiadiazolylium ring bonds to the mercury via the carbon. The salt was first used as a transfer agent for the dithiadiazolylium cation, the preparation of which is shown in Figure 2.1

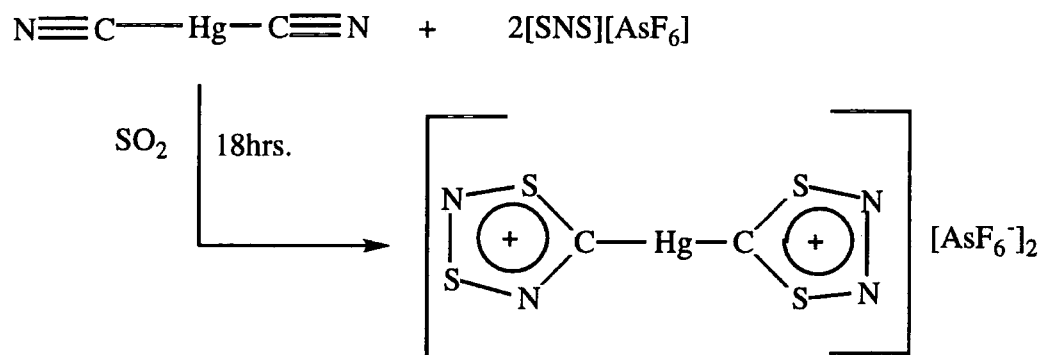


Figure 2.1 The structure of [Mercury-bis(1,3,2,4 dithiadiazolylium)hexafluoroarsenate]

The structure is analogous to $[\text{SNSNC.CNSNS}][\text{AsF}_6]_2$,⁵ but with Hg inserted into the C-C bond. The reactions of dithiadiazolyl radicals with Pt, Ni, and Pd have produced some interesting complexes,^{6,8} with novel bonding⁹ modes. The Pt and Pd complexes exhibit unusual structural and physical properties, for example their unusual e.s.r spectra, magnetic and biological properties.

Three different types of metal complexes have been synthesised (with +2 being the most common oxidation state) and studied, namely the monometallic, dimetallic and trimetallic species. In each case the metal is inserted into the S-S bond of the dithiadiazolyl. Both Pt and Pd are known to form square planar M^{2+} complexes for example $\text{K}_2[\text{Pt}(\text{CN})_4]\text{Cl} \cdot 0.3, 3\text{H}_2\text{O} (+2.0)$, $\text{K}_{1.75}[\text{Pt}(\text{CN})_4]1.50\text{H}_2\text{O} (+2.25)$ and $[\text{Pd}^{\text{II}}(\text{NH}_3)_2\text{Cl}_2]$.

In this chapter I outline the synthesis and properties of metal complexes. I also examine the bonding present within each complex, and some of their physical characteristics.

2.1.1 Synthesis of Some Metal Dithiadiazolyl Complexes.

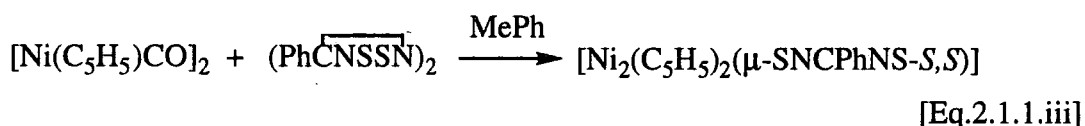
Several metal complexes have been synthesised using $(\text{PhCNSSN})_2$ as the ligand.⁸ The preparation of these complexes involves reacting the ligand with a variety of low valent (e.g. 0 or I) oxidation state metal complexes e.g. $\text{Pt}(\text{dppe})_2$, $\text{Pt}(\text{PPh}_3)_4$, $[\text{Ni}(\text{C}_5\text{H}_5)\text{CO}]_2$ and $\text{Pd}(\text{PPh}_3)_4$. The reaction proceeds via ligand replacement.

In addition to using the $(\text{PhCNSSN})_2$ species, some fluorine substituted and other halogenated dithiadiazolyls have been reacted with these phosphine complexes. Both monometallic and trimetallic species were produced. The synthetic methodology for these complexes is outlined below.

Nickel complexes react with $(\text{PhCN}_2\text{S}_2)$ producing dithiadiazolyl complexes via oxidative substitution.

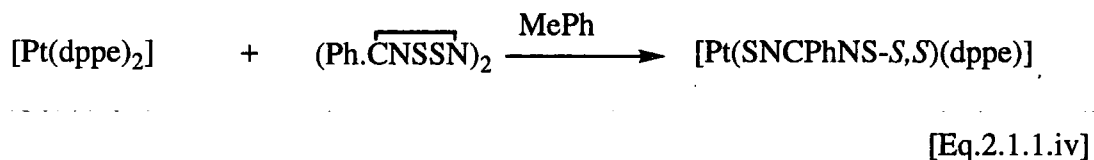
1(a) Preparation of $[\text{Ni}(\text{C}_5\text{H}_5)_2(\mu\text{-SNCPHNS-}S,S)]$ **7a,18**

Gorrell found that $[\text{Cp}_2\text{Ni}_2\text{PhCNSSN}]$ can be prepared by reacting $[\text{Ni}(\text{C}_5\text{H}_5)\text{CO}]_2$ with $(\text{PhCN}_2\text{S}_2)_2$ in toluene for 15 mins. followed by washing and drying *in vacuo.*, as shown in [Eq.2.1.1.iii].



1(b) Preparation of $[\text{Pt}(\text{SNCPHNS-}S,S)(\text{dppe})]$

Phosphine complexes also react with $(\text{PhCNSSN})_2$ [Eq.2.1.1.iv] via oxidative substitution.



2.1.2 Structural Studies of Monometallic Dithiadiazolyl Complexes.

As mentioned earlier, the metal complexes possess some unusual bonding modes⁹ and also structures with interesting biological properties.

A schematic representation of the monometallic dithiadiazolyl complexes, of the general formula $[M(\mu\text{-SNCPHNS-}S,S) L_x]$, is in Figure 2.1.2, where the metal is Pt or Pd and the ligand is either dppe or $(PPh_3)_4$.

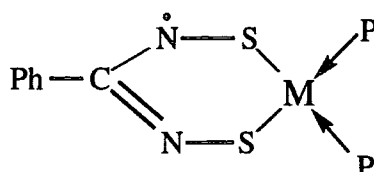


Figure 2.1.2 Structure of monometallic $[M(\mu\text{-SNCPHNS-}S,S)(P)_2]$.

The structure shows how the metal inserts into the S-S bond forming a six membered metallo-heterocycle,⁹ with the metal adopting a four co-ordinate planar geometry, giving a $16e^- M^{II}$ centre, and the complex retaining its free radical character.

Steric effects are very important (with respect to triphenylphosphine) in determining the structure and stereochemistry of these metallo-dithiadiazolyl complexes. These steric requirements are usually expressed by Tolman's cone angle ϕ . The cone angle encloses the van der Waal's surface of all the ligand atoms over all of the rotational orientations about the M-P bond.¹ The cone angle of triphenylphosphine is 145° .²³ The more bulky the substituent groups of the ligand the greater the cone angle will be. The large cone angle in triphenylphosphine has the effect of increasing the inter-bond P-M-P angle and decreasing the S-M-S angle.

The sum of the van der Waal's radii for a S-S bond (parallel to the bond) is 3.2\AA ($2 \times 1.6\text{\AA}$). The S---S bond distance in the monometallic platinum complex is just inside (3.168\AA) the sum of the van der Waal's radii (3.2\AA).²² This is still much greater than the S-S bond distance present in $(PhCNSSN)_2$ (2.089\AA).

2.1.3 Structural Studies of Dimetallic Complexes.

One dimetallic complex is known to date *viz* $[\text{NiCp}_2(\mu\text{-SNCPHNS-}S,S)]$. Its preparation ^{6,10} and structure have been previously reported.¹⁰ However recent research by Boeré *et al* has revealed that in the Fe complex (Figure 2.1.3(b)) $[\text{Fe}_2(\text{CO})_6(\mu\text{-SNCPHNHS-}S,S)]$, a nitrogen is protonated; this has the effect of removing its free radical character; with the ligand acting as a 2^- anion.

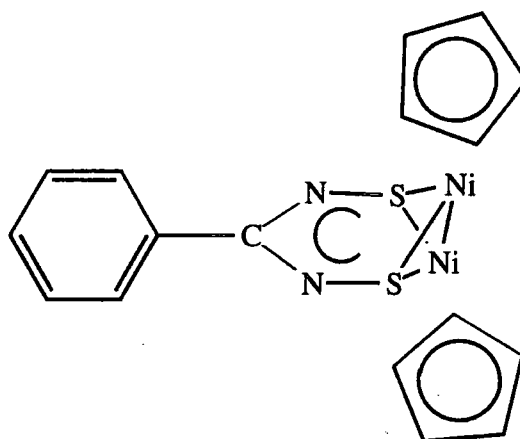


Figure 2.1.3(a) Structure of dimetallic $[\text{Ni}_2(\text{Cp})_2(\mu\text{-SNCPHNS-}S,S)]$

A tetrahedral configuration composed of 2Ni and 2S atoms is observed for the Ni complex as shown in Figure 2.1.3(a), with each Ni atom possessing $19e^-$ and adopting a butterfly configuration with the free radical character retained. In each case the S-S bond in the dithiadiazolyl opens up and bridges across the two metal centre complex.

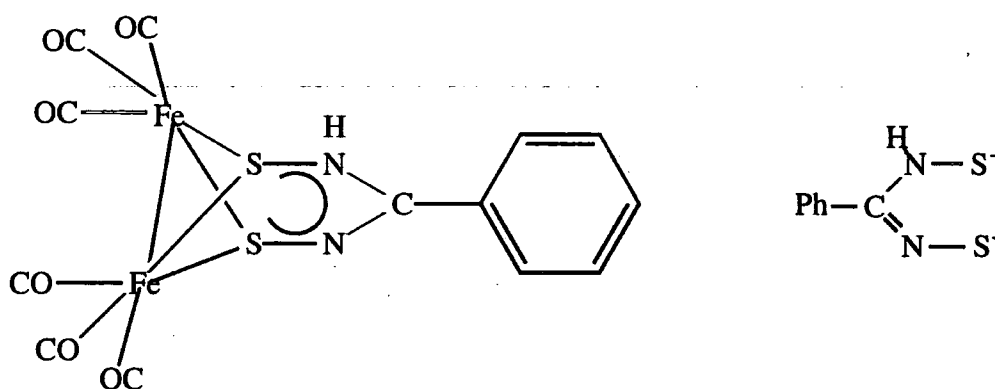


Figure 2.1.3(b) Structure of dimetallic $[\text{Fe}_2(\text{CO})_6(\mu\text{-SNCPHNHS-}S,S)]$ and its protonated anion.

2.1.4 Structural Studies of Trimetallic Complexes.

The monometallic complexes mentioned previously (section 2.1.2) are unstable in solution. They undergo rearrangement and decomposition to the corresponding trimetallic species (Figure 2.1.4). Alternatively the trimetallic complex can be synthesised directly,⁹ using the crystal growth procedure, (section 3.2.7). The structure shown (Figure 2.1.4) is composed of a Pt₃ linear chain which is bridged by two μ -SNCPPhNS ligands.

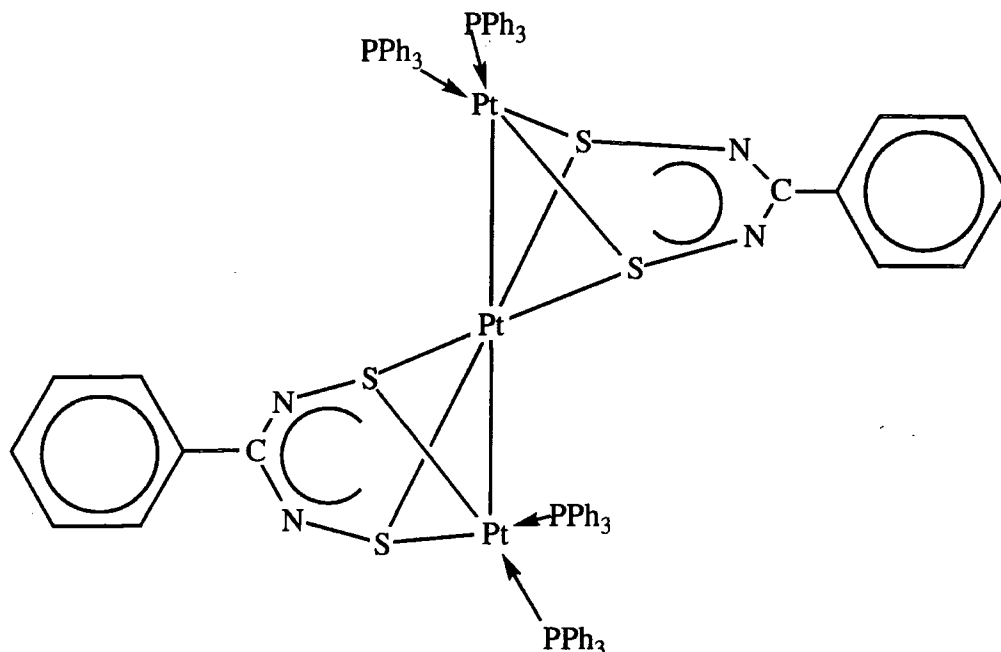


Figure 2.1.4 Structure of trimetallic $[\text{Pt}_3(\mu\text{-SNCPPhNS-S,S})_2(\text{PPh}_3)_4]$.

In the monometallic complex, the metal centre possess a square planar chelation environment i.e. $16e^- \text{Pt}^{\text{II}}$ centre. This has the effect of increasing the S---S bond length and decreasing the S-M-S bond angle.

The trimetallic species, (containing a crystallographic inversion centre), are structural analogues of the palladium complex $[\text{Pd}_3(\mu\text{-SNCPPhNS-S,S})_2(\text{PPh}_3)_4]$.¹² A decrease in the S---S bond length (Pd, 3.168(4)Å to Pt, 3.046(8)Å) is recorded and consequently an increase in P-M-P bond angle ($^\circ$), (100.01(7) to 103.3(2)).

The S--S bond distance in the trimetallic species (3.046Å) is within the sum of the van der Waal's radii (3.2Å).

2.5 Comparison of Bonding in Some Metal Dithiadiazolyl Complexes.

The S-S and S-M bond distances for some mono-, di- and trimetallic species are shown in Table 2.1.5. The differences can be attributed to two main factors.¹⁴ Firstly in the monometallic species (μ -SNCPPhNS) acts as a chelating ligand, while in the dimetallic and trimetallic species (μ -SNCPPhNS) acts as a bridging ligand. The second factor involves the degree of metal insertion. In the monometallic species the metal inserts more fully into the S-S bond of the dithiadiazolyl. This produces a much longer S-S distance than observed in the di- and trimetallic species, where the metal inserts to a much lower extent producing a shorter S-S distance.

COMPOUND	d _{S-S} Å	d _{S-M} Å	Ref.
(PhCN ₂ S ₂) ₂	2.09	-	11
[Pt(μ -SNCPPhNS - <i>S,S</i>)(PPh ₃) ₂]	3.168	2.301	9
[Pt(μ -SNCPPhNS - <i>S,S</i>)(dppe)]	3.281	2.293	2
[Ni ₂ (C ₅ H ₅) ₂ (μ -SNCPPhNS - <i>S,S</i>)]	2.905	2.172	6
[Fe ₂ (CO) ₆ (μ -SNCPPhNHS - <i>S,S</i>)]	2.930	2.225	9
[Pt ₃ (μ -SNCPPhNS - <i>S,S</i>) ₂ (PPh ₃) ₄]	3.046	2.387	8
[Pt ₃ (3,4-F ₂ .C ₆ H ₃ CN ₂ SSN) ₂ (PPh ₃) ₄]	3.040	2.340	21

Table 2.1.5 Bond lengths of various metal dithiadiazolyl complexes

Both PPh₃ and dppe are donor ligands, but their different relative bulk, effects the bonding in their respective complexes.¹⁴ As dppe is a chelating ligand, **15a,b** this could explain why the S-S bond length is observed to be longer in the monometallic dppe complex. The lower P-M-P angle (in the dppe complex) results in reduced repulsions between the bond pairs P-M and M-S, and hence an increase in the S-M-S angle, decrease in the P-M-P angle and lengthening of the S-S bond. The more bulky PPh₃ groups take up more space and thus decreases the S-M-S bond angle which increases the M-S bond distance and P-M-P angle.¹⁴

2.1.6 Biological Properties.

The anti-cancer interest in these metal complexes stems from their resemblance to cisplatin, $(\text{NH}_3)_2\text{PtCl}_2$ (Figure 2.1.6). Cisplatin known since 1845 as Peyrone's Chloride, was used by Chernyaev in developing his theory of the "Trans Effect".²⁰ It was not until 1969 that its efficacy as an anti-cancer agent was accidentally discovered.²⁰

Cisplatin belongs to a group of anti-cancer drugs which include inorganic co-ordination complexes, these are most commonly used for the treatment of testicular and ovarian cancers.

It has been reported that the effectiveness of the trans isomer (transplatin, Figure 2.1.6) is much lower than the cisplatin,²⁰ as the trans isomer is toxic towards both cancerous and non-cancerous body cells. The cisplatin isomer is more active and more selective towards cancerous cells because of its chelating ability towards biological molecules.

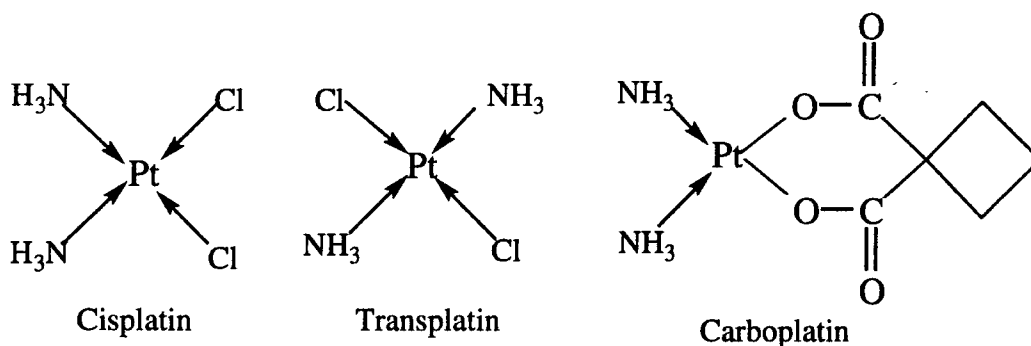


Figure 2.1.6 The structure of Cisplatin, Transplatin and Carboplatin.

Recent analogues of cisplatin²⁰ e.g. carboplatin, {1,1cyclobutanedicarboxylatyo-platinum(II) cis diammine} have been prepared which are more potent and less toxic than cisplatin.

Cytotoxicity studies, carried out by Johnson Matthey have shown that the monometallic Pt complex $[(\mu\text{-SNCRNS-S,S})\text{Pt}(\text{PPh}_3)_2]$ prepared by I. May is much more toxic and effective than the cisplatin. The toxicity of the monometallic complex is thought to arise from its free radical character.

Together with I. May,¹⁴ I have synthesised complexes with various substituted phenyl dithiadiazolyl complexes $[\text{Pt}(\mu\text{-SNCRNS,S})_2(\text{PPh}_3)_2]$ ($\text{R}=\text{p-Cl.C}_6\text{H}_4$; $\text{p-Br.C}_6\text{H}_4$; $\text{p-Me.C}_6\text{H}_4$; $3,4\text{-F}_2\text{.C}_6\text{H}_3$;). These complexes have been analysed and sent to Johnson Matthey for biological testing. (Results have yet to be received).

A number of culture cells were in the Johnson Matthey laboratory. The toxicity of the cisplatin is compared to that of the monometallic Pt complex, (shown in Table 2.1.6). The quantity of complex required to kill half of the culture cells IC_{50} (μM), was recorded for both complexes. In the majority of cases the Pt complex was shown to be much more toxic, but consequently less selective in targeting cancerous cells.

Table 2.1.6 The toxicity of cisplatin and the monometallic platinum complex.

IC_{50} (μM) Vs Cell Line

Culture Cells	Cisplatin	$[Pt(PhCNSSN)(PPh_3)_2] \cdot MeCN$
A2780	8.90	0.5
A2780 Cis ^R	29.0	0.35
CH1	0.082	0.43
CH1 ^R	0.33	0.43
CH1 ^{RF}	4.0	1
41M	0.22	0.66
41M Cis ^R	1.05	0.7
41M ^{RF}	4.7	1.1
SKOV-3	14.5	1.45
HX62	2.80	1.05

It is evident from the table that the Pt complex is more toxic than the cisplatin. The resistance factor (RF) is a measure of the ratio of the kill factor in the resistant strain against the kill factor in the nonresistant strains, i.e. how resistant the resistant cells actually are.²⁰ The lower the RF value the more toxic the complex is against both sensitive and resistant cells.

IC_{50} Resistant (Cis^R) Line

RF = Resistance Factor = -----

IC_{50} Sensitive Line

Although this monometallic platinum complex is more effective in inhibiting anti-cancer cells, the major drawback with the complex is its reduced selectivity.

The Pd(II) complexes have also been tested for their anti-cancer activity; however their toxicity is much lower than that of the monometallic Pt complexes.

2.2 EXPERIMENTAL.

2.2.1 Preparation of (C₆H₅CN₂SSN)₂

Li[N(SiMe₃)₂] (4.86g, 29.1mmol) and benzonitrile (3.0g, 29mmol) in anhydrous diethyl ether (ca. 50cm³), were stirred overnight at room temperature to give a straw coloured solution. A slight excess of SCl₂ was slowly added with cooling in ice, resulting in the instant formation of a yellow coloured precipitate. The mixture was stirred for a further 5 to 6 hrs. and then filtered and washed with Et₂O (ca. 3x15ml). The crude product was left drying *in vacuo* overnight. It was then transferred to a sealed extractor¹⁶ and extracted with SO₂(l) overnight.

After a few days, only white LiCl was visible on the extractor, indicating that the extraction was complete. The SO₂ was released slowly and the product was transferred to a two neck flask with Zn/Cu couple (0.6g, 9mmol) and THF (ca.15ml). The purple coloured solution was left stirring at room temperature overnight. The THF was removed and the residues dried *in vacuo*. The crude radical was transferred to a sublimation tube (0.70g, 3.9mmol), where prolonged heating in an oil bath released the pure radical. It was then placed in the glove box where the yield was recorded.

Appearance: Black crystalline solid.

Yield: 0.18g, 1.0 mmol, 25%.

Infra red: (Nujol mull, KBr plates) ν_{\max} ; 2359m, 1684br, 1461sh, 1376vs, 1136sh, 1018m, 834m, 802sh, 776sh, 767sh, 721vs, 689sh, 653s, sh; 507vs. cm⁻¹.

Elemental analysis: Found(%) C 45.28, H 2.60, N 15.13

Required (%) C 46.45, H 2.75, N 15.44.

Mass spectrum: (E.I.) 183(M⁺), 149(C₆H₄CN₂S⁺), 135(C₆H₄CNS⁺), 117(C₆H₄CN₂⁺), 103(C₆H₄CN⁺), 87(C₇H₅⁺), 78(C₆H₄⁺), 64(C₅H₃⁺), 46 (SN⁺).
(C.I.) 182(C₆H₄CN₂SSN⁺), 121(C₆H₄C(NH₂)₂⁺), 46(SN⁺).

DSC: Melting point 118.7 +/-1°C. Temperature of decomposition 259.1 +/-1°C.

2.2.2 Preparation of (*para*-Br.C₆H₄.CNSSN)₂

The procedure was applied as that described in section 2.1. Li[N(SiMe₃)₂] (2.73g, 16.4mmol) and *para*-bromobenzonitrile (3g, 16mmol) were stirred in anhydrous diethyl ether (ca. 50 cm³). The dithiadiazolyl was eventually sublimed *in vacuo* in a sublimation tube (0.63g, 2.4mmol) and the yield was recorded using the glove box balance.

Appearance: Dark brown crystalline material.

Yield: 0.04g, 0.12mmol, 6.1%.

Infra red: (Nujol Mull, KBr plates) $\bar{\nu}_{max}$; 1733msh; 1585m, 1461vs, br; 1375vs, 1264vw, 1099w, br; 1069m, 1010m, 969w, br; 833m, 775m, 772m, sh; 649m, 508m, sh; 478w, sh; 413vw, cm⁻¹.

Elemental analysis: Found(%) C 31.92, H 1.30, N 10.39

Required (%) C 32.32, H 1.53, N 10.77.

Mass spectrum: (E.I.) 261(M⁺), 215(Br.C₆H₄CNS⁺), 183(Br.C₆H₄CN⁺) 134(C₆H₄CNS⁺), 103(C₆H₄CN⁺), 89(C₇H₅⁺), 78(C₆H₄⁺), 76(C₆H₄⁺), 46(SN⁺) (C.I.) 261(M⁺), 48(S₂N⁺), 46(SN⁺).

DSC: Melting point 153.2 +/-0.5 °C. Decomposition temperature 269.2 +/-0.6 °C.

2.2.3 Preparation of (*para*-Cl.C₆H₄.CNSSN)₂

As was described in 2.2.1, Li[N(SiMe₃)₂] (1.54g, 9.2mmol) and *para*-chlorobenzonitrile (1.4g, 10mmol) were stirred in diethyl ether. The salt was reduced and sequently sublimed (0.85g, 3.9mmol), as described above.

Appearance: Black crystalline solid.

Yield: 0.2g, 0.93mmol, 24%.

Infra red: (Nujol mull, KBr plates) $\bar{\nu}_{max}$; 1600vw, 1475s,br; 1384s, 1310w, sh; 1154vw, sh; 1152w, 1096m, 1026m, 936vw, 838m, 774w, sh; 721vs, 656m, 484w, sh; 419vw, cm⁻¹.

Elemental analysis: Found (%) C 38.14, H 1.82, N11.71

Required (%) C 38.99, H 1.85, N 12.98.

Mass spectrum (E.I.) 215(M⁺), 169(Cl.C₆H₄CNS⁺), 151(Cl.C₆H₄CN₂⁺), 137(Cl.C₆H₄CN⁺), 102(C₆H₄CN⁺), 78(C₆H₄⁺), 76(C₆H₄), 46(SN⁺) (C.I.) 215(M⁺), 155(Cl.C₆H₄(NH₂)₂⁺), 78(S₂N⁺), 46(SN⁺).

DSC: Melting point 139.8 +/-0.3 °C. Decomposition temperature 250.4 +/-0.2 °C.

2.2.4 Preparation of (*para*-Me.C₆H₄.CNSSN)₂

The corresponding chloride salt, [*para*-Me.C₆H₄.CNSSN]Cl (0.55g, 2.4mmol) was prepared by C. Aherne, Durham University. It was reduced with Zn/Cu couple in THF; the THF was then removed *in vacuo* and the radical was then placed into a sublimation tube and heated in an oil bath. This was left on overnight and the crystals appeared as dark purple, black blocks and needles. The tube was cracked and put into the glove box where the radical was removed from the sides of the tube and the yield recorded.

Appearance: Dark purple black crystals.

Yield: 0.26g, 1.3mmol, 47%.

Infra red: (Nujol Mull, KBr plates) ν_{\max} ; 1740vw,br; 1460vs,br; 1376vs, 1304vw,br; 1179vw,sh; 996vw,br; 820vw, 804vw,br; 773vw,sh; 721s, 651m, 508w, cm⁻¹.

Elemental analysis: Found (%) C 48.92, H 3.46, N 16.26

Required (%) C 49.16, H 3.67, N 16.16.

Mass spectrum: (E.I.) 195(M⁺), 149(Me.C₆H₄CNS⁺), 117(Me.C₆H₄CN⁺),

91(Me.C₆H₄⁺), 89(C₇H₅⁺), 76(C₆H₄⁺), 64(S₂⁺), 46(SN⁺),

(C.I.) 195(M⁺), 135(Me.C₆H₄C(NH₂)₂⁺).

DSC: Melting point 132.8+/-0.4 °C. Decomposition temperature 241.8+/-0.3 °C.

2.2.5 Attempted Preparation of (*para*-Me₂N.C₆H₄.CNSSN)₂

Li[N(SiMe₃)₂] (3.40g, 20.4mmol) and *para*-dimethylaminobenzonitrile (3.0g, 20.4mmol) were stirred in diethyl ether, as described in section 2.2.1. On addition of SCl₂, a brown red coloured solution formed instead of the characteristic orange precipitate. After stirring for several hours the colour of the solution had changed to black-purple. The salt was reduced with Zn/Cu couple in THF. Following removal of the THF *in vacuo*, sublimation was attempted but this proved to be very difficult, yielding only yellow micro-crystals (sulfur) half way up the sublimation tube, along with some intractable brown solid. The intractable nature of the residue suggested that not all the THF was removed *in vacuo* prior to sublimation. An infra red spectrum of the chloride salt was run and the results are shown below.

Infra red: (Nujol mull, KBr plates) ν_{\max} ; 1685s, 1591w, 1464vs,br; 1376vs,

1306vw,br; 1208vw, 1130w, 1081w,br; 1050vw, 975vw,sh; 896w,br; 815vw,br; 724s, 678m, cm⁻¹.

2.2.6 Attempted Preparation of 2,4-Dimethoxydithiadiazolylium Chloride.

Li[N(SiMe₃)₂] (3.07g, 18.4mmol) and 2,4-dimethoxybenzonitrile (3.1g, 19mmol) were stirred overnight in diethyl ether (ca. 50ml). On addition of SCl₂, a dark brown colour developed. On filtering this solution some small white particles were observed on the filter stick. An infra red spectrum was carried out on the unknown white material and was found to be very similar to the infra red spectrum of the starting nitrile i.e 2,4 dimethoxybenzonitrile. The results of the infra red study are shown below.

Infra red: (Nujol Mulls, KBr plates) ν_{\max} ; 1165w,br; 1610m, 1574m, 1468vs,br; 1384 vs, 1302m, 1222m, 1174m, 1120w,sh; 1000s, 948m,sh; 804vw, 716vs, 566vw, 474m, cm⁻¹.

2.2.7 Preparation of Tetrakis(triphenylphosphine) platinum(0).

Triphenyl phosphine (2.9g, 10.9mmol) was dissolved in ethanol, and refluxed under a stream of nitrogen. A solution of potassium hydroxide (0.27g, 4.8mmol) was cannular transferred onto the refluxing triphenylphosphine solution. A second solution of potassium tetrachloroplatinate (1g, 2.4mmol) was also cannular transferred to the refluxing solution. After approximately 2 hours the solution was filtered and washed with ethanol/water, and dried *in vacuo*.

Appearance :Pale yellow solid.

Yield: 70%.

Infra red: (Nujol Mulls, KBr plates) ν_{\max} ; 3053m, 1959w, 1888w, 1816w, 1583m,sh; 1476s,sh ; 1305w, 1265w, 1198m, 1181m, 1154w, 1119m, 1803m, 1069w,sh; 1026sh, 998w, 743s, 721m, 694s, 619w, 542m, 507s,sh; 415s, cm⁻¹.

Elemental analysis: Found (%) C 69.51, H 4.76, N 0.00

Required (%) C 69.50, H 4.86, N 0.00.

DSC: Sharp exotherm (decomposition) recorded at 161.5+/-0.5 °C.

2.2.8 Preparation of Pt(dppe)₂.

Potassium tetrachloroplatinate (0.50g, 1.2mmol) was added to distilled water (ca. 10cm³), forming a red coloured solution. A second solution of dppe (0.95g, 1.6mmol) in ethanol was cannular transferred onto the aqueous K₂PtCl₄, producing a distinct pink coloured solution. This was allowed to reflux until a white grey coloured solution appeared. The reducing agent NaBH₄ was added slowly, in excess, resulting in the formation a bright yellow coloured solution .

Appearance: Bright yellow solid.

Yield: 80%.

Infra red: (Nujol Mulls, KBr plates) ν_{\max} ; 3048m, 1111w, 1890w, 1813w, 1583m, 1569w, 1432s,sh; 1407w, 1304w, 1272w, 1179w, 1156w, 1089m, 1066m, 1025m,999w 871m, 815m, 802m, 738s,sh; 693s,sh; 660m, 520s,sh; 513s,sh; 489m, 412m, cm⁻¹.

Elemental analysis: Found (%) C 62.90, H 4.90, N 0.00

Required (%) C 62.96, H 4.88, N 0.00.

DSC: Sharp exotherm (decomposition) at 230+/-1 °C.

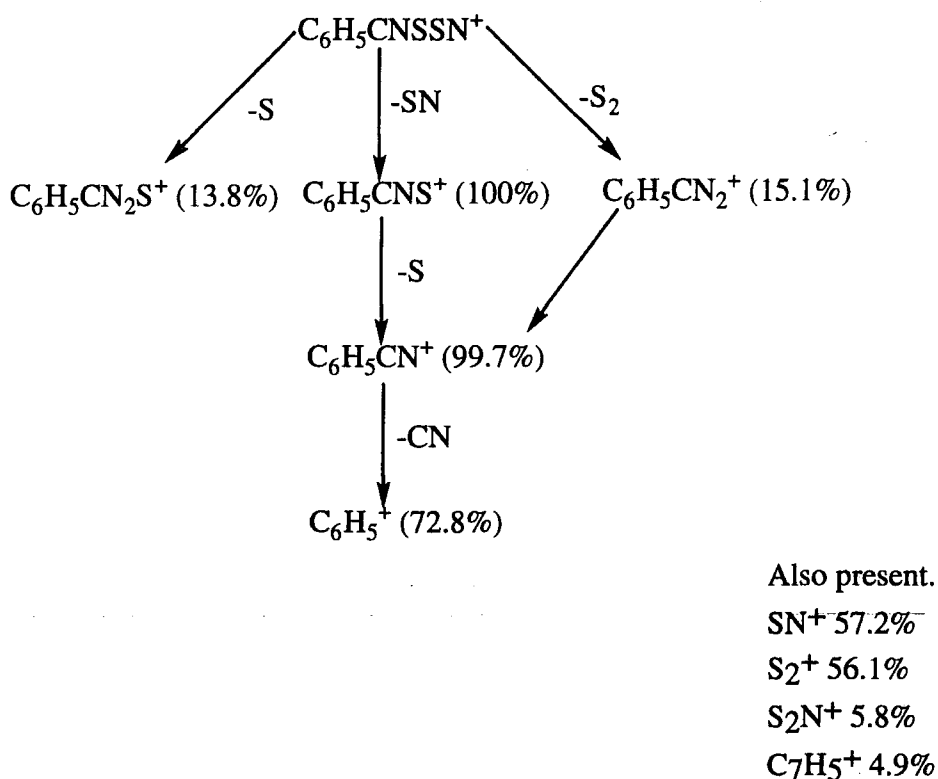
2.3 Results and Discussion.

2.3.1 Preparation of $(C_6H_5.CN_{SSN})_2$

The reaction of $Li[N(SiMe_3)_2]$ with benzonitrile in Et_2O (section 1.2c), produced phenyldithiadiazolyl. The infrared spectrum showed the absence of the CN peak at $2225cm^{-1}$; this indicated that cyclisation has successfully taken place.

The peak at $721cm^{-1}$ is thought to arise from an S-N bending mode, while the peak at $1308cm^{-1}$ could arise from C-N stretching.²¹ It can be seen that by changing the R substituents on the phenyl ring that the respective vibrational and stretching frequencies will shift. The mass spectrum (E.I.) breakdown pattern is shown in scheme 2.3.1. Together with excellent elemental analysis, it shows that the reaction proceeded successfully.

Scheme 2.3.1 Mass spectrum breakdown pattern of $(C_6H_5.CN_{SSN})_2$



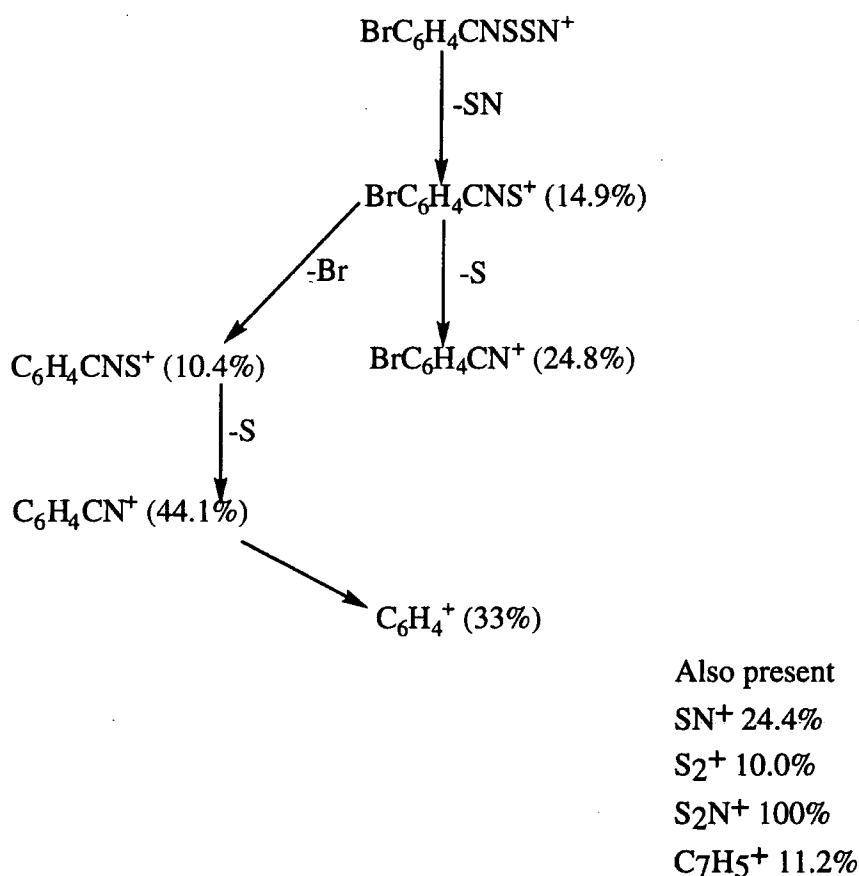
The DSC trace shows a sharp melting point (endotherm) at $118.7\pm 0.1^\circ C$, decomposition begins at around $259.1\pm 0.2^\circ C$.

2.3.2 Preparation of (*para*-Br.C₆H₄.CNSSN)₂

The reaction of Li[N(SiMe₃)₂] with *para*-bromobenzonitrile under similar conditions (in section 2.1c), produced the *para*-bromodithiadiazoly radical. The absence of any CN peak at 2225cm⁻¹ indicated that all the *para*-bromobenzonitrile had reacted.

The weak peak at 1321cm⁻¹ can be attributable to C-N stretching. It is likely that the strong peak at 722cm⁻¹ arises from S-N stretching within the dithiadiazoly radical. The mass spectrum breakdown pattern (E.I.) is shown below, it shows some similarities to that of (C₆H₅.CNSSN)₂, (see scheme 2.3.1).

Scheme 2.3.2 Mass spectrum breakdown pattern of (*para*-Br.C₆H₄.CNSSN)₂



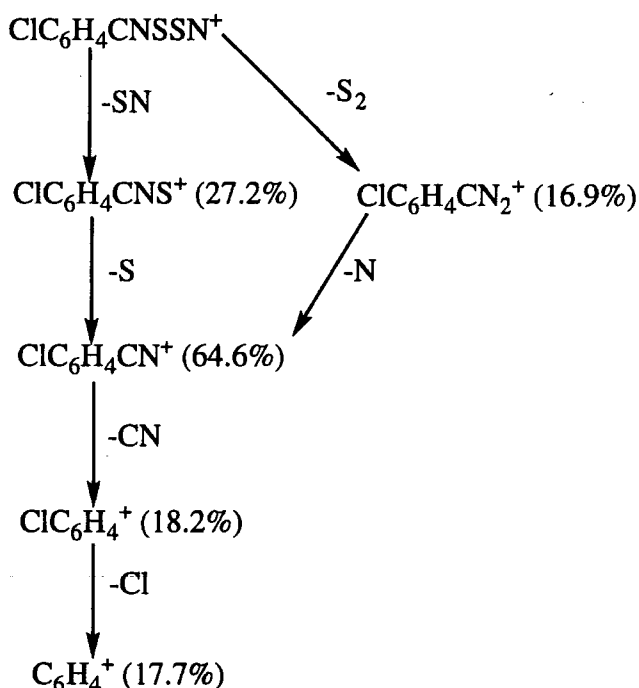
The DSC trace (see p. 43) shows a very sharp melting point at 153.2±0.5°C and a distinct decomposition or rearrangement process is occurring at 269.2±0.2°C. Along with the elemental analysis, it can be concluded that the preparation of (*para*-Br.C₆H₄.CNSSN)₂ was indeed a success.

2.3.3 Preparation of (*para*-Cl.C₆H₄.CNSSN)₂

As described in the previous section, 2.3.1 and 2.3.2. The reaction of Li[N(SiMe₃)₂] with *para*-chlorobenzonitrile and SCl₂ in anhydrous diethyl ether proceeded without any difficulties, producing (*para*-Cl.C₆H₄.CNSSN)₂. Firstly in the infrared spectrum, there is no evidence of the CN peak at 2225cm⁻¹. This indicates that cyclisation has successfully taken place. The vibrational frequency at 1310cm⁻¹ is believed to arise from the C-N stretching within the dithiadiazolyl.

The peaks between 1152 and 516cm⁻¹ are difficult to assign, but they are most likely to arise from the stretching within the benzene and dithiadiazolyl rings. The peak at 721cm⁻¹ can be assigned to S-N stretching. The mass spectrum breakdown shown in scheme 2.3.3 below, highlights the most abundant fragments which arise from electronic ionisation of the radical.

Scheme 2.3.3 Mass spectrum breakdown pattern of (*para*-Cl.C₆H₄.CNSSN)₂



Also present
SN⁺ 30.6%
S₂⁺ 3.9%
S₂N⁺ 100%

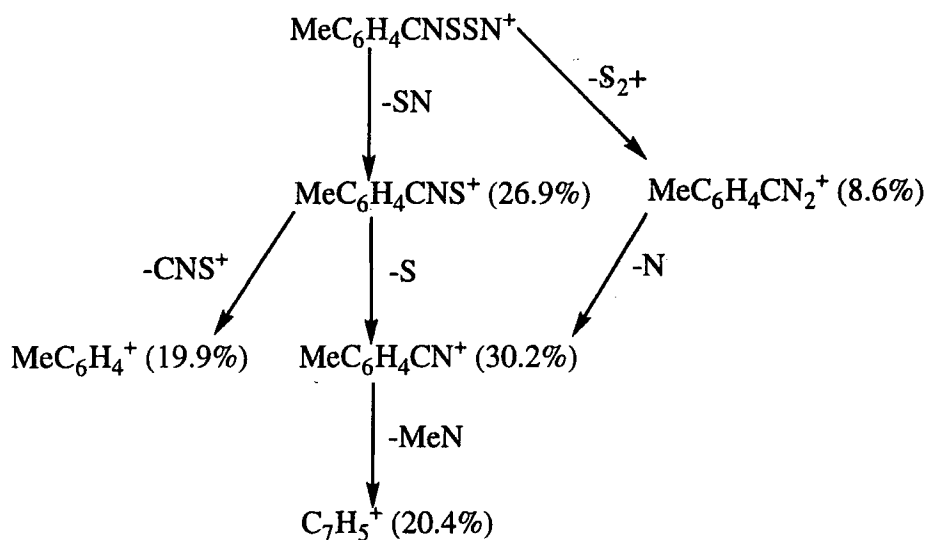
Good elemental analysis and the DSC indicate that the reaction proceeded successfully. The DSC reveals that melting begins at 139.8+/-0.2 °C and that decomposition occurs at 250+/-0.5 °C. The trace was similar to that shown on p.43.

2.3.4 Preparation of (*para*-Me.C₆H₄.CNSSN)₂

This radical was obtained from the chloride salt, (as in section 2.2.4) which had been previously prepared by C. Aherne.

As in the infrared spectrum of the other dithiadiazolyl radicals, the absence of the peak at 2250cm⁻¹ indicates that cyclisation has occurred. It is thought that the peak at 721cm⁻¹ and possibly that at 966cm⁻¹ are due to the S-N bending modes. The mass spectrum breakdown pattern (E.I.) is shown in scheme 2.3.4 below.

Scheme 2.3.4 Mass spectrum breakdown pattern of (*para*-Me.C₆H₄.CNSSN)₂



Also present.

S₂⁺ 9.8%

SN⁺ 13.9%

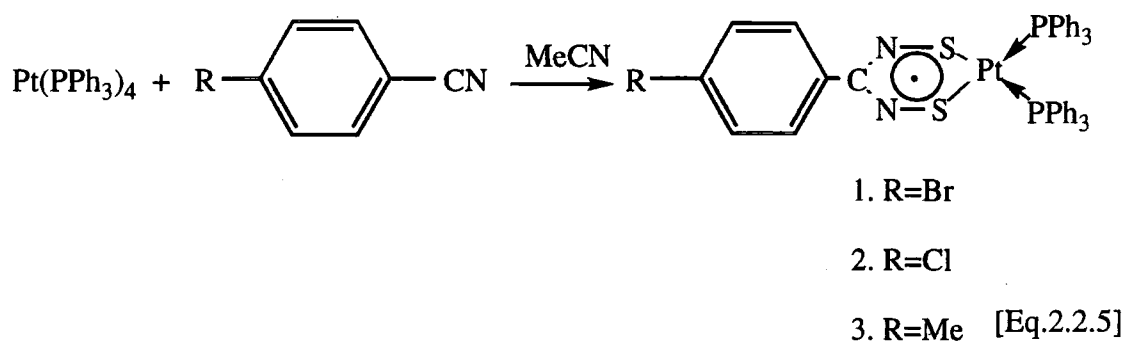
S₂N⁺ 100%

Good elemental analysis were obtained and the DSC shows that melting begins at 132.8±0.2 °C and that decomposition occurs at 242±1 °C.

2.3.5 The Reaction of $\text{Pt}(\text{PPh}_3)_4$ with (*para*-Br.C₆H₄.CNSSN)₂

The addition of MeCN (ca. 15ml) to a mixture of $\text{Pt}(\text{PPh}_3)_4$ and *para*-bromobenzonitrile, led to the formation of a dark blue micro crystalline precipitate under a blue-green solution. ¹⁷ After stirring in a Schlenk, (ca. 20mins.), the solution was filtered off and the filtrate washed with MeCN (3x5ml).

Comparison of the infrared spectrum of the complex with that of the dithiadiazolyl, highlights some differences. The peaks at 1733cm^{-1} and 1585cm^{-1} have disappeared, and a peak at 2359cm^{-1} has appeared. The reaction sequence [Eq.2.2.5] for the preparation of *para*-substituted metallo-dithiadiazolyl complexes.



Excellent elemental analysis figures were obtained. Ultraviolet/visible spectroscopic studies were carried out on all the newly synthesised complexes. The complexes were dissolved in dichloromethane, and the spectra recorded between 400nm and 1000nm.

The initial colour of the complex was blue-green. After completion of the scan, the solution appeared green. An intense absorption peak was observed at 684nm (absorbance 2.26) while a much weaker band was observed at 509nm (absorbance 0.8). This had disappeared on completion of the second scan, while at the same time there was a significant reduction in intensity at the peak at 684nm.

The DSC shows that the complex begins to decompose (exotherm) at $240 \pm 0.5^\circ\text{C}$, with further decomposition occurring at $303 \pm 1^\circ\text{C}$.

Elemental analysis: Found(%) C 51.44, H 3.26, N 3.28

Required(%) C 52.96, H 3.72, N 3.53.

2.3.6 The Reaction of Pt(PPh₃)₄ with (*para*-Cl.C₆H₄.CNSSN)₂

Tetrakis(triphenylphosphine)platinum(0) and *para*-chlorobenzonitrile were stirred in MeCN (ca. 15ml) for about 30mins. A green blue micro crystalline solid in a blue coloured solution developed; this was subsequently filtered and washed with MeCN (3x5ml).

On comparing the infrared spectrum of the starting dithiadiazolyl radical with that of the metal complex, the following peaks were observed. A peak arises at 2359cm⁻¹ and the peak at 721cm⁻¹ had decreased in intensity. As in the infrared spectrum of the *para* bromo dithiadiazolyl complex, many of the peaks remain unassigned. However the presence of the platinum metal clearly has an effect on the peak absorption's and intensities.

Ultraviolet/visible spectroscopic studies were carried out, as described in section 2.3.5. The solution initially appeared as a dark emerald green colour, eventually turning to a lighter shade of green on completion of the scan. The strongest absorption peak appeared at 684nm (absorbance 1.72). The solution was recorded between 400nm and 1000nm. The main peak intensity decreased with time as the complex decomposed.

The DSC appeared to be very similar to that of [Pt(PPh₃)₂(Br.C₆H₄.CNSSN)] with melting beginning at 147°C ± 1°C, and decomposition occurring at 344°C ± 2°C.

Excellent elemental analysis were obtained:

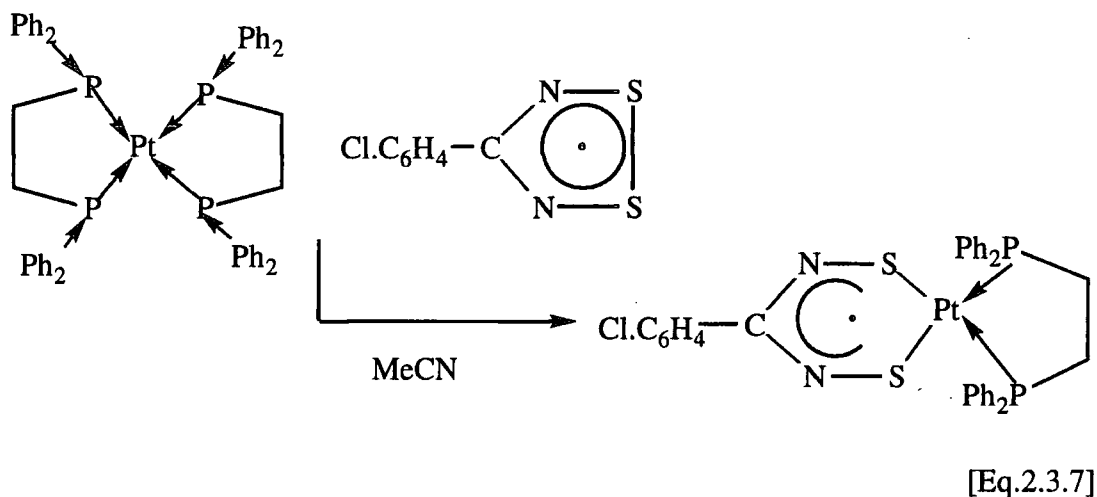
Found (%) C 52.91, H 3.58, N 3.02

Required (%) C 52.91, H 3.59, N 2.87.

2.3.7 Reaction of Pt(dppe)₂ with (*para*-Cl.C₆H₄CN₂SSN)₂

Pt(dppe)₂ and *para*-chlorobenzonitrile were stirred in MeCN in a Schlenk, (ca.15mins), [Eq.2.3.7]. A blue micro crystalline precipitate under a blue-green coloured solution was observed. The solution was filtered and washed with MeCN (3x5ml). It was dried *in vacuo*.

The infrared spectrum of the new complex shows a peak at 2360cm⁻¹, while a peak at 525cm⁻¹ has also appeared. The peak at 1600cm⁻¹, which was present in the spectrum of the starting dithiadiazolyl, disappeared.



Elemental analysis was obtained on the complex:

Found (%) C 48.59, H 3.17, N 3.13

Required (%) C 48.94, H 3.45, N 3.46.

Ultraviolet/visible spectroscopic studies showed that when the complex was dissolved in dichloromethane it developed a deep blue colour. The spectrum was recorded between 400nm and 1000nm. The absorption intensity was strongest at 662nm (absorbance 2.63) and at 622nm (absorbance 2.13). On completion of the scan the complex had changed colour emerald green. The intensity of the absorption peaks decreased with time as the complex decomposed (indicated by colour change).

The DSC showed that melting began at 128°C \pm 1°C, and that the complex began decomposing at 240.7 \pm 0.5°C.

2.3.8 Reaction of Pt(PPh₃)₄ with (*para*-Me.C₆H₄CN₂SSN)₂

Para-methyldithiadiazolyl was reacted with Pt(PPh₃)₄ in MeCN (ca. 15ml) and left stirring in a Schlenk (ca. 30mins). A dark green micro crystalline solid appeared in a green coloured solution. As described previously (section 2.3.7). This solution was filtered and washed with MeCN (3x5ml). It was allowed to dry overnight *in vacuo*.

Comparison of the infrared spectrum of the newly synthesised complex with the spectra of (*para*-Me.C₆H₄.CN₂SSN)₂ indicated several changes. The peak at 721cm⁻¹ on the spectrum of the dithiadiazolyl has shifted to 730cm⁻¹, while a new peak at 2366cm⁻¹ appears on the spectrum of the new complex.

Ultraviolet/visible spectroscopic studies carried out on the complex revealed that weak absorption occurs at 698nm (absorbance 0.385). The spectrum was recorded between 200nm and 1000nm. The initial colour of the complex was green-blue, while on completion of the scan the complex had adopted a light green colour and peak intensity had decreased.

The DSC trace showed that melting began at 283.8+/-1 °C.

Elemental analysis:

Found (%) C 56.28, H 4.22, N 4.72,

Required (%) C 57.81, H 4.29, N 4.39.

These Platinum dithiadiazolyl complexes prepared (section 2.3.5 to 2.3.8) are considerably more air stable than uncomplexed dithiadiazolyls.

2.4 Differential Scanning Calorimetry Studies.

DSC analysis was carried out on some *para* substituted phenyl dithiadiazolyl radicals, the DSC trace of (*para*-Br.C₆H₄.CNSSN) is shown below, Figure 2.4.1.

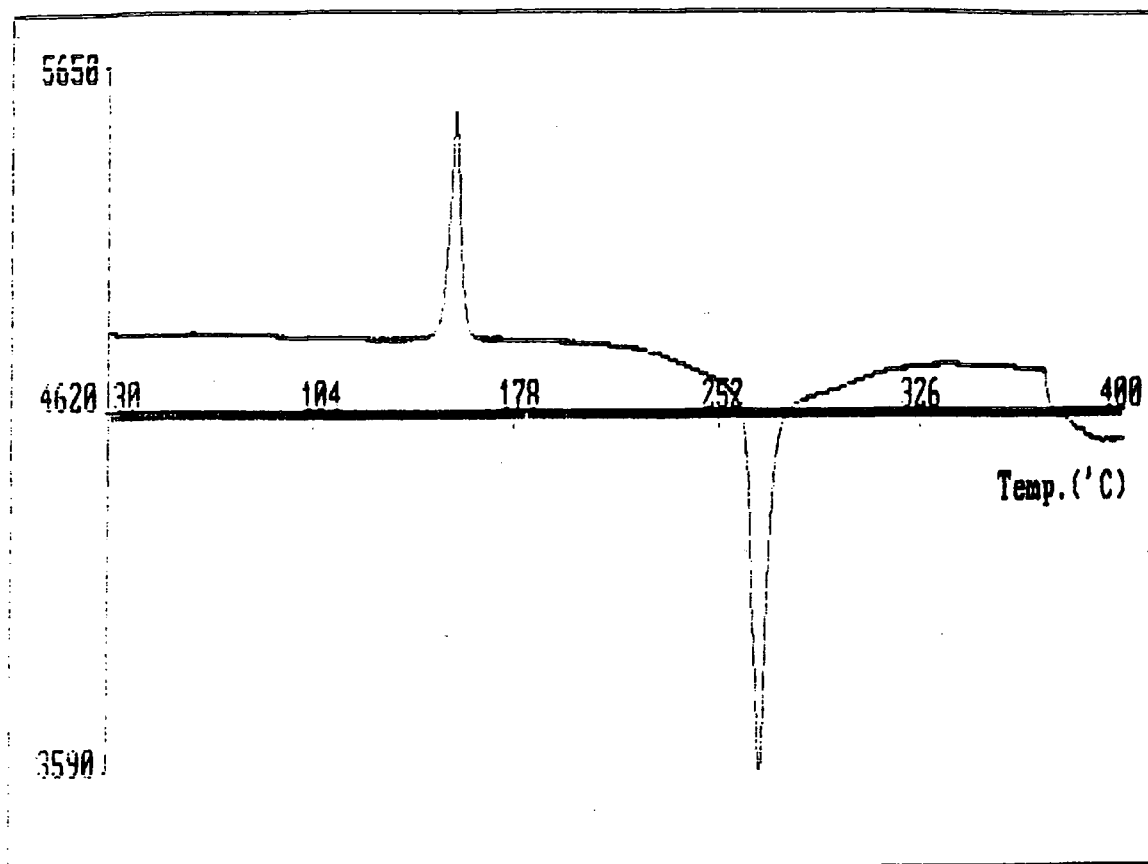


Figure 2.4.2 The DSC trace of (*para*-Br.C₆H₄.CNSSN)₂ recorded from 30°C to 400°C, at a scan rate of 5°C/min, under an argon atmosphere.

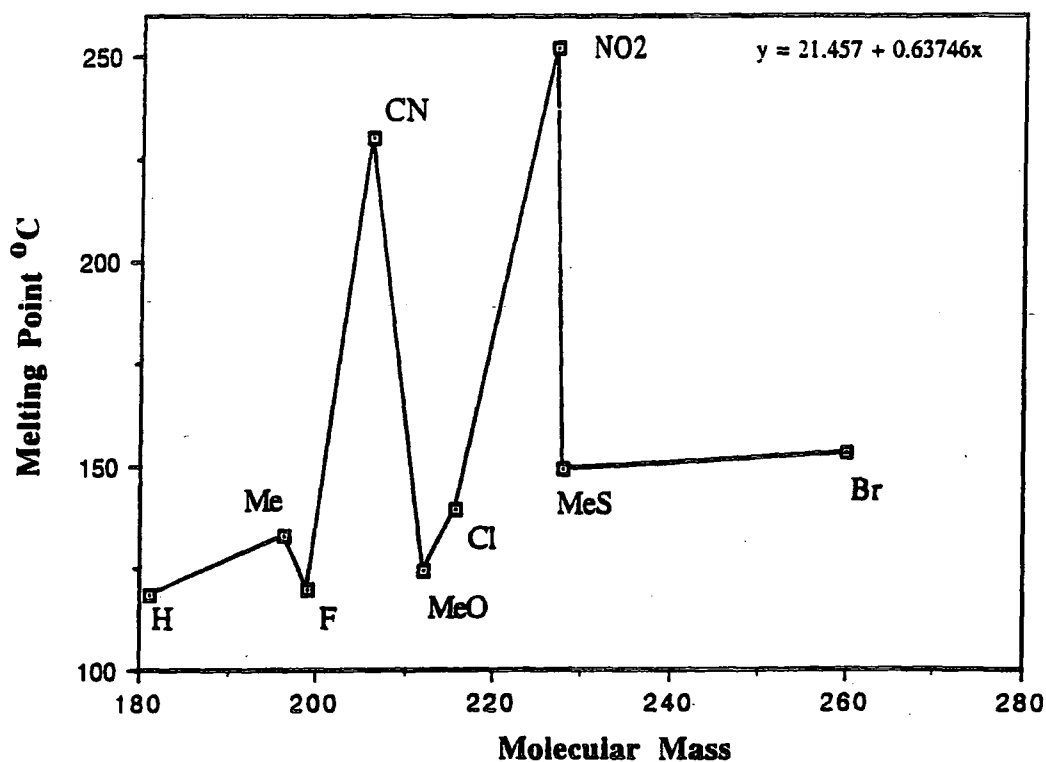
A sharp endotherm (indicative of melting which absorbs energy), is observed at 153.2±0.2°C, while an intense exotherm (indicative of decomposition which releases energy) is observed at 269.2±0.1°C. All other DSC traces have their own characteristic exotherms and endotherms.

Table 2.4.1 is a summary of the melting points recorded for each DSC trace carried out on the *para* substituted phenyl dithiadiazolyls.

Compound	Melting Point (°C)	Molecular Mass	Hammett values (σ_p)
(C ₆ H ₅ CN ₂ SSN) ₂	118.7	181.2	0.000
(FC ₆ H ₄ CN ₂ SSN) ₂	120	199.19	0.062± 0.020
(MeOC ₆ H ₄ CN ₂ SSN) ₂	124.5	212.0	-0.268± 0.020
(MeC ₆ H ₄ CN ₂ SSN) ₂	132.8	196.27	-0.170± 0.020
(ClC ₆ H ₄ CN ₂ SSN) ₂	139.8	215.61	0.227± 0.020
(MeSC ₆ H ₄ CN ₂ SSN) ₂	149.5	228	0.000± 0.100
(BrC ₆ H ₄ CN ₂ SSN) ₂	153.2	260.1	0.232± 0.020
(CNC ₆ H ₄ CN ₂ SSN) ₂	230.1	206.21	0.660± 0.020
(NO ₂ C ₆ H ₄ CN ₂ SSN) ₂	252	227.0	0.778± 0.020

Table 2.4.1 Relationship between molecular mass, melting point and Hammett values.

Molecular Mass v. Melting Point (°C) of some *para* substituted Dithiadiazolyls.

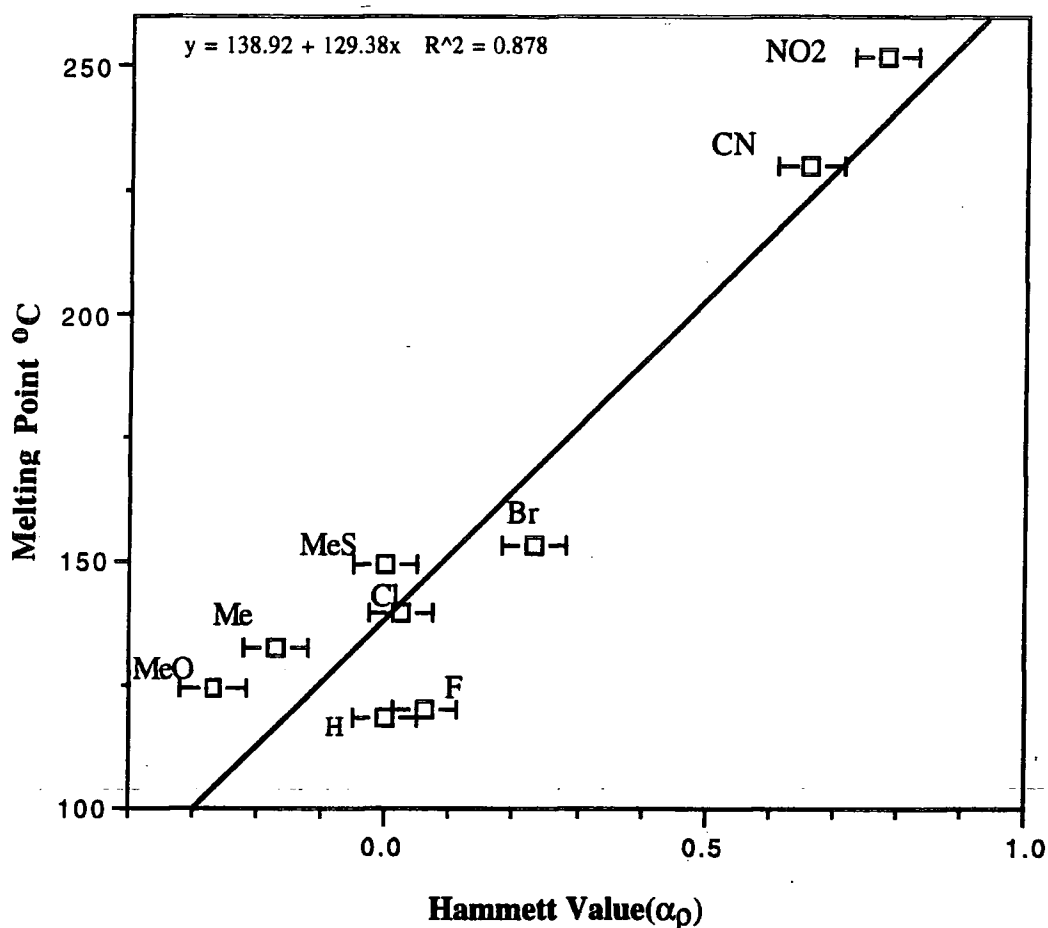


Graph 2.4.1(a) The relationship between melting point °C and molecular mass of some *para* substituted dithiadiazolyls.

This does not follow the expected linear relationship, it suggests however that the melting point is not fully dependent upon the molecular weight of the dithiadiazolyl, and that other factors influence the melting process.

The Hammett value indicates the electron withdrawing/donating ability of the substituents. The value for each dithiadiazolyl was plotted against the respective melting points, graph 2.4.1(b).

Melting Point °C v. Hammett Value ($\alpha\rho$) of some para-substituted Dithiadiazolyls.



Graph 2.4.1(b) The relationship between melting point and Hammett potential.

A good correlation is achieved, which indicates that the melting point of these dithiadiazolyls are more dependent upon the substituent and consequently the molecular packing, rather than on the molecular mass alone. The exceptionally high melting points of the *para*-NO₂ and *para*-CN derivatives shown in graph 2.4.1(a), arise from the fact that these substituents provide stronger inter dimer interactions, arising from the interaction of the highly negatively charged CN and NO₂ groups with the positively charged sulfur atoms within the dithiadiazolyl ring.

2.5 Ultraviolet/vis. Studies on some Metal Dithiadiazolyls Complexes.

The ultraviolet/visible spectroscopic studies which were performed on the complexes reveal some correlation between absorption frequency and the type of ligand present on the dithiadiazolyl. Table 2.5 highlights this information and possible explanations for the relevant absorptions are outlined.

The absorbance of the relevant chromophore, is known to be directly proportional to the concentration.¹⁹ The relevant extinction coefficients for each complex were derived from the Beer-Lambert Law, which can be written as.

$$A = \epsilon.c.l$$

A = absorbance

c = concentration

l = path length

ϵ = extinction coefficient.

All the ultraviolet/visible spectra were recorded under the same conditions. Figure 2.5 shows the typical ultraviolet/visible spectra for a dithiadiazolyl metal complex. The main absorption peaks for all recorded spectra appeared between 670 and 710nm.(the visible region of the spectra).

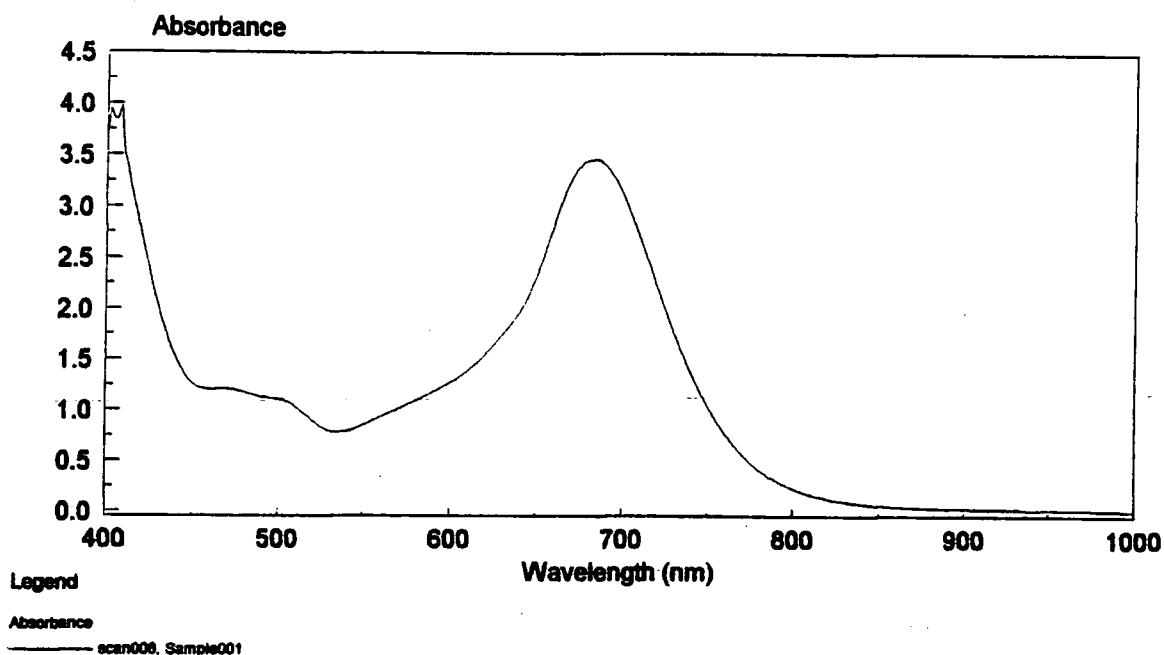


Figure 2.5 The ultraviolet/visible spectrum of [(3,4-F₂.C₆H₃.CNSSN) Pt(PPh₃)₂] recorded at a bandwidth of 2.0nm and a wavelength of 325nm.

Table 2.5 is a summary of the main absorption peaks for each spectrum recorded, and their relevant extinction coefficients, calculated from the Beer-Lambert Law.

Complex	Absorption nm		Concentration $M^{-1} \times 10^{-3}$	Extinction Coefficient
[Pt(PPh ₃) ₂ C ₆ H ₄ CN ₂ SSN]	680	3.606	3.11	1161
[Pt(dppe)C ₆ H ₄ CN ₂ SSN]	658	2.720	3.10	153
[Pt(PPh ₃) ₂ ClC ₆ H ₄ CN ₂ SSN]	684	1.730	5.6	309
[Pt(dppe)ClC ₆ H ₄ CN ₂ SSN]	662	2.650	6.8	390
[Pt(PPh ₃) ₂ BrC ₆ H ₄ CN ₂ SSN]	684	2.300	4.4	523
[Pt(dppe)3,4F ₂ C ₆ H ₃ CN ₂ SSN]	660	3.75	6.78	553
[Pt(PPh ₃) ₂ 3,4F ₂ C ₆ H ₃ CN ₂ SSN]	682	3.505	5.1	687

Table 2.5 Ultraviolet/visible data on the Pt complexes prepared.

The absorbance range of the main peaks in all the complexes studied was between 660-694nm. The predominant colours observed were blue-green and green, which arise from absorption in the red and purple regions of the spectra. The complexes with the dppe ligand absorb around 661nm and 620nm, while complexes containing the unidentate bonding ligand PPh₃ absorb at around 686nm. As the rate of decomposition of the complexes is so fast, indicated by a sharp decrease in peak intensity this would explain why the extinction coefficient values are much lower than expected thus making it difficult to conclude whether the transition can be classified as metal to ligand or ligand to metal.

However metal to the ligand transitions are most commonly observed in complexes which contain aromatic ligands.^{15a} Since all transitions are occurring in the visible region of the spectrum, they can all be designated as symmetry allowed n to π^* transitions. As the spare electron resides predominately on the ligand, then electronic transitions are most likely to arise from the ligand to the metal.¹⁴

2.6 References.

1. F.A. Cotton and G. Wilkinson ; *Advanced Inorganic Chemistry*, Wiley ,3rd edition.
2. S.E. Lawrence, Ph.D. Thesis, University of Durham, 1995.
3. O. Ruff and E. Geisel, *Ber Dtsh Chem Ges*, 1904, **37**, 1573
4. A.J. Banister, I. Lavender, S.E. Lawrence, J.M. Rawson and W. Clegg, *J.Chem.Soc.,Dalton Trans.*, 1994, 29.
5. A.J. Banister, J.M. Rawson,W. Cleggand S.L. Birky, *J.Chem. Soc.,Dalton Trans.*, 1991, 1099.
- 6a. A.J. Banister, I.B. Gorrell, W. Clegg and K.A. Jørgensen, *J.Chem.Soc.Dalton Trans.*, 1991, 1105.
- 6b. R.B. King and P.N. Kapoor, *Inorganic Chemistry.*, 1972, 11(7), 1524.
- 7a. C.A. Tolman, W.C. Steidel and D.H. Gerlach, *J. Am. chem.Soc*, 1971, 2669.
- 7b. L. Malatesta and C. Cariello *ibid.*, 1958, 2323.
8. A.J. Banister and I. May *Phosphorous,Sulfur and Silicon.*, 1994, **93**, 447.
9. A.J. Banister, I.B. Gorrell, S.E. Lawrence, C.W. Lehmann, I.May, G.Tate, A.J. Blake and J.M. Rawson, *J.Chem.Soc.,Chem. Commun.*, 1994, 1779.
10. A.J. Banister, I.B. Gorrell, W. Clegg and K.A. Jørgensen, *J.Chem.Soc.Dalton Trans.*, 1984, 2229.
11. A.J. Banister and J.M. Rawson, *Chemistry of Inorganic Ring Systems*, R. Steudel, ed.R. Steudal, Elsevier, Amsterdam, 1992, 323-348.
12. J.M. Rawson, Ph.D Thesis, University of Durham, 1990.
13. A.J. Banister, M.I. Hansford, Z.V. Hauptman, A.W. Luke, S.T. Wait, W. Clegg and K.A. Jørgensen. *J.Chem.Soc.Dalton Trans.*, 1990, 2793.
14. I. May, personal communication, University of Durham.
- 15a. D.F. Shriver, P.W. Atkins, and C.H. Langford, *Inorganic Chemistry*, Oxford University press, 1990.
- 15b. Dr.J.M. Rawson, personal communication University of Durham.
16. P.D.B. Belluz, A.W. Cordes, E.M. Kristof, P.V. Kristof, S.W. Liblong and R.T. Oakley, *J.Am.Chem.Soc.*, 1992, 3097.
17. R.W.H. Small, A.J. Banister and Z.V. Hauptman, *J.Chem.Soc., Dalton Trans.*, 1984, 1374.
18. I.B. Gorrell, Ph.D. Thesis, University of Durham, 1989.

19. D.C. Harris, *Quantitative Chemical Analysis*, Freeman, New York, 1987.
20. F.R. Hartley, *Chemistry of Platinum Group Metals*, Elsevier, Amsterdam, 1991, p.594 and references therein.
21. T. Hibbert, M.Sc. Thesis, University of Durham, 1994.
22. S.C. Nyburg and C.H. Faerman, *Acta Cryst.* 1985, **B41**, 274.
23. N.N. Greenwood and A. Earnshaw, *Chemistry Of The Elements*, Pergamon Press, 1984.

CHAPTER 3

PREPARATION AND CHARACTERISATION OF SOME FLUORINE SUBSTITUTED DITHIADIAZOLYLS AND THEIR PLATINUM COMPLEXES.

3.1 Introduction.

As outlined in the previous chapters the chemistry of dithiadiazolylium compounds has been widely studied.^{1,2} Many new structures have been determined since 1977, when the first dithiadiazolyl X-Ray structure, $(\text{PhCN}_2\text{S}_2)_2$ was determined.³ The chemistry of the 1,2,3,5 dithiadiazolyl is more widely known, and are most commonly prepared as the chloride salt.

Oakley *et al* found that the conductivity of dithiadiazolylys could be improved by simple p-type doping of the energy bands. Samples of $(\text{HCNSSN})_2$ have been doped with iodine^{5,6} and their conductivity has been investigated. By co-subliming the 1,2,3,5 dithiadiazolyl in the presence of iodine, with a molar ratio of $5(\text{HCNSSN}):1(\text{I})$ he found that an iodine-doped hexagonal phase was formed $(\text{HCNSSN})_6(\text{I})_{1.1}$

However very little is known about the fluorinated dithiadiazolylys. The first 1,2,3,5 fluorinated dithiadiazolylys prepared²³ were $(\text{F.CNSSN})_2$ and $(\text{CF}_3.\text{CNSSN})_2$. The attempted fluorinated reaction of $(\text{C}_6\text{H}_5.\text{CNSSN})_2$ with tetrafluorohydrazine⁸ N_2F_4 , in liquid SO_2 , yielded the trifluorosulfate salt, $[\text{PhCNSSN}][\text{SO}_2\text{F}_3]$.

The thermally stable (4,5-bis(trifluoromethyl)1,3,2 dithiazolyl) $(\text{CF}_3.\text{CSNSCCF}_3)_2$ was prepared and its gas phase structure has been determined, by J.Passmore *et al*.⁹ It was shown to be a diamagnetic solid at room temperature, with the potential to act as a charge transfer conducting salt.¹⁰

Since the successful isolation of $(\text{F.CNSSN})_2$ and $(\text{CF}_3.\text{CNSSN})_2$,²³ several other fluorinated derivatives have been prepared, eq. $(\text{C}_6\text{F}_5.\text{CNSSN})_2$ and $(\text{C}_5\text{NF}_4.\text{CNSSN})_2$. These fluorinated derivatives usually exist as dimeric units in the solid state¹² and are diamagnetic. However the fluorine substituents present result in a decrease in the diamagnetic character, as these substituents are net electron donating, which weakens the S---S interactions.

The preparation of (*para*-NC.C₆F₄.CNSSN)¹³ has marked a new beginning in the preparation of magnetic materials. This dithiadiazolyl is the only one known to-date, to retain its paramagnetic character in the solid state. All other previously reported dithiadiazolylys are diamagnetic in the solid state. ESR studies indicate that the unpaired electron resides predominantly on the sulfur/nitrogen ring, thus enhancing orbital overlap. It has been successfully prepared in two phases, namely the α and the β -phase.¹³

It seems that the presence of the cyano group has helped prevent dimerisation by strongly competing with the out of plane S--S interactions. The closest contact to the disulfur bridge is that from the nitrogen of the cyano group; this interaction gives rise to a co-facial layered structure.¹⁴ The close intermolecular S--S contacts which are characteristic of dithiadiazolylys are no longer present.

3.1.1 Structural Studies of Fluorine Substituted Dithiadiazolyls.

The most common solid state structure adopted by phenyl derivatives of the 1,2,3,5 dithiadiazolyls is the cis configuration.¹⁶ This configuration exposes the sulfur atoms, in such a way that maximum secondary interactions (S---S and S---N) are achieved; this gives rise to a compact crystal unit cell.¹⁷

In the solid state the fluorinated dithiadiazolyl ($C_6F_5.CNSSN$)₂ is associated as dimer pairs which are held together through two S--S interactions, leading to a cis-oid configuration.

The net electron donating capacity of these fluorine substituents into the π e^- framework, results in a significantly stronger bonding interaction between the monomer units. This is manifested through shorter S--S contacts, as shown in Table 3.1.2 and with their lower volatility. The pyridyl derivative ($p-C_5NF_4.CNSSN$)₂²⁴ exists in an array of spin paired radicals (Figure 3.1.1(a)), also adopting a cis-oid arrangement (S-S 2.10 (1) \AA and S--S 3.11(1) \AA) (sum of the van der Waal's radii perpendicular to the bond is 4.06 \AA while parallel to the bond it is 3.2 \AA)³⁶ In comparison alkyl substituted dithiadiazolyls ($CF_3.CNSSN$)₂, ($Me.CNSSN$)₂ and ($Bu^t.CNSSN$)₂ adopt a more twisted eclipsed configuration^{23,19,26} similar to that observed in ($Me_2N.CNSSN$)₂.¹⁹

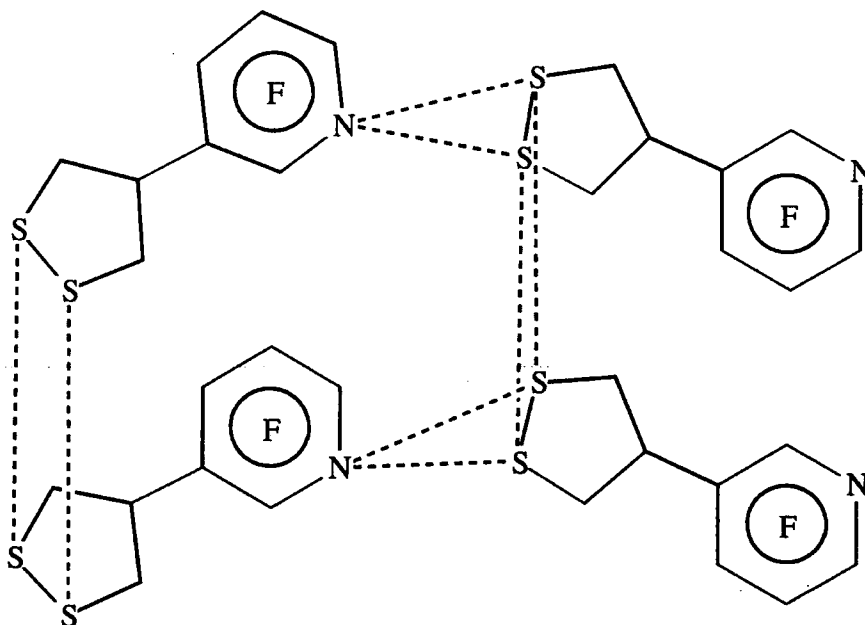


Figure 3.1.1(a) Solid State arrangement of ($p-C_5NF_4.CNSSN$)₂

The *para*-cyano derivative was prepared in two phases, namely the α and β phase.^{13,22} Both show similarities, they exist as monomers in the solid state and pack in a head to tail arrangement in chains.

α phase of (p-NC.C₆F₄.CNSSN)

In the α phase the intermolecular CN--S contacts are longer than in the β phase, and the dithiadiazolyl chains are arranged in opposite directions.(see Figure 3.1.1(a)).

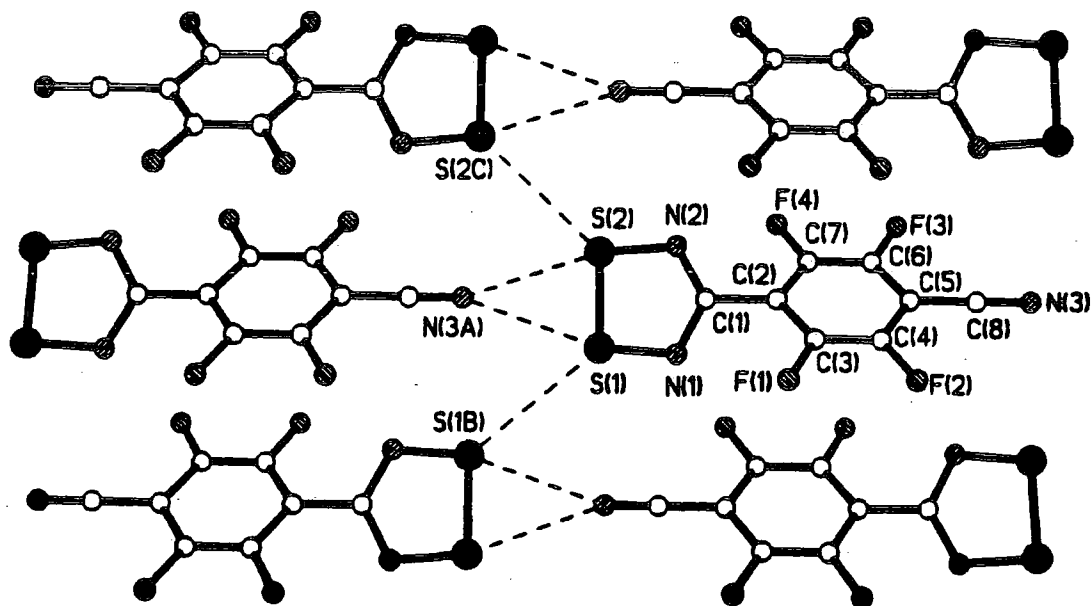


Figure 3.1.1(a) The Solid State monomeric packing arrangement of α -(p-NC.C₆F₄CNSSN).

A layered structure with weak S--S and S--N intermolecular contacts is formed. The monomers are packed in the layers in a cis-oid arrangement, with a significantly longer monomer separation (S---S' 4.6Å).(see Table 3.1.2). The dominant interactions are that of the CN--S-S type, with some S--F intramolecular contacts present.

β -phase of (p-NC.C₆F₄.CNSSN)

A notable difference on comparing the α and β -phases is highlighted in Figure 3.1.1(c). Here the chains are aligned in the same direction, with the CN--S-S interactions clearly visible; however the dithiadiazolyl ring is twisted by about 58° about the C-C bond.(compared with 32.2° in the α phase).

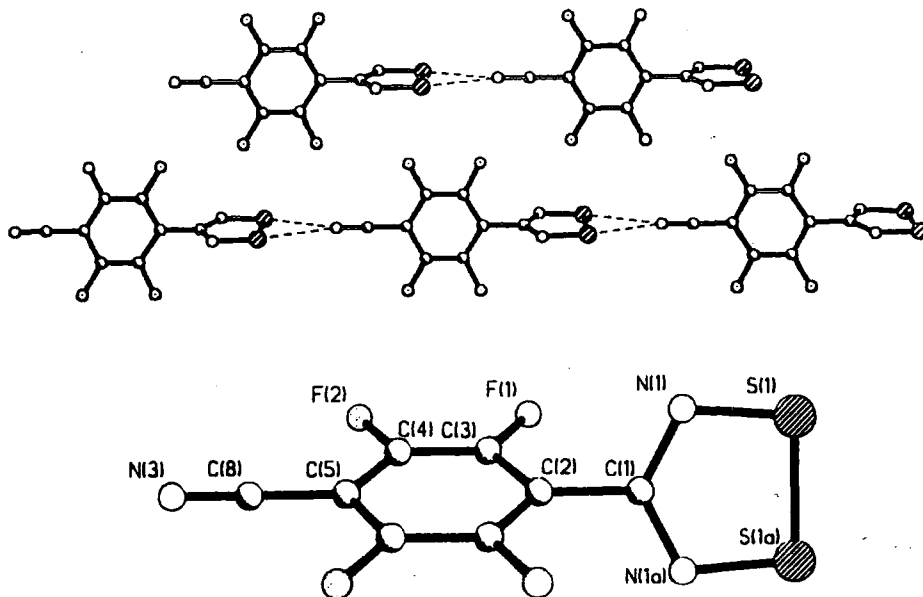


Figure 3.1.1(c) The crystal structure of β -(p-NC.C₆F₄.CNSSN).

Recently the structure of the (*meta*-NC.C₆F₄.CNSSN)₂ has been determined. The dithiadiazolyls adopt an unusual trans configuration, (see Figure 3.1.2(d) with some weak S-F interactions also).

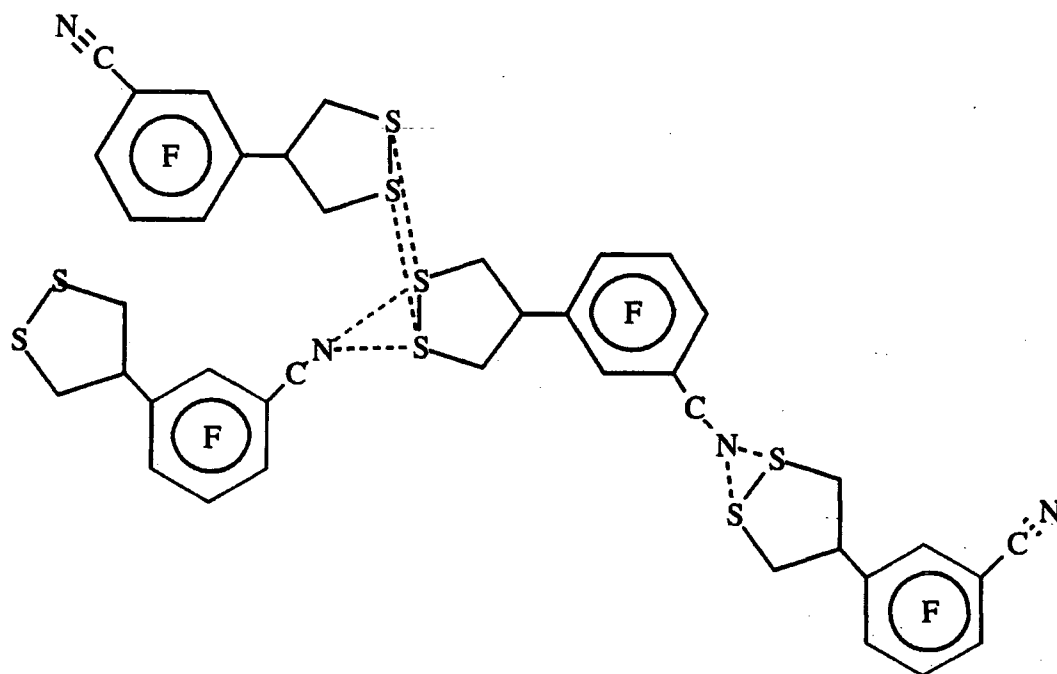


Figure 3.1.1(d) The configuration of (*meta*-CN.C₆F₄.CNSSN)₂

3.1.2 Bonding in Fluorine Substituted Dithiadiazolyls.

As was mentioned earlier the bonding modes present in dithiadiazolyls and their derivatives, very much depend upon the R substituent group present.

The configuration adopted whether cis, trans or twisted will result in changes in the interdimer S---S' intradimer S---S distances and intramolecular S-S and S-N bond lengths. A comparison of these bond lengths is tabulated below, (Table 3.1.2). The effects on the bond lengths of adding fluorine substituents can be seen by comparing the protonated with the fluorinated phenyl dithiadiazolyls and *para*-NCC₆F₄CN₂SSN with *para*-NCC₆H₄CN₂SSN.

In the pyridyl derivative (C₅NF₄.CN₂SSN)₂ the long intradimer S--S contact (3.111(1)Å) can be attributed to the repulsion between the two fluorinated dithiadiazolyl rings, and the cis-oid configuration adopted.

Compound	d _{S---S} Å	d _{S-S} Å	d _{S-N} Å	Reference
C ₆ H ₅ CN ₂ SSN	3.102	2.089(5)	1.63	18,20
C ₆ F ₅ CN ₂ SSN	3.067(1)	2.097(1)	1.640	12,21
CF ₃ CN ₂ SSN	2.998(2)	2.087(2)	1.630(5)	19,20
C ₅ NF ₄ CN ₂ SSN	3.111(1)	2.100(1)	1.640(2)	21
m-CNC ₆ F ₄ CN ₂ SSN	-	3.132		22
p-NCC ₆ F ₄ CN ₂ SSN	-	2.09(14)	1.638(2)	13
p-NCC ₆ H ₄ CN ₂ SSN	3.10(2)	2.081(1)	1.63	26
α.mNCC ₆ H ₄ CN ₂ SSN	3.13(2)	2.080(3)	1.63	26
β.mNCC ₆ H ₄ CN ₂ SSN	3.141(1)	2.087	1.626	22

Table 3.1.2 The intradimer and intramolecular bond distances of some dithiadiazolyls.

In general the protonated derivatives possess a greater intradimer S---S bond length, than present in the fluorinated derivatives. As can be seen from Table 3.1.2, the intramolecular S-S and S-N distances are very similar.

The greatest monomer separation is observed in (p-CN.C₆F₄.CN₂SSN), (4.613Å) see p.53, which is outside the sum of the van der Waal's radii perpendicular to the bond (4.06Å).³⁶ This accounts for the monomeric structure observed.¹³ In the (m-CN.C₆F₄.CN₂SSN) a trans antarafacial arrangement is observed, the intradimer contact is 3.132Å with no close interdimer contacts present.²²

3.1.3 Conclusion.

It can be concluded that most aryl-substituted dithiadiazolyls take up a predominantly cis configuration, although few take up a trans arrangement. In both cases the dimers are held together by a four centre $2e^-$ spin-paired interaction. Twisted configurations have only been observed for alkyl dithiadiazolyls, where a bulky substituent hinders any possibility of a highly ordered packing arrangement.

In this chapter, I have described the synthesis and structure of $(2,3-F_2.C_6H_3CNSSN)_2$ and $(2,5-F_2.C_6H_3.CNSSN)$. Although the 2,3 fluorine substituted dithiadiazolyl has an aryl planar substituent, a twisted configuration is adopted and not the expected cis (or trans) configuration. The synthesis and structure of the trimetallic platinum complex $Pt_3[PPh_3]_4[3,4-F_2.C_6H_3CNSSN]_2$ is also discussed; its structure is similar to that previously reported²⁴ by I.May *et al* for the protonated analogue.

3.2 Experimental.

3.2.1 Preparation of (2,6-F₂.C₆H₃.CNSSN)₂

Li[N(SiMe₃)₂] (3g, 17.92mmol) and 2,6-difluorobenzonitrile (2.0ml, 14.3mmol) was stirred in anhydrous diethyl ether (ca.50cm³), overnight at room temperature. Addition of SCl₂ yielded the characteristic orange coloured chloride suspension. This was then filtered on a filter stick. The bright orange precipitate was dried *in vacuo* and extracted using SO₂(l). On this occasion the chloride salt was reduced in liquid SO₂ using a Zn/Cu couple; a brown black coloured solution was observed.

The radical (0.17g, 0.78mmol) was sublimed *in vacuo* using electrical heating tape, at 30watts of power; the sublimation proved unsuccessful. By simply carrying out the sublimation at a lower voltage and by leaving it running overnight, green coloured regular shaped crystals appeared near the top of the sublimation tube. Sublimation had to be repeated on several occasions in order to obtain a high enough yield for complete analysis.

Appearance: Green black crystals.

Yield: 0.02g, 0.13mmol, 11%.

Infra red: (Nujol mull, KBr plates) ν_{\max} ; 2730w, 2672vw,br; 2046vw,br; 1681s, 1626s, 1596s, 1462vs,br; 1376vs,br; 1308w,sh; 1238w, 1158w,sh; 1009s, 836s, 788s,sh; 721vs, 562s, cm⁻¹.

Elemental analysis: Found (%) C 38.06, H 1.49, N12.58

Required (%) C 38.36, H 1.37, N 12.77.

Mass spectrum: The mass spectrum breakdown pattern is very similar for all the fluorinated dithiadiazolyls.

(E.I.) 217(M⁺), 171(2,6-F₂.C₆H₃CNS⁺), 139(2,6-F₂.C₆H₃CN⁺), 113(2,6-F₂.C₆H₃⁺), 78(S₂N⁺), 64(S₂⁺), 46(SN⁺),

(C.I.) 217(M⁺), 157(2,6-F₂.C₆H₃C(NH₂)₂⁺).

DSC: Broad endotherm (melting) at 104+/-2°C, exotherm (decomposition) at 213.3+/-0.4°C.

3.2.2 Preparation of (3,4-F₂.C₆H₃.CNSSN)₂

Li[N(SiMe₃)₂] (1.8g, 10.78mmol) and 3,4 difluorobenzonitrile (1.58g, 11.36mmol), were stirred in diethyl ether. The addition of SCl₂ produced an orange yellow precipitate which was filtered, extracted and reduced as described before (section 3.2.1) and subsequently sublimed *in vacuo* (0.470g, 3.38mmol) in an oil bath.

Appearance: Purple black micro crystalline material.

Yield: 0.074g, 0.53mmol, 16%.

Infra red: (Nujol Mulls, KBr plates) ν_{max} ; 2728m, 2684vw,br; 2396vw,br; 2034vw,br; 1612m,sh; 1386vs, 1310w,sh; 1282w, 1234vw, 1154vw,sh; 972w,sh; 884m, 778s,sh; 721vs, 672m, 622w, 516m, cm⁻¹.

Elemental analysis: Found (%) C 38.68, H 1.48, N 12.69

Required (%) C 38.36, H 1.37, N 12.77.

Mass spectrum: (E.I.) 217(M⁺), 171(3,4-F₂.C₆H₃CNS⁺), 139(3,4-F₂.C₆H₃CN⁺), 113(3,4-F₂.C₆H₃⁺), 78(S₂N⁺), 64(S₂⁺), 46(SN⁺).

(C.I.) 217(M⁺), 157(3,4-F₂.C₆H₃C(NH₂)₂⁺), 78(S₂N⁺).

DSC: Sharp endotherm at 129.2±0.2 °C, while an exotherm was observed at 360±1 °C.

3.2.3 Preparation of (2,3-F₂.C₆H₃.CNSSN)₂

The chloride salt was previously prepared by C.Aherne, according to the standard synthetic procedure.¹⁴ Reduction in THF with a Zn/Cu couple produced an oily material. The salt (0.218g, 0.89mmol) was reduced in SO₂(l) with Zn/Cu couple in a two limbed vessel. The reaction mixture was allowed to stir overnight; the SO₂ was released slowly and the vessel was placed in the glove box. The vessel was then cracked and the yield of the dark purple dimer was recorded.

The radical was then sublimed *in vacuo* using heating tape; after overnight sublimation fine dark green coloured crystals developed in the sublimation tube. These were analysed and the X-Ray structure was determined.

Appearance: Dark purple.

Yield: 0.03g, 0.14mmol, 14%.

Infra red: (Nujol Mulls, KBr plates) ν_{max} . 2724m, 2676w,br; 2304vw,br; 1600vw,br; 1468vs, 1376vs, 1314m,sh; 1282w, 1158w,sh; 1076vw, 976vw,br; 896vw,sh; 838vw, 794m,sh; 726s, 610w, cm⁻¹.

Elemental analysis: Found(%) C 38.02, H 1.54, N 12.32

Required(%) C 38.36, H 1.37, N 12.77.

Mass spectrum: (E.I.) 217(M⁺), 171(2,3-F₂.C₆H₃CNS⁺), 139(2,3-F₂.C₆H₃CN⁺), 113(2,3-F₂.C₆H₃⁺), 78(S₂N⁺), 64(S₂⁺).

(C.I.) 217(M⁺), 157(2,3-F₂.C₆H₃C(NH₂)₂⁺), 78(S₂N⁺).

3.2.4 Preparation of (C₆F₅.CNSSN)₂

The chloride salt, [C₆F₅.CNSSN]Cl, was provided by Dr.J.M. Rawson. The salt was placed (0.23g, 0.75mmol) in the lower leg of a "dog" along with Zn/Cu couple. SO₂ was then vacuum transferred into the same limb and the mixture was allowed to stir overnight. The following day, the SO₂(l) was removed by slowly opening the Youngs tap on the "dog" while at the same time keeping the bulbs warm.

The dithiadiazolyl was transferred to a sublimation tube in the glove box. This was then sublimed in an oil bath. The sublimation yielded only one single block-shaped (cubical) crystal which appeared at the top of the sublimation tube. Some yellow red coloured material was also visible around the middle of the tube. This was probably sulfur.

With such a small yield obtained, there was insufficient quantity for complete analysis. Solution Electron Spin Resonance studies were carried out on the single crystal, which were complexed with Pt(PPh₃)₄ *in situ.*, the results of which are discussed in section 3.4.

3.2.5 Preparation of (3,5-F₂.C₆H₃.CNSSN)₂

This was prepared as the chloride salt; it was then reduced in SO₂(l) and Zn/Cu couple and left stirring overnight in a "dog". The dithiadiazolyl (2.11g, 15.17mmol) was sublimed using an oil bath. Crystals appeared as purple coloured needles and large clusters. The yield obtained was very low; as a result several sublimations were carried out in order for a high enough yield for complete analysis.

Appearance: Purple clusters.

Yield: 0.016g, 0.115mmol, 0.76%

Infra red: (Nujol Mulls, KBr plates) ν_{\max} ; 2724w, 2676vw,br; 2402vw,br; 2046vw,br; 1854vs, 1692w, 1608m, 1460vs,br; 1382vs, 1314w,sh; 1266vw, 1122w,1028w, 810vw, 726vs, 649vw, 618vw,br; 546vw, cm⁻¹.

Elemental analysis: Found (%) C 38.69, H 1.45, N 12.32

Required (%) C 38.36, H 1.37, N 12.77.

Mass spectrum: (E.I.) 217(M⁺), 171(3,5-F₂.C₆H₃CNS⁺), 139(3,5-F₂.C₆H₃CN⁺), 113(3,5-F₂.C₆H₃⁺), 78(S₂N⁺), 64(S₂⁺), 46(SN).

(C.I.) 217(M⁺), 157(3,5-F₂.C₆H₃C(NH₂)₂⁺).

DSC: Melting point was recorded at 133.7+/-0.5 °C, decomposition at 254.8+/-0.3 °C.

3.2.6 Preparation of (2,5-F₂.C₆H₃.CNSSN)·

The chloride salt was previously prepared by C. Aherne, according to the standard synthetic procedure.¹⁴ Reduction in THF using Zn/Cu couple overnight yielded the relative radical. The THF was removed under vacuum; the released radical was dried *in vacuo* overnight and transferred into a subliming tube (in the glove box). The sublimation process yielded some crystalline material; the yield was recorded in the glove box.

Appearance: Grey black crystalline material

Yield: 9%.

Infra red: (Nujol Mulls, KBr plates) ν_{\max} ; 2856vw,br; 2362vw, 2344vw,sh;

1644vw, 1460m,sh; 1370s, 1242s,sh; 1206s, 1058vs, 1024s,sh; 944s, 881w,sh; 790vs, 650s,sh; cm⁻¹.

Mass spectrum (E.I.) 217(M⁺), 171(2,5-F₂.C₆H₃CNS⁺), 139(2,5-F₂.C₆H₃CN⁺), 113(2,5-F₂.C₆H₃⁺), 78(S₂N⁺), 64(S₂⁺), 46(SN).

(C.I.) 217(M⁺), 157(2,5-F₂.C₆H₃C(NH₂)₂⁺), 78(S₂N⁺).

DSC Melting was recorded at 105.1+/-0.2°C, decomposition occurred at 228°C +/-1°C.

3.2.7 Attempted Preparation of [H₂N-C₆F₄.CNSSN]⁺Cl⁻.

Li[N(SiMe₃)₂] (0.44g, 2.63mmol) and 4-amino-2,3,5,6-tetrafluorobenzonitrile (0.5g, 2.6mmol) was stirred in anhydrous diethyl ether (ca.40cm³) overnight. A creamy white solution with pink coloured streaks was observed. A solution of sulfur dichloride/dichloromethane (in a 1:10 ratio) was then added very slowly, by cannular transfer. Prior to the transfer, the creamy solution was cooled down with an acetone/CO₂(s) bath, (-65°C).

The solution was then allowed to stir for 4 to 5 hrs, slowly changing colour to purple-brown. The precipitate was filtered on a filter stick and dried *in vacuo*. An infra red spectrum was recorded on this material; the results show that the chloride salt may well have been successfully synthesised.

Appearance: Purple non-crystalline material.

Infra red: (Nujol Mull, KBr plates) ν_{\max} , 1636vs,br;1402vs,sh; 1621w, 1196w, 1108vs, 961s,sh; 944vs, 801vw, 708vs, 581m, 431s, cm⁻¹.

3.2.8 Attempted Crystal Growth of $[\text{Pt}(\text{PPh}_3)_2 \cdot (3,4\text{-F}_2\text{C}_6\text{H}_3\text{CNSSN})_2]$.

The $(3,4\text{-F}_2\text{C}_6\text{H}_3\text{CNSSN})_2$ dithiadiazolyl (0.09g, 0.65mmol) was placed in one bulb of a two bulb flask i.e the "dog" with $\text{Pt}(\text{PPh}_3)_4$ (0.2g, 0.016mmol) in the other bulb MeCN (ca. 10cm^3) was added to each bulb under a stream of nitrogen. The fluorine dithiadiazolyl gave a dark brown orange coloured solution, while the $\text{Pt}(\text{PPh}_3)_4$ solution was a bright yellow.

The reaction vessel was then inverted, which allowed both solutions to mix by slow diffusion through a medium porous glass sinter (see p.104). The diffusion of both solutes produced a green coloured micro crystalline precipitate, in a green blue coloured solution (previously orange and yellow). These crystals were left for a few days, the crystals never developed well enough to warrant a crystal structure determination.

After a few days of growing, a dark brown orange coloured micro crystalline suspension had developed, this is believed to be that of the corresponding trimetallic species. The structure is reported in section 3.3

3.3 Solid State Structures.

The solid state structures of the fluorine substituted trimetallic platinum dithiadiazolyl, $\text{Pt}_3[\text{PPh}_3]_4[3,4\text{-F}_2\text{C}_6\text{H}_3\text{.CNSSN}]_2$ (a), the 2,3 fluorine dithiadiazolyl, $(2,3\text{-F}_2\text{C}_6\text{H}_3\text{.CNSSN})_2$ (b) and 2,5-F₂.C₆H₃.CNSSN (c) were determined by the author with the help of Dr.A. Batsanov and Dr.J.M. Rawson at the Department of Chemistry, University of Durham. Table 3.3 highlights the differences in bond lengths and bond angles, between (a) and its non fluorinated platinum analogue $[\text{Pt}_3(\mu\text{-SNSPhNS-S,S})_2(\text{PPh}_3)_4]$ (a)1.

The crystal parameters for (a), crystal data, atomic co-ordinates and selected bond lengths are given in Tables 3.3.1, 3.3.2 and 3.3.3 respectively. Crystal parameters for (b) and (c) crystal data, atomic co-ordinates and selected bond lengths are given in Tables 3.3.4, 3.3.5, 3.3.6, 3.3.7, 3.3.8 and 3.3.9 respectively. The remaining crystallographic data, anisotropic displacement parameters and hydrogen atom co-ordinates for (a), (b) and (c) are highlighted in Appendix II. (Table 3.3(a)i and 3.3(a)ii, Table 3.3(b)i and 3.3(b)ii, Table 3.3(c)i and 3.3(c)ii).

The structure of (a) shown in Figure 3.3(a) can be thought of as a Pt atom being sandwiched between two monometallic $[\text{Pt}(\mu\text{-SNCRNS})(\text{PPh}_3)_2]$ ligands. The structure is analogous to the non fluorinated platinum species, $[\text{Pt}_3(\mu\text{-SNSPhNS-S,S})_2(\text{PPh}_3)_4]$ ²⁸ and its palladium analogue.

On comparing the bond lengths of (a) with its non fluorinated Pt analogue (a)1, the following differences were observed. First of all the Pt---Pt interaction in (a) of 2.9026(4)Å is longer than that observed in (a)1, 2.865(1)Å. (cf. M---M in $[\text{Ni}(\text{C}_5\text{H}_5)_2(\mu\text{-SNCPHNS-S,S})]$ of 2.441Å)

There is no difference between the Pt(1)-S(2) bond distance. The Pt(1)-S(2) bond in (a) is recorded as 2.380(7) Å, while it is 2.387(4)Å in (a)1. There is a significant decrease in the P(1)-Pt(2)-P(2) bond angle; it has decreased from 103.3(2)° (a)1 to 99.06(8)° in (a). These minor differences are perhaps due to the different solvents of crystallisation in each case (i.e. PhMe and CDCl₃ respectively).

The stability of the complex is most likely to arise from the 16e⁻/16e⁻/16e⁻ M₃ system and the 5d_z², 6p_z orbital overlap between the three M atoms which is observed in both the Pd₃ and Pt₃ structures.

The skeletal structure of (a) is composed of a linear Pt chain, which is bridged by two ligands. As is observed in the structure reported by I.May, the terminal Pt atoms have a PtP₂S₂ environment, while the central Pt atom is bound only to the dithiadiazolyl S atoms. This gives rise to a PtS₄ co-ordination geometry.

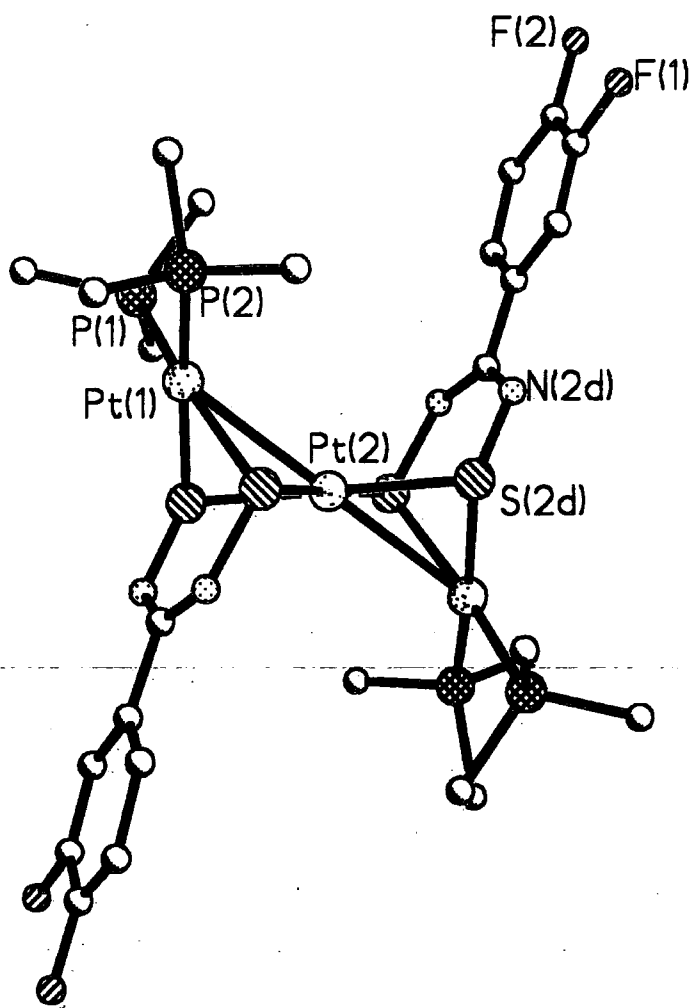


Figure 3.3(a) Crystal structure of $\text{Pt}_3[\text{PPh}_3]_4[3,4\text{-F}_2\text{C}_6\text{H}_3\text{.CNSSN}]_2$ in $\text{P2}_1/\text{c}$

A comparison of bond lengths (Å) and bond angles(°) is highlighted in Table 3.3 below, for [Pt₃(μ-SNSPhNS-S,S)₂(PPh₃)₄] and the 3,4-difluorine substituted analogue Pt₃[PPh₃]₄[3,4-F₂.C₆H₃.CNSSN]₂.

Bond Length (Å)	Trimetallic Pt Complex	3,4-F ₂ Trimetallic Pt Complex
M(1)-S(1)	2.367(4)	2.383(2)
M(1)-S(2)	2.387(4)	2.380(7)
M(1)-P(1)	2.300(5)	2.297(2)
M(1)-P(2)	2.301(4)	2.305(2)
M(2)-S(1)	2.332(5)	2.344(2)
M(2)-S(2)	2.344(4)	2.340(2)
S(1)-N(1)	1.66(1)	1.669(7)
S(2)-N(2)	1.64(1)	1.667(7)
Pt(1)-Pt(2)	2.865(1)	2.9026(4)
S(1)..S(2)	3.019(6)	3.038(6)
C(1)-N(1)	1.31(2)	1.315(12)
C(1)-N(2)	1.34(2)	1.325(12)
Bond Angle(°)		
S(1)-M(1)-S(2)	78.8(2)	79.29(8)
S(1)-M(2)-S(2)	80.4(2)	80.90(2)
P(1)-P(1)-Pt(2)	103.3(2)	99.06(8)
P(1)-M(1)-S(2)	87.8(2)	91.37(8)
M(1)-S(1)-N(1)	113.2(5)	113.3(3)
M(1)-S(2)-N(2)	111.1(5)	107.4(3)
M(2)-S(1)-N(1)	109.3(5)	107.4(3)
M(2)-S(2)-N(2)	107.4(6)	107.4(3)
S(1)-N(1)-C(1)	122.5(13)	123.9(6)
S(2)-N(2)-C(1)	126.1(13)	123.9(7)
M(1)-M(2)M(1)	180.0	180.0

Table 3.3 Selected bond lengths and angles for the two trimetallic platinum complexes.

Table 3.3.1 Crystal data and structure refinement for (a).

Identification code	owenabs
Empirical formula	C90 H70 Cl12 F4 N4 P4 Pt3 S4
Formula weight	2546.29
Temperature	150(2) K
Wavelength	0.71073 Å
Crystal system	Monoclinic
Space group	P21/c
Unit cell dimensions	a = 13.5111(13) Å alpha = 90 deg. b = 20.902(2) Å beta = 111.330(5) deg. c = 17.588(2) Å gamma = 90 deg.
Volume	4626.9(8) Å ³
Z	2
Density (calculated)	1.828 Mg/m ³
Absorption coefficient	5.086 mm ⁻¹
F(000)	2472
Crystal size	0.2 x 0.2 x 0.2 mm
Theta range for data collection	1.62 to 25.98 deg.
Index ranges	-16 ≤ h ≤ 16, -19 ≤ k ≤ 25, -21 ≤ l ≤ 15
Reflections collected	19745
Independent reflections	8048 [R(int) = 0.0735]
Refinement method	Full-matrix least-squares on F ²
Data / restraints / parameters	8048 / 0 / 548
Goodness-of-fit on F ²	1.186
Final R indices [I > 2σ(I)]	R1 = 0.0531, wR2 = 0.1223
R indices (all data)	R1 = 0.0595, wR2 = 0.1265
Extinction coefficient	0.00076(6)
Largest diff. peak and hole	1.807 and -2.177 e.Å ⁻³

Table 3.3.2 Atomic co-ordinates ($\times 10^4$) and equivalent isotropic displacements parameters ($\text{\AA}^2 \times 10^3$) for (a). $U(\text{eq})$ is defined as one third of the trace of the orthogonalized U_{ij} tensor.

	x	y	z	$U(\text{eq})$
Pt(1)	4270(1)	1057(1)	8862(1)	26(1)
Pt(2)	5000	0	10000	26(1)
S(1D)	5084(2)	-1083(1)	9685(1)	27(1)
S(2D)	6745(2)	-218(1)	10866(1)	27(1)
P(2)	5311(2)	1921(1)	8823(1)	27(1)
P(1)	3714(2)	758(1)	7515(1)	28(1)
N(2D)	7401(6)	-479(4)	10286(4)	29(2)
C(126)	1986(8)	-98(5)	7054(6)	37(2)
N(1D)	6048(6)	-1127(3)	9305(5)	28(2)
C(111)	2703(7)	1278(4)	6826(5)	28(2)
C(112)	2238(8)	1731(5)	7175(7)	38(2)
C(113)	1443(8)	2133(5)	6687(7)	45(3)
C(114)	1114(8)	2102(5)	5853(7)	48(3)
C(115)	1546(8)	1646(6)	5497(7)	45(3)
C(116)	2328(8)	1224(5)	5979(6)	36(2)
C(121)	3090(7)	-34(4)	7330(5)	29(2)
C(122)	3708(8)	-575(4)	7553(6)	34(2)
C(123)	3246(9)	-1181(5)	7482(6)	43(3)
C(124)	2165(9)	-1236(5)	7195(7)	45(3)
C(125)	1521(9)	-695(5)	6988(7)	46(3)
C(131)	4842(8)	659(4)	7194(5)	31(2)
C(132)	4837(7)	804(4)	6415(5)	29(2)
C(133)	5723(8)	688(5)	6226(6)	39(2)
C(134)	6643(9)	430(5)	6805(6)	40(2)
C(135)	6650(8)	294(5)	7573(6)	35(2)
C(136)	5758(7)	403(5)	7768(6)	34(2)
C(210)	6560(8)	1967(5)	7853(6)	35(2)
C(211)	6726(8)	2091(5)	7128(6)	38(2)
C(212)	5903(9)	2342(5)	6452(6)	43(3)
C(213)	4939(9)	2461(4)	6511(6)	37(2)
C(214)	4753(8)	2331(4)	7222(5)	31(2)
C(211)	5574(8)	2085(4)	7903(5)	31(2)
C(221)	6630(7)	1905(4)	9624(5)	29(2)
C(222)	7208(8)	2451(5)	9945(6)	38(2)
C(223)	8200(9)	2404(5)	10583(7)	48(3)
C(224)	8602(8)	1820(5)	10894(7)	43(2)
C(225)	8049(8)	1266(5)	10562(7)	45(3)
C(226)	7056(8)	1300(5)	9936(6)	37(2)
C(231)	4722(7)	2672(4)	8978(5)	28(2)
C(232)	3939(8)	2670(5)	9315(6)	32(2)
C(233)	3501(9)	3243(5)	9442(6)	43(3)
C(234)	3834(9)	3825(5)	9225(6)	39(2)
C(235)	4593(8)	3836(4)	8869(6)	36(2)
C(236)	5042(8)	3263(4)	8754(6)	33(2)
C(1D)	6964(8)	-830(4)	9620(6)	31(2)
C(2D)	7646(8)	-899(5)	9104(6)	34(2)
C(3D)	8568(8)	-542(5)	9284(6)	38(2)
C(4D)	9126(8)	-583(5)	8771(7)	44(3)
C(5D)	8777(9)	-959(5)	8077(6)	42(3)
C(6D)	7878(10)	-1314(6)	7888(7)	49(3)

C(7D)	7299(9)	-1294(5)	8409(6)	38(2)
F(2)	9364(5)	-976(4)	7587(4)	58(2)
F(1)	10009(6)	-244(4)	8908(5)	70(2)
C1(1S)	9858(3)	1103(2)	7666(2)	78(1)
C1(2S)	9448(3)	1367(2)	9136(2)	77(1)
C1(3S)	11131(4)	2034(2)	8823(3)	85(1)
C(1S)	10419(9)	1310(6)	8695(7)	51(3)
C1(4S)	7215(2)	4391(2)	9772(2)	61(1)
C1(5S)	8672(2)	5258(2)	10913(2)	57(1)
C1(6S)	9484(3)	4143(2)	10375(2)	70(1)
C(2S)	8490(9)	4721(6)	10092(7)	46(3)

Table 3.3.3 Selected bond lengths [Å] and angles for (a).

Pt(1)-P(1)	2.297(2)
Pt(1)-P(2)	2.305(2)
Pt(1)-S(2D)#1	2.380(2)
Pt(1)-S(1D)#1	2.383(2)
Pt(1)-Pt(2)	2.9026(4)
Pt(2)-S(2D)	2.340(2)
Pt(2)-S(2D)#1	2.340(2)
Pt(2)-S(1D)	2.344(2)
Pt(2)-S(1D)#1	2.344(2)
Pt(2)-Pt(1)#1	2.9026(4)
S(1D)-N(1D)	1.669(7)
S(1D)-Pt(1)#1	2.383(2)
S(2D)-N(2D)	1.667(7)
S(2D)-Pt(1)#1	2.380(2)
N(2D)-C(1D)	1.325(12)
N(1D)-C(1D)	1.315(12)
C(1D)-C(2D)	1.517(13)
C(2D)-C(3D)	1.386(14)
C(2D)-C(7D)	1.406(13)
C(3D)-C(4D)	1.373(14)
C(4D)-F(1)	1.332(13)
C(4D)-C(5D)	1.38(2)
C(5D)-C(6D)	1.36(2)
C(5D)-F(2)	1.368(11)
C(6D)-C(7D)	1.407(14)
P(1)-Pt(1)-P(2)	99.06(8)
P(1)-Pt(1)-S(2D)#1	90.61(8)
P(2)-Pt(1)-S(2D)#1	170.29(8)
P(1)-Pt(1)-S(1D)#1	165.45(8)
P(2)-Pt(1)-S(1D)#1	91.37(8)
S(2D)#1-Pt(1)-S(1D)#1	79.29(8)
P(1)-Pt(1)-Pt(2)	113.95(6)
P(2)-Pt(1)-Pt(2)	123.96(6)
S(2D)#1-Pt(1)-Pt(2)	51.43(5)
S(1D)#1-Pt(1)-Pt(2)	51.51(5)
S(2D)-Pt(2)-S(2D)#1	180.0
S(2D)-Pt(2)-S(1D)	80.90(8)
S(2D)#1-Pt(2)-S(1D)	99.10(8)
S(2D)-Pt(2)-S(1D)#1	99.10(8)
S(2D)#1-Pt(2)-S(1D)#1	80.90(8)
S(1D)-Pt(2)-S(1D)#1	180.0
S(2D)-Pt(2)-Pt(1)	127.33(5)
S(2D)#1-Pt(2)-Pt(1)	52.67(5)
S(1D)-Pt(2)-Pt(1)	127.28(5)
S(1D)#1-Pt(2)-Pt(1)	52.72(5)
S(2D)-Pt(2)-Pt(1)#1	52.67(5)
S(2D)#1-Pt(2)-Pt(1)#1	127.33(5)
S(1D)-Pt(2)-Pt(1)#1	52.72(5)
S(1D)#1-Pt(2)-Pt(1)#1	127.28(5)
Pt(1)-Pt(2)-Pt(1)#1	180.0
N(1D)-S(1D)-Pt(2)	105.0(3)
N(1D)-S(1D)-Pt(1)#1	113.3(3)
Pt(2)-S(1D)-Pt(1)#1	75.77(6)
N(2D)-S(2D)-Pt(2)	107.4(3)
N(2D)-S(2D)-Pt(1)#1	110.9(3)

Pt(2)-S(2D)-Pt(1)#1	75.90(7)
C(1D)-N(2D)-S(2D)	123.9(7)
C(1D)-N(1D)-S(1D)	123.9(6)
N(1D)-C(1D)-N(2D)	133.1(9)
N(1D)-C(1D)-C(2D)	112.7(8)
N(2D)-C(1D)-C(2D)	114.2(8)
C(3D)-C(2D)-C(7D)	120.2(9)
C(3D)-C(2D)-C(1D)	120.2(9)
C(7D)-C(2D)-C(1D)	119.5(9)
C(4D)-C(3D)-C(2D)	118.6(10)
F(1)-C(4D)-C(3D)	121.1(11)
F(1)-C(4D)-C(5D)	117.3(10)
C(3D)-C(4D)-C(5D)	121.6(10)
C(6D)-C(5D)-F(2)	120.2(10)
C(6D)-C(5D)-C(4D)	121.0(9)
F(2)-C(5D)-C(4D)	118.8(10)
C(5D)-C(6D)-C(7D)	119.0(11)
C(2D)-C(7D)-C(6D)	119.7(11)

Symmetry transformations used to generate equivalent atoms:
#1 -x+1, -y, -z+2

Crystals of $(2,3\text{-F}_2\text{.C}_6\text{H}_3\text{.CNSSN})_2$ were recently grown by the author; the structure is discussed below.

Figure 3.3(b)i overleaf shows the asymmetric unit cell of $(2,3\text{-F}_2\text{.C}_6\text{H}_3\text{.CNSSN})_2$; containing one molecule. Figure 3.3(b)ii highlights the twisted configuration which the dimers adopt, with only one close intradimer S--S interaction present, (cf. $(\text{CF}_3\text{.CNSSN})_2$ and $(\text{Bu}^t\text{.CNSSN})_2$).^{1,28}

Figure 3.3(b)iii (p.73) shows the solid state packing arrangement. A zig-zag conformation is adopted, with channels clearly visible between the dimeric units. The S--F and S---N interdimer contacts are well established along with (possibly) intermolecular F--F contacts.

As was mentioned earlier the phenyl derivatives which contain planar substituents usually adopt a cis configuration; ^{2,27} while a twisted configuration is usually observed in dithiadiazolyls which contain bulky, non planar substituents. {cf. $(\text{Me}_2\text{N.CNSSN})_2$, $(\text{Bu}^t\text{.CNSSN})_2$ }. The R group accounts for the unusual solid state structure (Figure 3.3(b)ii); the close S---S' interdimer contact present gives rise to overlap between the P_z orbitals on the sulfur atoms.

Earlier e.s.r. studies have shown that the use of fluorine substituents leads to an increase in spin density at the heterocyclic sulfur which leads to stronger bonding between the monomeric units. The intradimer S--S distances in $(\text{C}_6\text{H}_5\text{.CNSSN})_2$ and $(2,3\text{-F}_2\text{.C}_6\text{H}_3\text{.CNSSN})_2$ are recorded as 3.102 and 3.020(3)Å (which is inside the sum of the van der Waal's radii of 4.06Å perpendicular to the bond).³⁶ The increased spin density at the sulfurs is accommodated by stronger out-of plane interactions between the sulfur atoms.

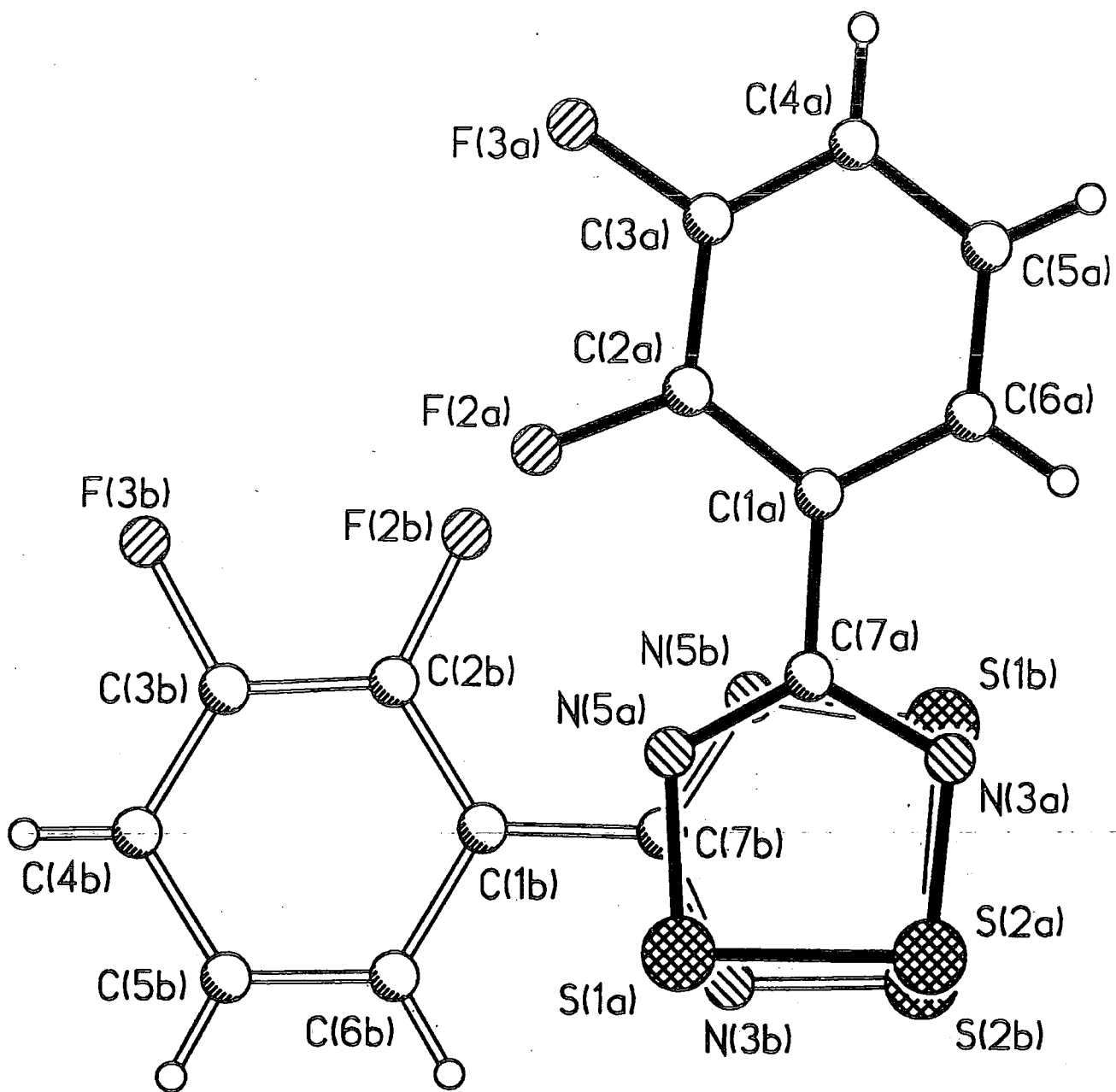


Figure 3.3(b)i The unit asymmetric cell of (2,3-F₂.C₆H₃.CNSSN)₂

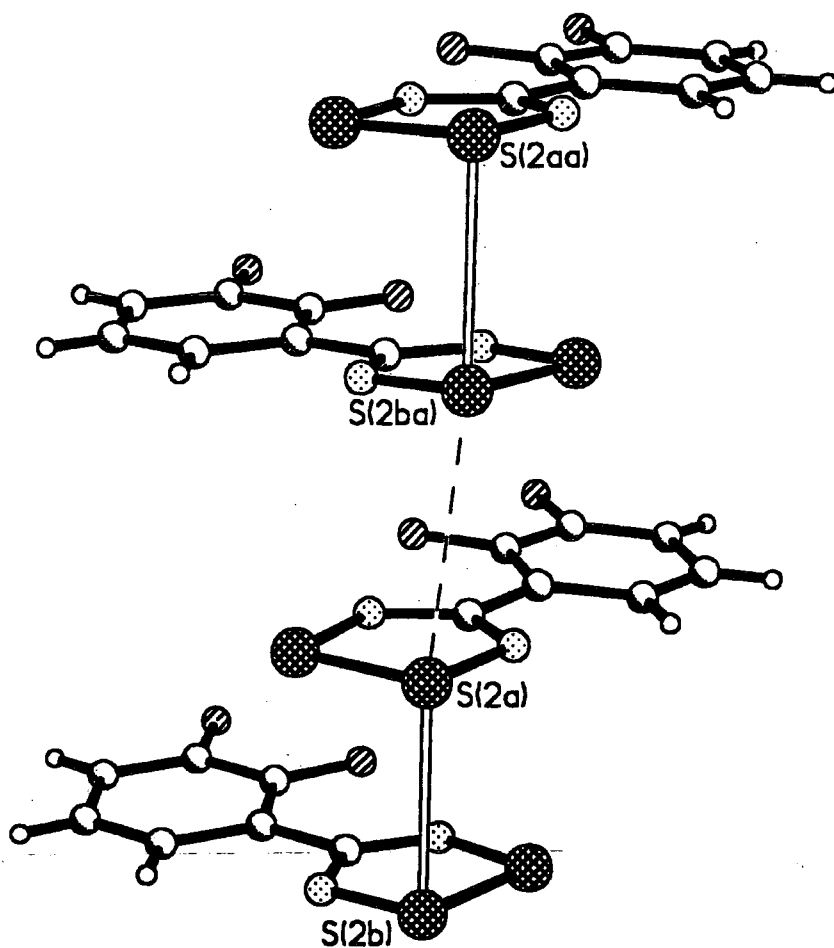


Figure 3.3(b)ii The overlap of the sulfur P_z orbitals in $(2,3-F_2.C_6H_3.CNSSN)_2$

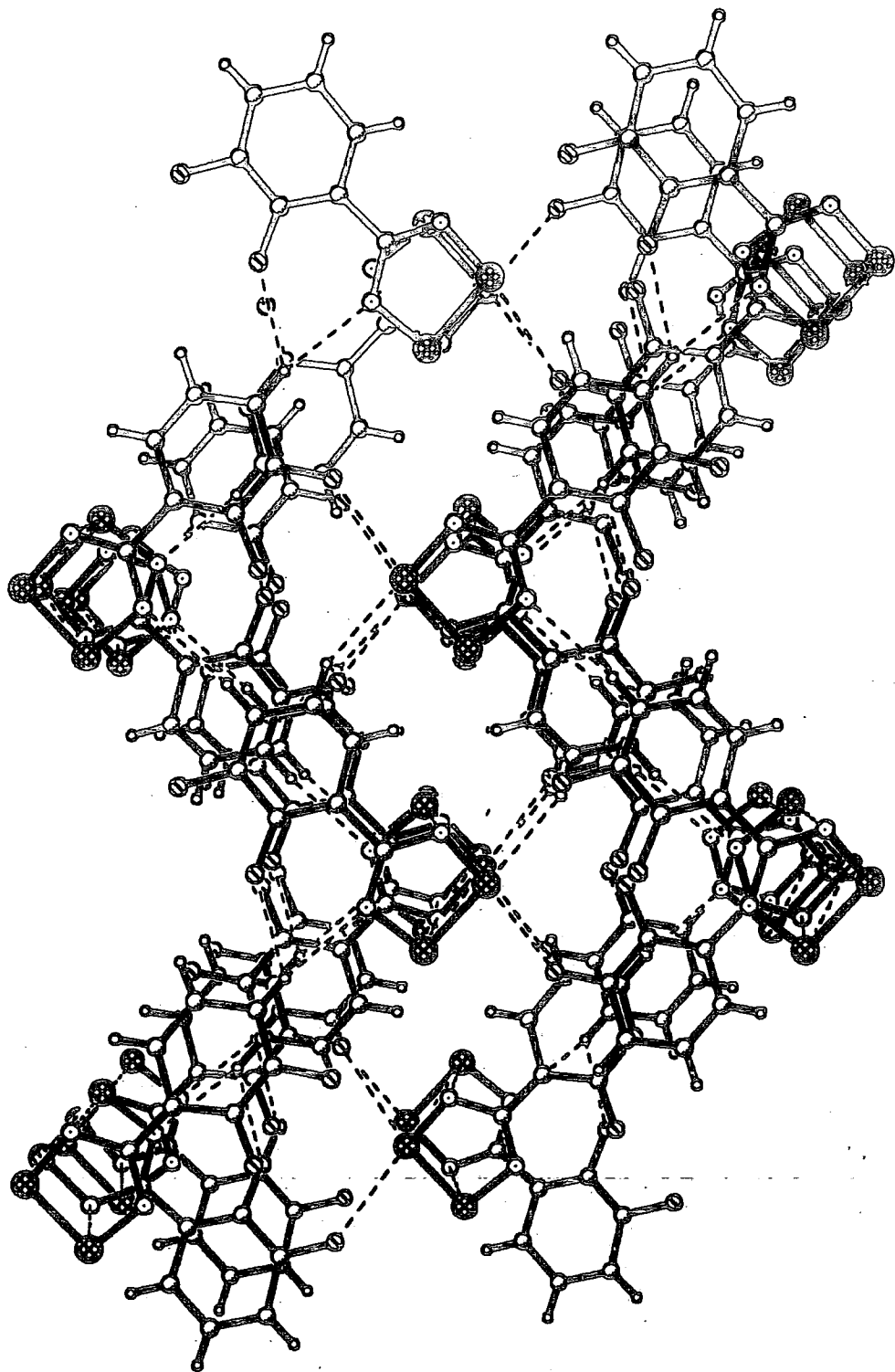


Figure 3.3(b)iii The solid state packing of (2,3-F₂.C₆H₃.CNSSN)₂

Table 3.3.4 Crystal data and structure refinement for (b).

Identification code	95sr7090
Empirical formula	C7 H3 F2 N2 S2
Formula weight	217.23
Temperature	150(2) K
Wavelength	1.54184 Å
Crystal system	Triclinic
Space group	P-1
Unit cell dimensions	a = 6.637(6) Å alpha = 88.79(6) b = 8.768(11) Å beta = 86.37(5) c = 13.546(5) Å gamma = 80.40(5)
Volume	775.6(12) Å ³
Z	4
Density (calculated)	1.860 g/cm ³
Absorption coefficient	6.144 mm ⁻¹
F(000)	436
Crystal size	0.40 x 0.10 x 0.10 mm
Theta range for data collection	3.27 to 75.00 deg.
Index ranges	-8<=h<=8, -10<=k<=0, -16<=l<=16
Reflections collected	2365
Independent reflections	2365 [R(int) = ?]
Absorption correction	None
Refinement method	Full-matrix least-squares on F ²
Data / restraints / parameters	2365 / 0 / 236
Goodness-of-fit on F ²	1.114
Final R indices [I>2sigma(I)]	R1 = 0.0698, wR2 = 0.1683
R indices (all data)	R1 = 0.0886, wR2 = 0.1970
Extinction coefficient	0.0016(6)
Largest diff. peak and hole	.745 and -.837 e.Å ⁻³

Table 3.3.5 Atomic co-ordinates ($\times 10^4$) and equivalent isotropic displacements parameters ($\text{\AA}^2 \times 10^3$) for (b). $U(\text{eq})$ is defined as one third of the trace of the orthogonalized U_{ij} tensor.

	x	y	z	$U(\text{eq})$
S(1A)	5904(3)	4454(2)	1286(1)	30(1)
S(2A)	5584(3)	6114(2)	2411(2)	31(1)
N(3A)	6051(10)	4869(7)	3299(5)	28(2)
N(5A)	6428(11)	2998(7)	2055(4)	26(2)
C(1A)	6817(12)	2170(8)	3772(5)	20(2)
C(2A)	7389(12)	601(8)	3576(5)	24(2)
C(3A)	7720(12)	-449(8)	4348(5)	26(2)
C(4A)	7511(13)	-20(9)	5320(5)	29(2)
C(5A)	6958(14)	1539(9)	5520(6)	33(2)
C(6A)	6614(13)	2606(9)	4775(6)	28(2)
C(7A)	6420(12)	3373(8)	2993(5)	23(2)
F(2A)	7648(9)	48(5)	2655(3)	42(1)
F(3A)	8246(8)	-1969(5)	4110(3)	41(1)
S(1B)	1446(3)	4409(2)	3688(1)	31(1)
S(2B)	1034(3)	6070(2)	2551(1)	30(1)
N(3B)	1219(10)	4827(8)	1675(5)	30(2)
N(5B)	1721(11)	2953(8)	2930(4)	30(2)
C(1B)	1835(12)	2146(8)	1203(5)	24(2)
C(2B)	2409(12)	560(8)	1388(5)	22(2)
C(3B)	2698(11)	-468(8)	605(5)	22(2)
C(4B)	2481(12)	-22(9)	-361(5)	24(2)
C(5B)	1892(12)	1552(8)	-542(5)	26(2)
C(6B)	1622(12)	2612(9)	209(5)	26(2)
C(7B)	1584(12)	3333(9)	1984(5)	27(2)
F(2B)	2658(8)	-1(5)	2306(3)	37(1)
F(3B)	3206(8)	-2000(5)	839(3)	36(1)

Table 3.3.6 Bond lengths [A] and angles for (b)

S(1A)-N(5A)	1.636(6)	S(1A)-S(2A)	2.105(3)
S(2A)-N(3A)	1.617(6)	N(3A)-C(7A)	1.362(10)
N(5A)-C(7A)	1.319(9)	C(1A)-C(2A)	1.392(10)
C(1A)-C(6A)	1.412(10)	C(1A)-C(7A)	1.479(9)
C(2A)-F(2A)	1.337(8)	C(2A)-C(3A)	1.383(9)
C(3A)-F(3A)	1.361(9)	C(3A)-C(4A)	1.369(10)
C(4A)-C(5A)	1.383(11)	C(5A)-C(6A)	1.366(10)
S(1B)-N(5B)	1.634(7)	S(1B)-S(2B)	2.095(3)
S(2B)-N(3B)	1.613(7)	N(3B)-C(7B)	1.353(10)
N(5B)-C(7B)	1.323(9)	C(1B)-C(2B)	1.401(10)
C(1B)-C(6B)	1.407(10)	C(1B)-C(7B)	1.482(11)
C(2B)-F(2B)	1.338(7)	C(2B)-C(3B)	1.390(10)
C(3B)-F(3B)	1.365(8)	C(3B)-C(4B)	1.367(10)
C(4B)-C(5B)	1.392(10)	C(5B)-C(6B)	1.375(11)
N(5A)-S(1A)-S(2A)	93.4(2)	N(3A)-S(2A)-S(1A)	95.2(3)
C(7A)-N(3A)-S(2A)	113.6(5)	C(7A)-N(5A)-S(1A)	115.3(5)
C(2A)-C(1A)-C(6A)	116.9(6)	C(2A)-C(1A)-C(7A)	123.6(6)
C(6A)-C(1A)-C(7A)	119.4(6)	F(2A)-C(2A)-C(3A)	117.6(6)
F(2A)-C(2A)-C(1A)	122.5(6)	C(3A)-C(2A)-C(1A)	119.9(6)
F(3A)-C(3A)-C(4A)	119.9(6)	F(3A)-C(3A)-C(2A)	117.2(6)
C(4A)-C(3A)-C(2A)	122.9(7)	C(3A)-C(4A)-C(5A)	117.5(7)
C(6A)-C(5A)-C(4A)	121.1(8)	C(5A)-C(6A)-C(1A)	121.6(7)
N(5A)-C(7A)-N(3A)	122.4(6)	N(5A)-C(7A)-C(1A)	121.0(7)
N(3A)-C(7A)-C(1A)	116.5(6)	N(5B)-S(1B)-S(2B)	93.6(2)
N(3B)-S(2B)-S(1B)	95.0(2)	C(7B)-N(3B)-S(2B)	114.3(5)
C(7B)-N(5B)-S(1B)	115.2(6)	C(2B)-C(1B)-C(6B)	116.9(7)
C(2B)-C(1B)-C(7B)	123.4(6)	C(6B)-C(1B)-C(7B)	119.5(7)
F(2B)-C(2B)-C(3B)	118.7(6)	F(2B)-C(2B)-C(1B)	121.6(7)
C(3B)-C(2B)-C(1B)	119.7(6)	F(3B)-C(3B)-C(4B)	119.7(7)
F(3B)-C(3B)-C(2B)	116.6(6)	C(4B)-C(3B)-C(2B)	123.6(7)
C(3B)-C(4B)-C(5B)	116.6(7)	C(6B)-C(5B)-C(4B)	121.6(7)
C(5B)-C(6B)-C(1B)	121.5(7)	N(5B)-C(7B)-N(3B)	121.8(7)
N(5B)-C(7B)-C(1B)	121.8(7)	N(3B)-C(7B)-C(1B)	116.4(6)

Crystals of the (2,5-F₂.C₆H₃.CNSSN)· fluorine substituted dithiadiazolyl have recently been grown in a sublimation tube by the author, and its X-Ray structure has been resolved which is described below .

As expected from planar substituents a cis configuration^{2,27} is adopted. Figure 3.3(c)i shows the asymmetric unit cell of the molecule. The fluorine atoms have a 66% occupancy in the 2,5 position, while the remaining 33% is in the 3,6 position. Figure 3.3(c)ii highlights the packing arrangement of the dithiadiazolyl along the Z-axis, the disorder present is visible in this diagram.

Figure 3.3(c)iii shows the intermolecular S--S and S--N contacts developed as the rings interact with each other. It appears from Figure 3.3(c)iii that one dithiadiazolyl ring interacts between two neighbouring rings.

Finally; Figure 3.3(c)iv shows the solid state packing arrangement, with S--F contacts visible a complex network of H-bonding is also present but it has been left out in order to highlight the S--S and S--N contacts. This packing is unique as there is only one S--S distance between each molecule (3.544Å) (throughout the packing arrangement) and this is above the S-S single bond distance (~2.0Å) but slightly shorter than the sum of the van der Waal's radii (4.06Å) perpendicular to the bond.³⁶ This polymeric packing has produced interest into investigating its conductivity and magnetic properties. Only further research will indicate whether this most recent fluorinated dithiadiazolyl will produce interesting magnetic materials.

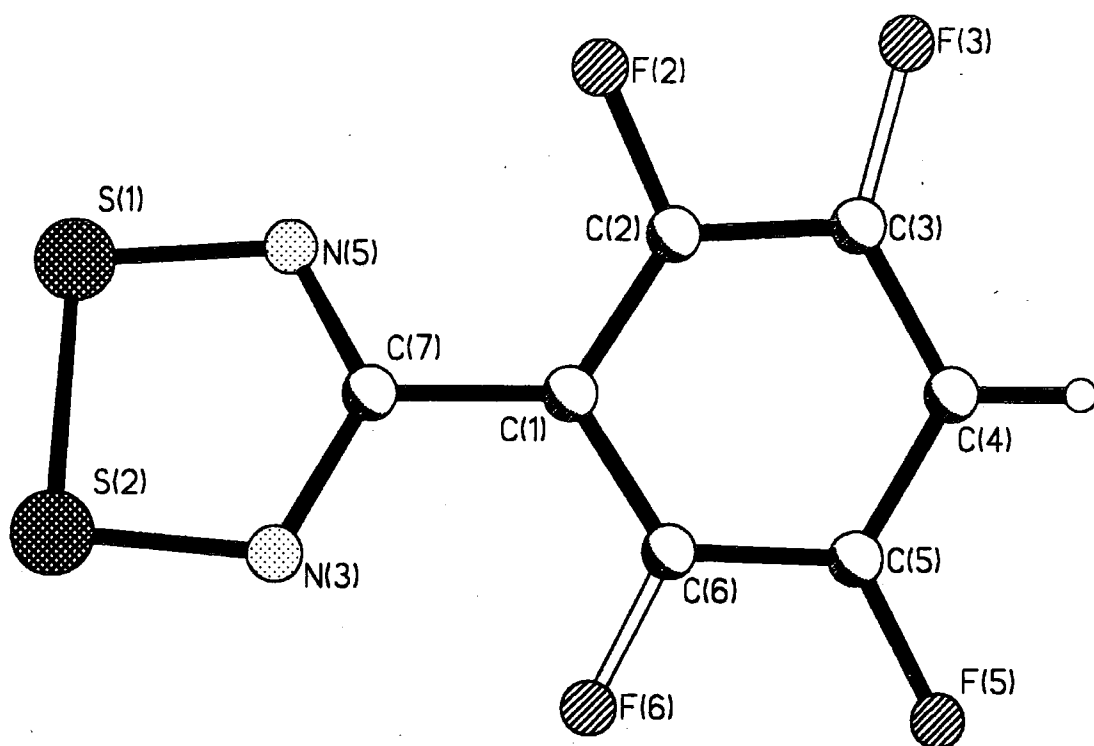


Figure 3.3(c)i The asymmetric unit cell of (2,5-F₂.C₆H₃.CNSSN)

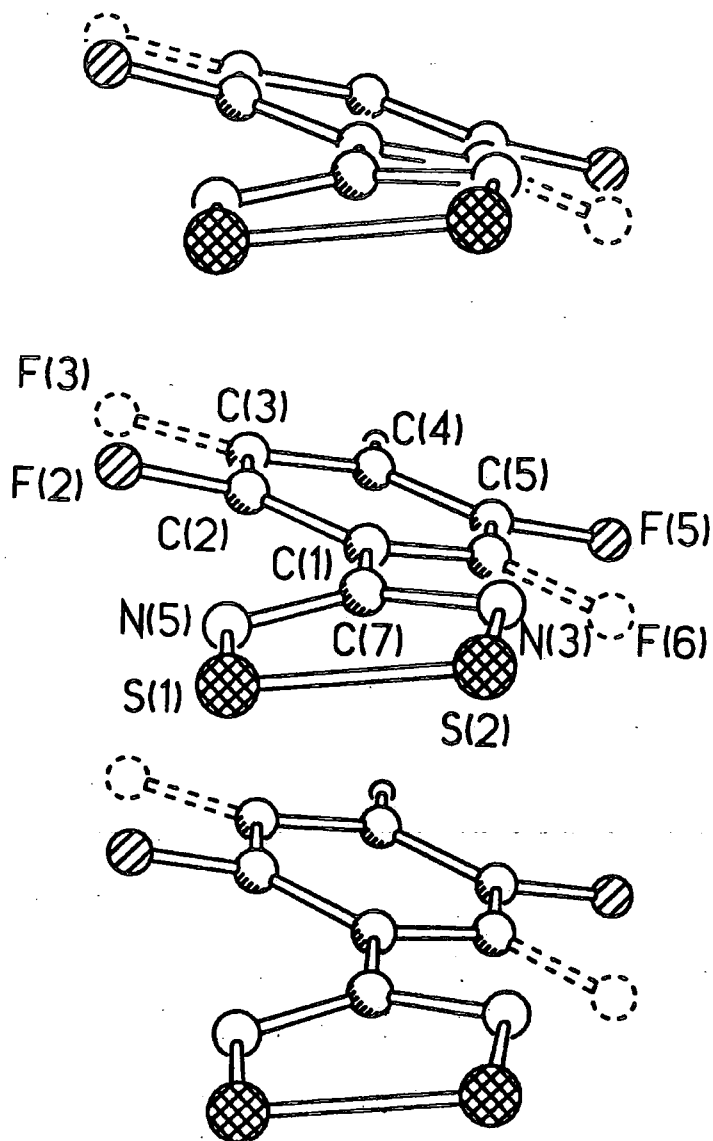


Figure 3.3(c)ii Packing along the Z-axis in (2,5-F₂.C₆H₃.CN)SSN)

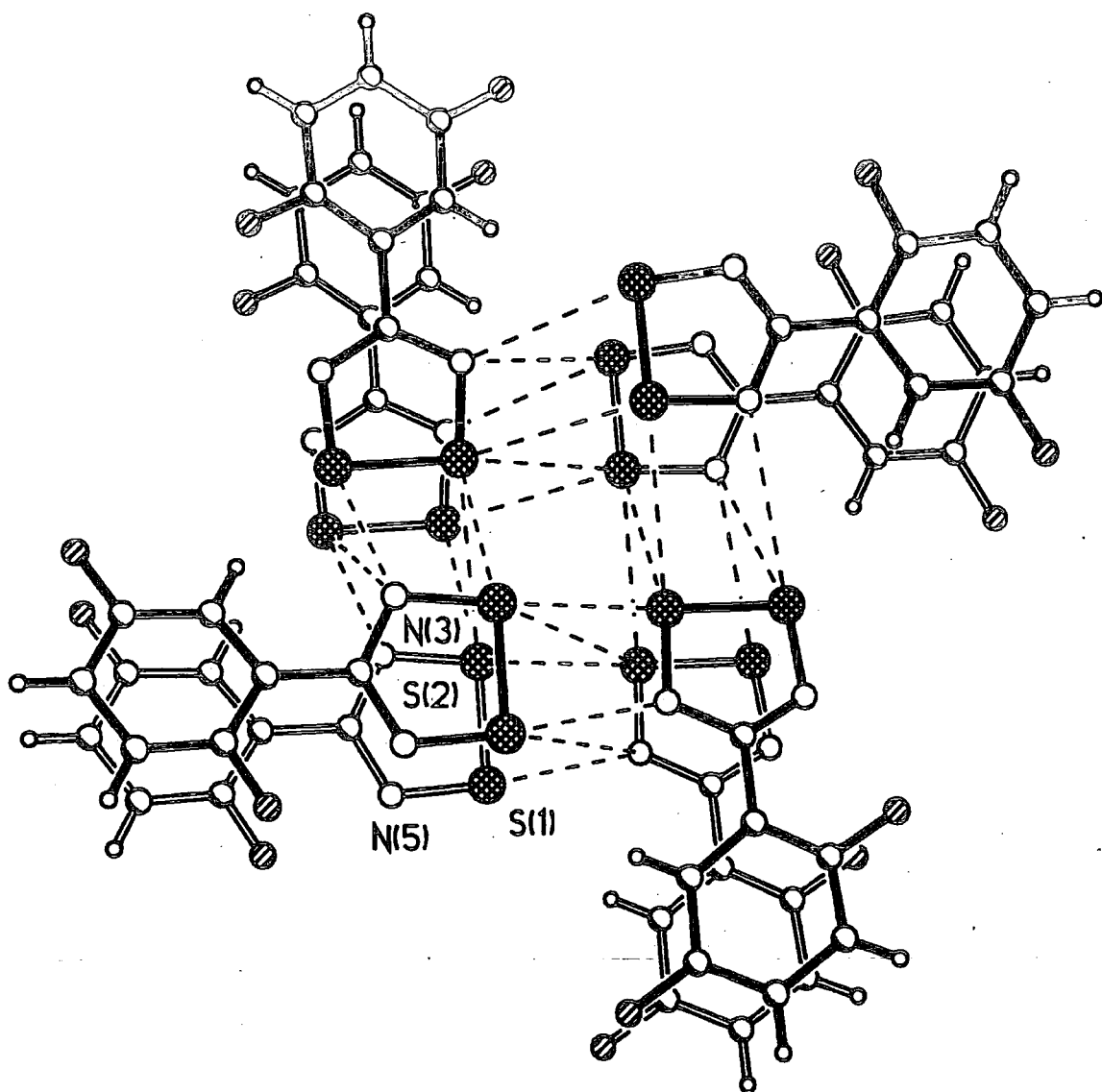


Figure 3.3(c)iii The interaction between two rings in (2,5-F₂.C₆H₃.CNSSN).

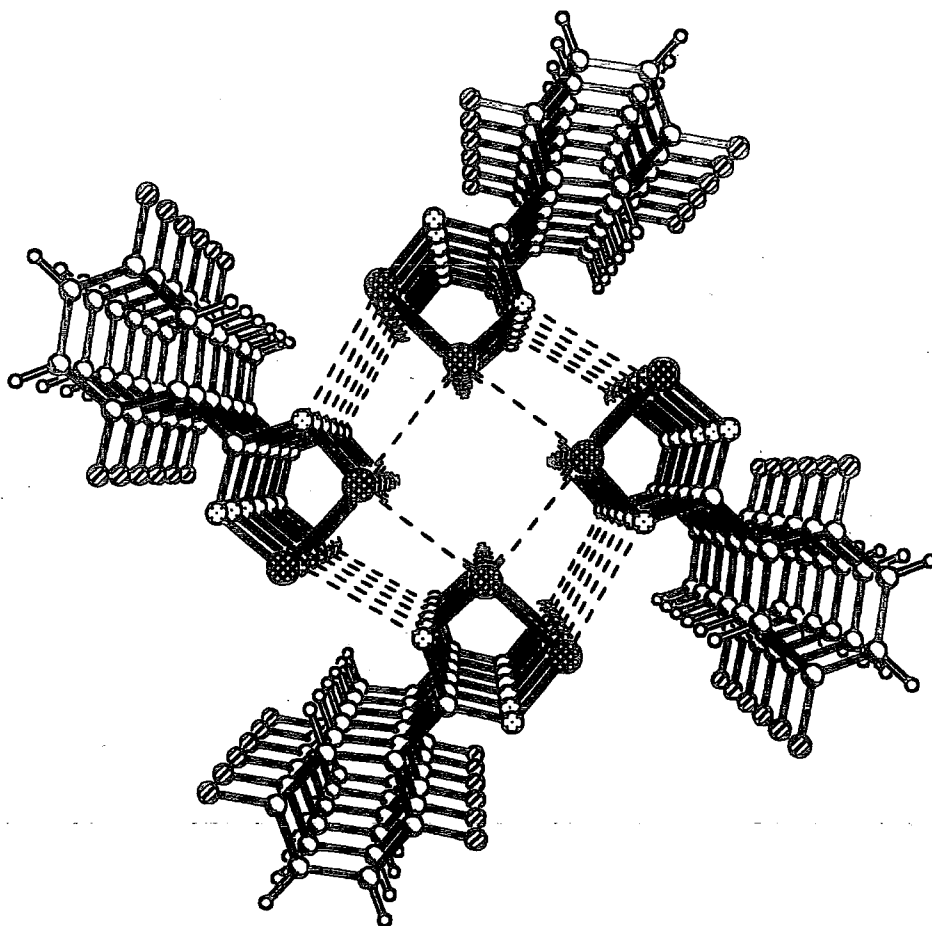


Figure 3.3(c)iv Solid state packing arrangement in (2,5-F₂.C₆H₃.CNSSN).

Table 3.3.7 Crystal data and structure refinement for (c).

Identification code	95srv106
Empirical formula	C7 H3 F2 N2 S2
Formula weight	217.23
Temperature	150(2) K
Wavelength	1.54184 Å
Crystal system	Tetragonal
Space group	P4(2)/n
Unit cell dimensions	a = 21.277(3) Å alpha = 90 deg b = 21.277(3) Å beta = 90 deg c = 3.544(6) Å gamma = 90 deg.
Volume	1604(3) Å ³
Z	8
Density (calculated)	1.799 Mg/m ³
Absorption coefficient	5.940 mm ⁻¹
F(000)	872
Crystal size	0.40 x 0.20 x 0.20 mm
Theta range for data collection	4.16 to 74.95 deg.
Index ranges	0<=h<=26, 0<=k<=26, -4<=l<=3
Reflections collected	2457
Independent reflections	1438 [R(int) = 0.0875]
Absorption correction	Semi-empirical from psi-scans
Max. and min. transmission	1.0000 and 0.6845
Refinement method	Full-matrix least-squares on F ²
Data / restraints / parameters	1438 / 6 / 136
Goodness-of-fit on F ²	1.092
Final R indices [I>2sigma(I)]	R1 = 0.0900, wR2 = 0.2339
R indices (all data)	R1 = 0.1624, wR2 = 0.2808
Largest diff. peak and hole	.547 and -.670 e.Å ⁻³

Table 3.3.8 Atomic co-ordinates ($\times 10^4$) and equivalent isotropic displacement parameters ($\text{\AA}^2 \times 10^3$) for (c). $U(\text{eq})$ is defined as one third of the trace of the orthogonalized U_{ij} tensor.

	x	y	z	$U(\text{eq})$
S(1)	6621(1)	4138(1)	2190(10)	65(1)
S(2)	7355(1)	3490(1)	2567(8)	57(1)
N(3)	7904(3)	4015(3)	3172(20)	41(2)
N(5)	7081(3)	4742(3)	2715(24)	48(2)
C(1)	8133(4)	5137(3)	3635(20)	30(2)
C(2)	7957(4)	5733(4)	4774(25)	45(2)
C(3)	8350(5)	6232(4)	5231(28)	58(3)
C(4)	8996(5)	6134(5)	4510(29)	60(3)
C(5)	9204(4)	5550(5)	3300(23)	45(2)
C(6)	8763(4)	5070(3)	2994(24)	37(2)
C(7)	7679(4)	4614(3)	3202(23)	35(2)
F(2)	7377(3)	5866(3)	5713(22)	44(2)
F(5)	9816(3)	5436(4)	2451(25)	56(2)
F(3)	7992(10)	6733(7)	6235(60)	92(7)
F(6)	8988(7)	4541(5)	1661(47)	48(4)

Table 3.3.9 Bond lengths [A] and angles for (c).

S(1)-N(5)	1.627(7)	S(1)-S(2)	2.087(3)
S(2)-N(3)	1.633(7)	N(3)-C(7)	1.361(9)
N(5)-C(7)	1.314(11)	C(1)-C(6)	1.368(11)
C(1)-C(2)	1.384(10)	C(1)-C(7)	1.480(11)
C(2)-F(2)	1.309(8)	C(2)-C(3)	1.360(13)
C(3)-F(3)	1.358(10)	C(3)-C(4)	1.413(14)
C(4)-C(5)	1.389(13)	C(5)-F(5)	1.358(8)
C(5)-C(6)	1.390(11)	C(6)-F(6)	1.312(9)
N(5)-S(1)-S(2)	93.7(3)	N(3)-S(2)-S(1)	95.3(2)
C(7)-N(3)-S(2)	112.9(6)	C(7)-N(5)-S(1)	115.7(5)
C(6)-C(1)-C(2)	114.2(8)	C(6)-C(1)-C(7)	122.9(7)
C(2)-C(1)-C(7)	122.9(7)	F(2)-C(2)-C(3)	112.4(8)
F(2)-C(2)-C(1)	121.8(8)	C(3)-C(2)-C(1)	125.7(8)
F(3)-C(3)-C(2)	107.4(12)	F(3)-C(3)-C(4)	135.1(14)
C(2)-C(3)-C(4)	117.5(8)	C(5)-C(4)-C(3)	119.8(9)
F(5)-C(5)-C(4)	122.3(9)	F(5)-C(5)-C(6)	119.9(8)
C(4)-C(5)-C(6)	117.8(8)	F(6)-C(6)-C(1)	120.5(9)
F(6)-C(6)-C(5)	114.4(9)	C(1)-C(6)-C(5)	124.9(7)
N(5)-C(7)-N(3)	122.3(7)	N(5)-C(7)-C(1)	119.3(7)
N(3)-C(7)-C(1)	118.3(7)		

3.4 Electron Spin Resonance.

3.4.1 Introduction

Electron Spin Resonance is employed to probe the electronic structure of radicals. An e.s.r. signal can only be detected only when unpaired electrons are present. Variable temperature e.s.r. permits some thermodynamic data to be determined for the monomer-dimer equilibrium in solution.²

The g-tensor, which is the e.s.r. equivalent of the chemical shift, gives us an idea of the main peak resonance. It can be calculated from the formula shown below.

$$h=6.626179 \times 10^{-27}$$

$$\mu_0=0.92732 \times 10^{-20}$$

$$g=h/\mu_0 \times \nu/H$$

ν =Operating frequency

H =Magnetic field of resonance position.

The unpaired electron exists in the SOMO, and its spin will couple with any nucleus which contributes to the SOMO. In the case of dithiadiazolyls, the largest electron density is at the two sulfur atoms.¹⁶ However since ³³S (I=1/2) has a low abundance and ³²S (I=0) spin nucleus, no hyperfine coupling to sulfur is observed.² However the ¹⁴N nuclei possess a I=1 spin. Thus coupling to the two equivalent N nuclei gives rise to a well resolved 1:2:3:2:1 pentet.^{27,1,2, 28}

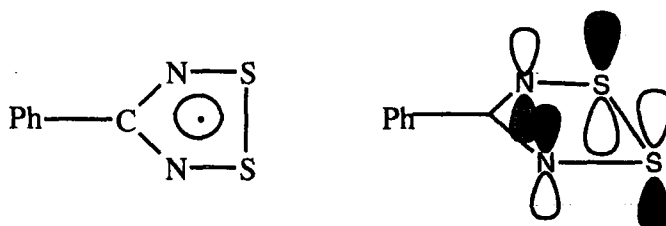


Figure 3.4.1 The $2a_2$ SOMO of 4-phenyl -1,2,3,5 dithiadiazolyl.

Because of the a_2 symmetry, only a small spin population is observed on the ring carbon, however significant spin density is located on the sulfur atoms.³¹

The e.s.r. spectra of the fluorinated dithiadiazolyls, $(CF_3.CNSSN)^\cdot$ and $(C_6F_5.CNSSN)^\cdot$ has been previously reported.³² The study showed that the fluorine substituents cause a drift of electron spin density away from the nitrogen $2p_x$ orbitals, towards the $3p_x$ orbitals of the sulfur atoms. Recent e.s.r. measurements³³ have shown that the enthalpy of dimerisation of fluorinated dithiadiazolyls is similar to that observed for the protonated analogues.

3.4.2 Results and Discussion

ESR studies were carried out on the following fluorinated dithiadiazolyls.

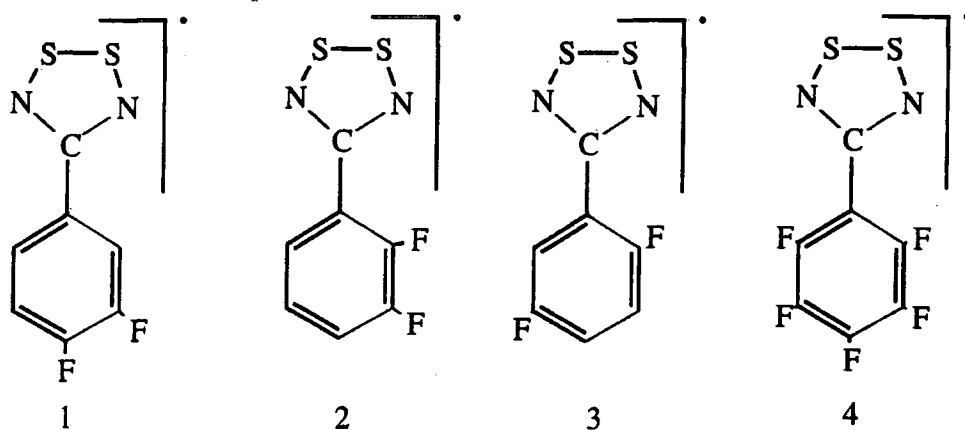


Figure 3.4.2 The fluorinated dithiadiazolyls ($3,4\text{-F}_2\text{.C}_6\text{H}_3\text{.CNSSN}$). (1), ($2,3\text{-F}_2\text{.C}_6\text{H}_3\text{.CNSSN}$). (2) ($2,5\text{-F}_2\text{.C}_6\text{H}_3\text{.CNSSN}$). (3) and ($\text{C}_6\text{F}_5\text{.CNSSN}$). (4).

Their preparation was previously outlined in section 3.2. Each radical was dissolved in CH_2Cl_2 and the second derivative X-band e.s.r. spectra were recorded at room temperature the results are discussed below.

($3,4\text{-F}_2\text{.C}_6\text{H}_3\text{.CNSSN}$). (1)

This spectrum reveals the characteristic quintet which arises from the coupling to two equivalent ^{14}N nuclei, Figure 3.4.4 below. The fluorine coupling was not resolved. The parameters of the spectrum are recorded in Table 3.4.

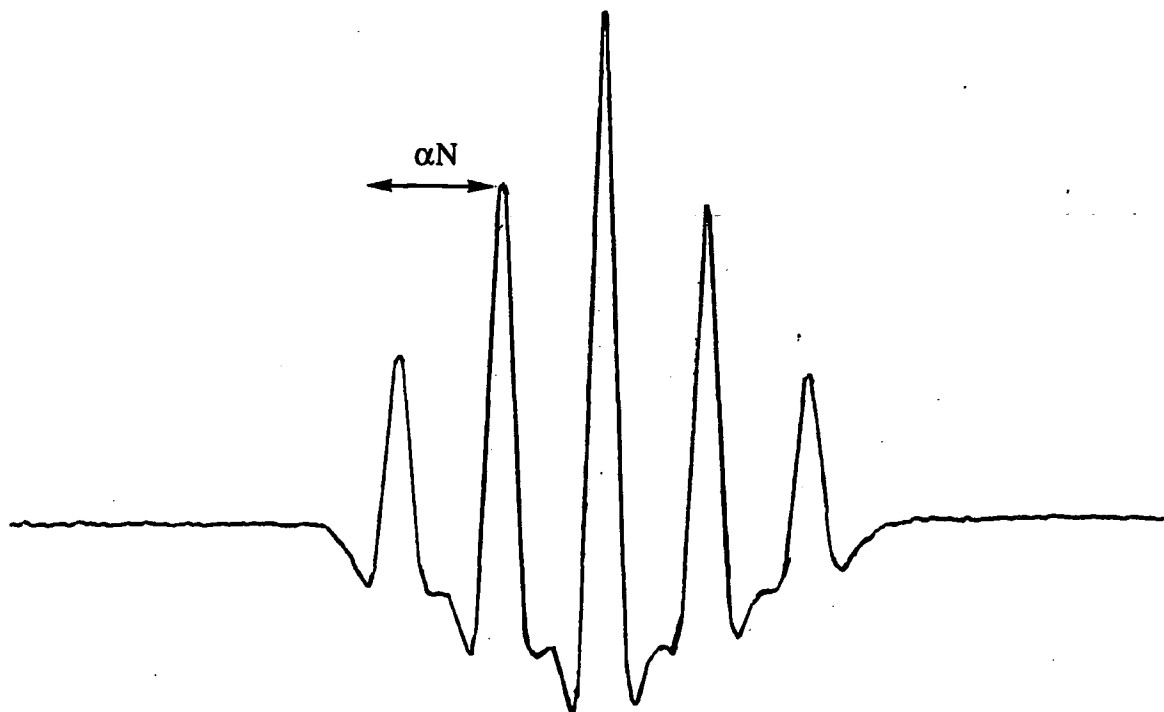


Figure 3.4.4 Second-derivative X-band e.s.r. spectrum of ($3,4\text{-F}_2\text{.C}_6\text{H}_3\text{.CNSSN}$). in CH_2Cl_2 at room temperature.

(2,3-F₂.C₆H₃CN₂SSN)· (2)

The spectrum was recorded at room temperature; the isotropic spectrum is composed of a 1:2:3:2:1 quintet. The spectral parameters are listed in Table 3.4; no coupling to the fluorine was resolved.

(2,5-F₂.C₆H₃.CN₂SSN)· (3)

The spectrum obtained for this derivative, appeared to be very similar to that observed in (1) and (2). The five line quintet is reported. While no fluorine coupling appears, the spectra were recorded at room temperature. The spectral parameters are listed in Table 3.4.

ESR Parameters

Compound	g _{iso}	a _{Pt}	a _P	a _N
(C ₆ H ₅ .CN ₂ SSN)·	2.012	--	--	0.517
(3,4-F ₂ .C ₆ H ₃ .CN ₂ SSN)·	2.019	--	--	0.512
(2,3-F ₂ .C ₆ H ₃ .CN ₂ SSN)·	2.018	--	--	0.511
(2,5-F ₂ .C ₆ H ₃ .CN ₂ SSN)·	2.018	--	--	0.512
Pt[C ₆ F ₅ .CN ₂ SSN][PPh ₃] ₂	2.04696	5.5135	--	0.5405
Intermediate	2.0097	5.135	2.567	

Table 3.4 ESR parameters for (C₆H₅.CN₂SSN)·, (3,4-F₂.C₆H₃.CN₂SSN)· (1), (2,3-F₂.C₆H₃.CN₂SSN)· (2), (2,5-F₂.C₆H₃.CN₂SSN)· (3), Pt[C₆F₅.CN₂SSN][PPh₃]₂ (4) and an intermediate (5).

Reaction of (C₆F₅.CN₂SSN)· with Pt(PPh₃)₄ in CH₂Cl₂.

The first e.s.r. spectrum for a metallo-dithiadiazolyl complex³⁴ indicated that the spin density is delocalised over the N₂S₂PtP₂ core.²⁷ Addition of a small amount of (C₆F₅.CN₂SSN)· to Pt(PPh₃)₄ in an e.s.r. tube in CH₂Cl₂ led to the immediate formation of a blue coloured solution, which eventually turned orange. This *in situ* reaction is believed to proceed in a manner similar to that reported³⁴ for (C₆H₅.CN₂SSN)· and Pt(PPh₃)₄. The unstable monometallic complex eventually decomposed to the more stable trimetallic species, Pt₃[C₆F₅.CN₂SSN][PPh₃]₄ as indicated by the colour change.

The second derivative spectrum (Figure 3.4.5(a)) highlights the ^{195}Pt and ^{31}P coupling, it also shows minor contributions from the intermediate formed during the reaction. All the parameters are recorded in Table 3.4, shown below. The second spectrum (Figure 3.4.5(b)) was recorded when the reaction was complete. The main peak in the centre of the spectrum arises from ^{14}N hyperfine coupling, while the two peaks to the left and the right of the centre peak are Pt satellites arising from ^{195}Pt coupling. No fluorine coupling was resolved. All parameters are shown in Table 3.4.

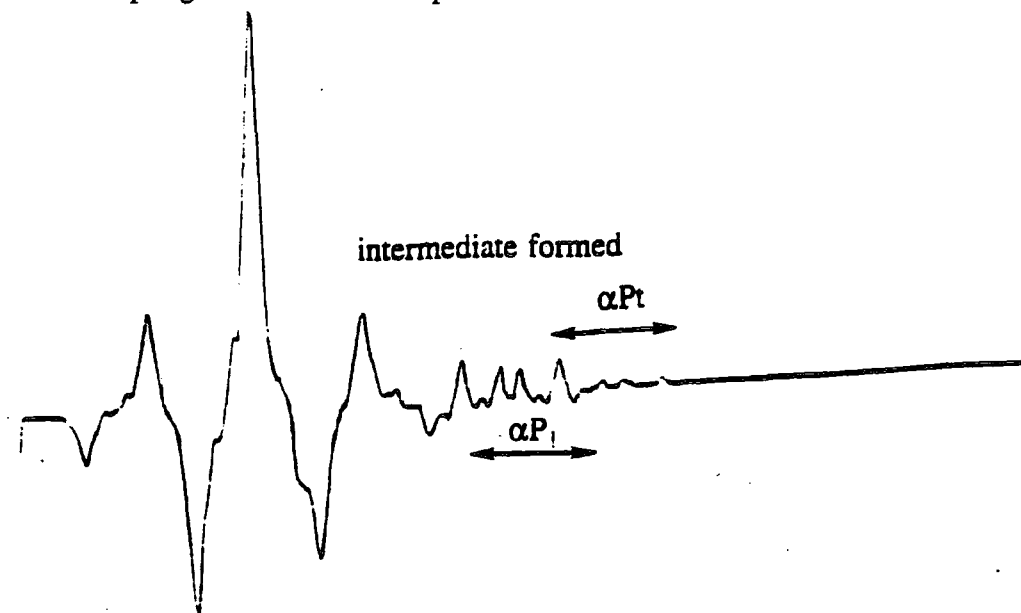


Figure 3.4.5(a) Second derivative e.s.r. spectrum of $(\text{C}_6\text{F}_5)_2\text{CNSSN}\cdot$ freshly added to $\text{Pt}(\text{PPh}_3)_4$, in CH_2Cl_2 at room temperature. (First run).

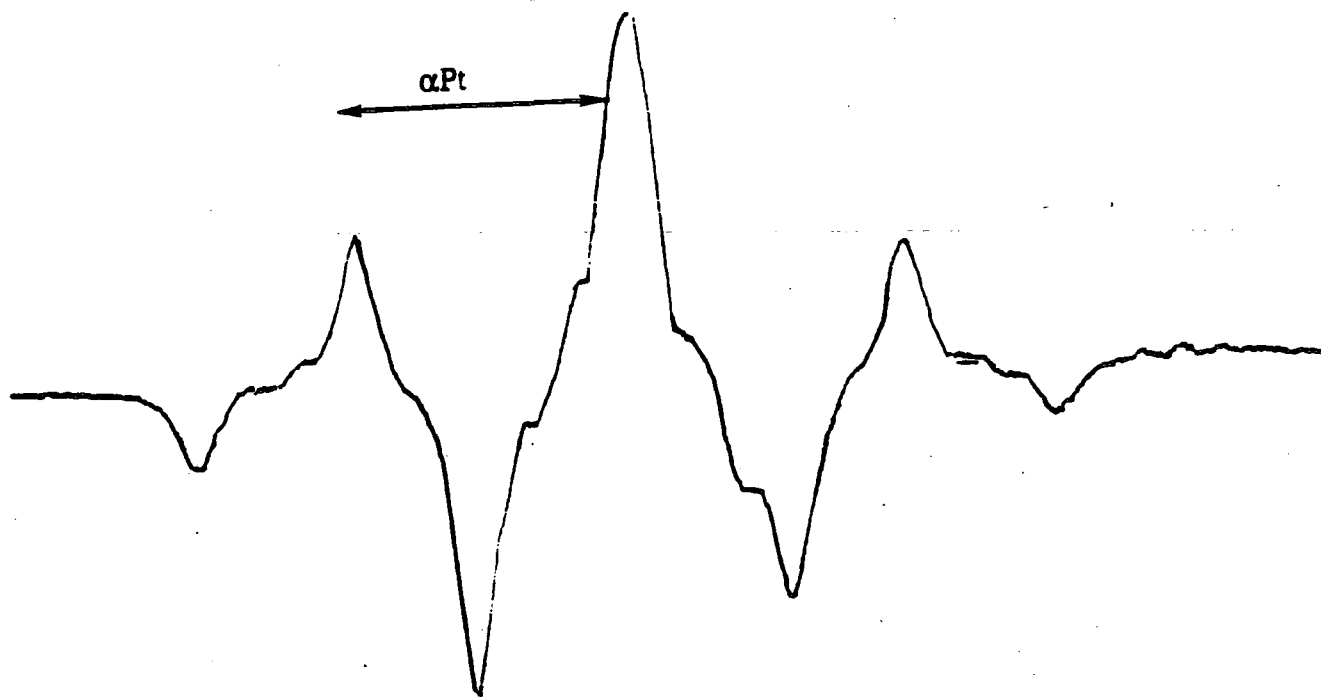


Figure 3.4.5(b) Second derivative isotropic X-band spectrum of $(\text{C}_6\text{F}_5)_2\text{CNSSN}\cdot$ and $\text{Pt}(\text{PPh}_3)_4$ in CH_2Cl_2 at room temperature. (Reaction complete).

3.5 N.M.R. Study of $\text{Pt}_3[\text{PPh}_3]_4[3,4\text{-F}_2\text{.C}_6\text{H}_3\text{.CNSSN}]_2$

A comprehensive n.m.r. study (^{31}P , ^1H and ^{19}F) was undertaken on the trimetallic platinum complex (reported in section 3.3). The previously synthesised blue monometallic species $[\text{Pt}(\text{PPh}_3)_2(3,4\text{-F}_2\text{.C}_6\text{H}_3\text{.CNSSN})_2]$ was dissolved in CDCl_3 and various n.m.r. spectra were recorded immediately and at various time intervals. Over a period of 2-3 days the solution turned from blue to brown to orange, upon decomposition to the trimetallic complex. After a few days, crystals of the trimetallic species began to crystallise from solution.

The n.m.r. spectra ^1H , ^{19}F of the monometallic species revealed little significant information. This is due to the paramagnetic nature of the initial monometallic species which broadens the n.m.r. spectra.¹⁵ The ^{31}P spectra of the trimetallic species are summarised in Table 3.5 below.

Complex/ Species	δ (ppm)	$J_{\text{Pt-P}}$ (Hz)
$[\text{Pt}_3(\text{PPh}_3)_4(3,4\text{-F}_2\text{.C}_6\text{H}_3\text{.CNSSN})]$	18.0	2805
Unknown (a)	15.33	3555
Unknown (b)	19.45/14.64	22.6 (J _{P-P})
$[\text{Pt}_3(\mu\text{-SNCPHNS-S,S})_2(\text{PPh}_3)_4]$	18.5	3282
Unknown	15.36	3551
PPh_3S	-5.13	----
PPh_3	43.60	----
$[\text{Pt}(\text{PPh}_3)_2(1,5\text{Ph}_4\text{P}_2\text{N}_4\text{S}_2)]$	18.3	2861

Table 3.5 The chemical shifts (ppm) and J values (Hz) for the ^{31}P n.m.r. spectra of $\text{Pt}_3[\text{PPh}_3]_4[3,4\text{-F}_2\text{.C}_6\text{H}_3\text{.CNSSN}]_2$ and related species.

The trimetallic platinum complex $[\text{Pt}_3(\text{PPh}_3)_4(3,4\text{-F}_2\text{.C}_6\text{H}_3\text{.CNSSN})]$ and the unknown (a) peak both appear as singlets. This would suggest that the PPh_3 groups are chemically/magnetically equivalent. This is presumably due to rotation about the C-Ph single bond on the chalcogen ring system.

The unknown (b) signals could arise from a protonated analogue of the monometallic complex, (Figure 3.5.1). This would make the two PPh₃ groups chemically inequivalent and thus result in the formation of a doublet of doublets

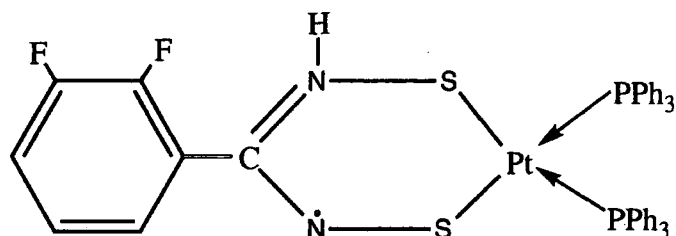


Figure 3.5.1 The protonated monometallic complex.

The ³¹P n.m.r. spectrum of the 2,3-F₂ Pt complex consists of a single peak (δ 17.98) with platinum satellites ($J_{\text{Pt-P}}=2805$ Hz) with a much less intense peak being observed close to it (δ 15.33) again with platinum satellites ($J_{\text{Pt-P}}=3555$ Hz).

After a few hours the spectrum was run again, the only difference observed was the increase in the intensity of free Ph₃P and the Ph₃PS peaks. As the trimetallic species begins to decompose, the dithiadiazolyl rings begin to break-up; this could account for loss of PPh₃ and the abstraction of S. As the PPh₃ groups are lost the intensity of this signal decreases, while the intensity of the Ph₃PS peak increases.

It is possible that the unknown (b) peak, could arise from a higher oligomer species. On comparison of the results with those obtained by I. May, (who studied the non fluorinated analogue) see Table 3.5, no major differences in chemical shift are apparent. The sulfur based complex³⁶ [M(PPh₃)₂(1,5-Ph₄P₂N₄S₂)] where M=Pt or Pd (Figure 3.5.2 below) which has a similar structure to the monometallic and trimetallic Pt species, has similar chemical shift (δ ppm) and $J_{\text{Pt-P}}$ coupling (Hz) data to both trimetallic Pt complexes.

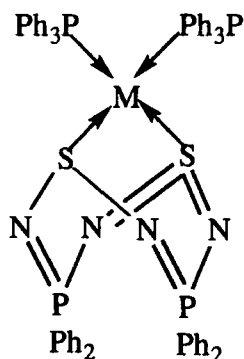
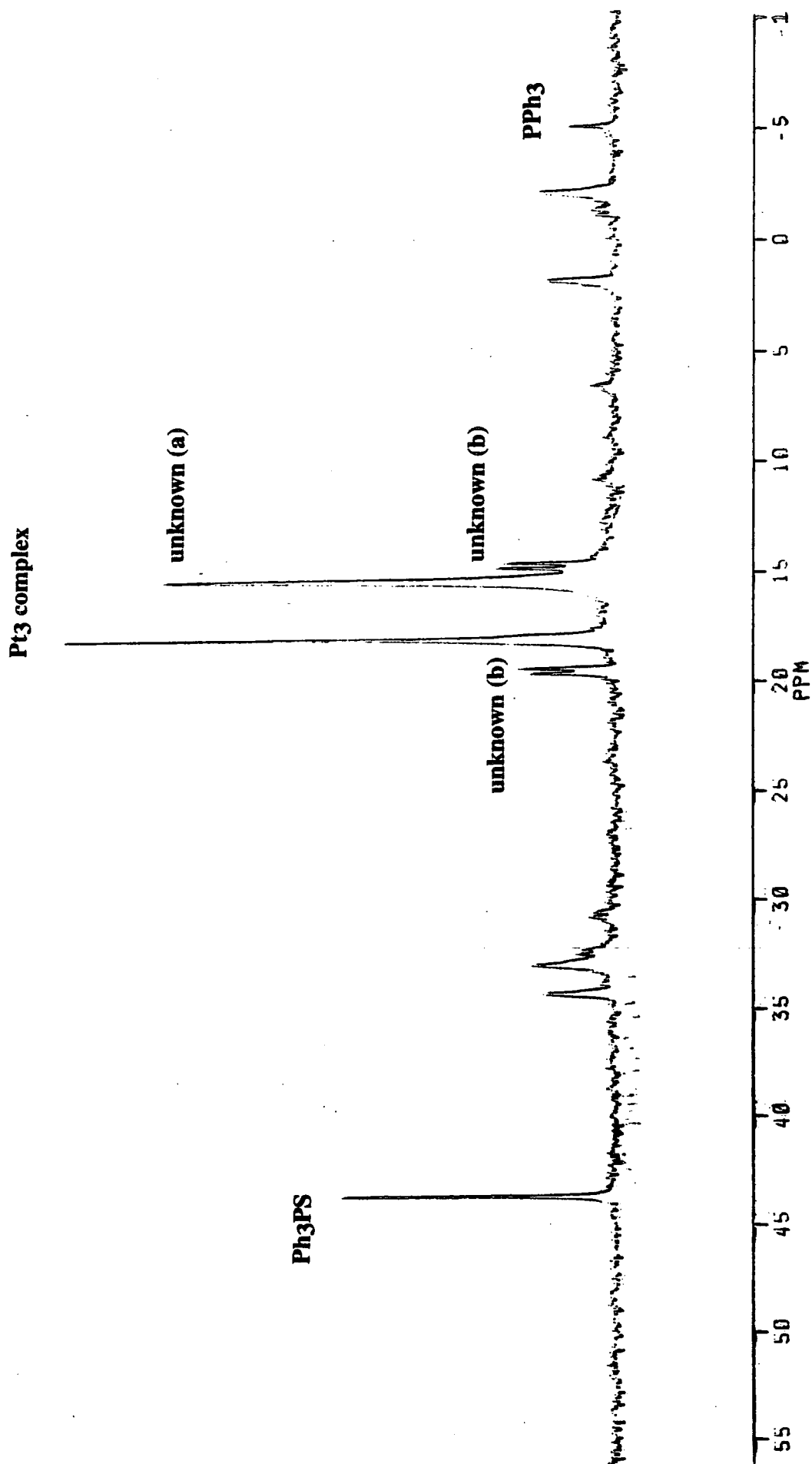


Figure 3.5.2 [M(PPh₃)₂(1,5-Ph₄P₂N₄S₂)].

Figure 3.5.3 The ^{31}P n.m.r. spectrum of $[\text{Pt}_3(\text{PPh}_3)_4(3,4\text{-F}_2\text{C}_6\text{H}_3\text{CNSSN})]$.



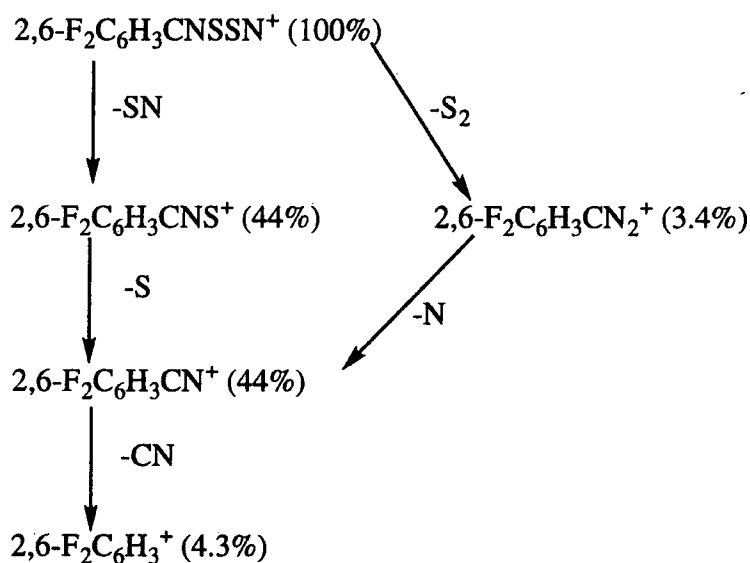
3.6 Results and Discussion.

3.6.1 Preparation of (2,6-F₂C₆H₃CN₂SSN)₂

The reaction between Li[N(SiMe₃)₂] and the 2,6 difluorobenzonitrile in diethyl ether produced a straw coloured solution characteristic of the lithium salt of the silylated amidine. Addition of SCl₂ yielded a bright orange precipitate of the chloride salt. This was then filtered on a filter stick, and subsequently extracted with SO₂(l) and the released dithiadiazolyl was sublimed.

The infrared spectrum of the dithiadiazolyl appeared to be very similar to those of the other fluorinated analogues. The absence of the CN peak at 2225cm⁻¹ is significant as it indicates that cyclisation has successfully taken place. The peaks at 1308cm⁻¹ and between 906 and 1009cm⁻¹ are believed to arise from the C-N stretching modes within the dithiadiazolyl ring.³⁴

Scheme 3.5.1 Mass spectrum breakdown pattern of (2,6-F₂C₆H₃CN₂SSN)₂



Also present.

SN⁺ 24.1%

S₂⁺ 21.2%

S₂N⁺ 97.5%

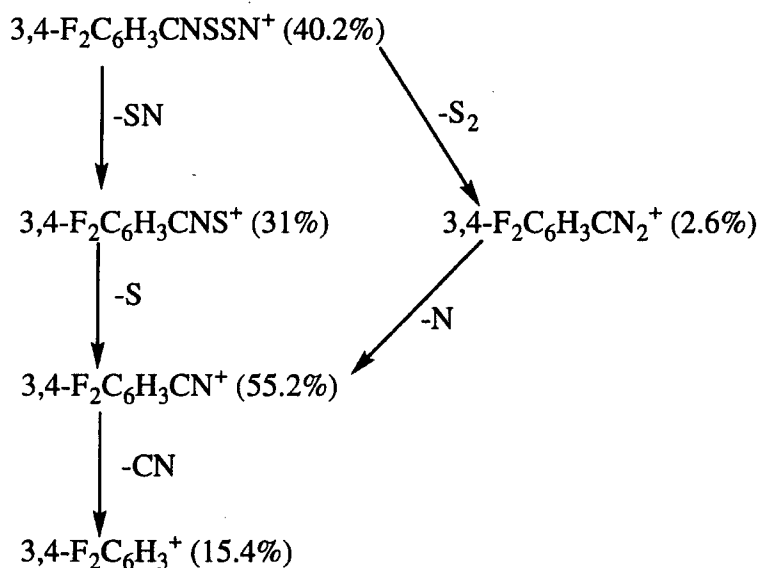
DSC studies showed that a very broad endotherm(melting) appears at 104+/-2°C and that decomposition starts around 213.3+/-0.5°C.

3.6.2 Preparation of (3,4-F₂C₆H₃CN₂SSN)₂

The reaction between Li[N(SiMe₃)₂] with 3,4-difluorobenzonitrile produced a yellow coloured solution (section 3.6.1). Addition of SCl₂ produced an orange coloured precipitate. This was then filtered and washed on a filter stick; the filtrate was then extracted with SO₂(l), and subsequently reduced in THF with Zn/Cu couple. Finally the dithiadiazolyl was sublimed using electrical heating tape.

In the infrared spectrum the absence of the CN peak at 2225cm⁻¹; proves that cyclisation successfully took place. The strong peak at 721cm⁻¹ is thought to arise from S-N stretching while the peaks at 966cm⁻¹ and 1308cm⁻¹ could possibly arise from C-N stretching frequencies within the dithiadiazolyl ring. It was not possible to assign all the peaks successfully.

Scheme 3.6.2 Mass spectrum breakdown pattern of (3,4-F₂C₆H₃CN₂SSN)₂



Also present
SN⁺ 38.7%
S₂⁺ 9.8%
S₂N⁺ 100%

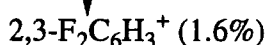
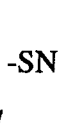
DSC studies shows a sharp endotherm at 129.2±0.4 °C.

3.6.3 Preparation of (2,3-F₂.C₆H₃.CNSSN)₂

The chloride salt, which was previously synthesised by C. Aherne University of Durham, was reduced with Zn/Cu couple in SO₂(l) and successfully sublimed. The infrared spectrum appeared to be similar to that obtained for the 3,4 difluorinated dithiadiazolyl. The absence of any CN peak at 2250cm⁻¹ indicates that cyclisation has occurred. The peak at 727cm⁻¹ which is present in the infrared spectrum of the other fluorinated compounds, arises from the S-N stretching, while the peaks at 976 and 1314cm⁻¹ are probably due to C-N stretching within the dithiadiazolyl ring.

The mass spectrum breakdown pattern (scheme 3.6.3) is very similar to that of the other fluorinated dithiadiazolyls highlighted previously.

Scheme 3.6.3 Mass spectrum breakdown pattern of (2,3-F₂.C₆H₃.CNSSN)₂



Also present

SN⁺ 8.2%

S₂⁺ 0.6%

S₂N⁺ 21%

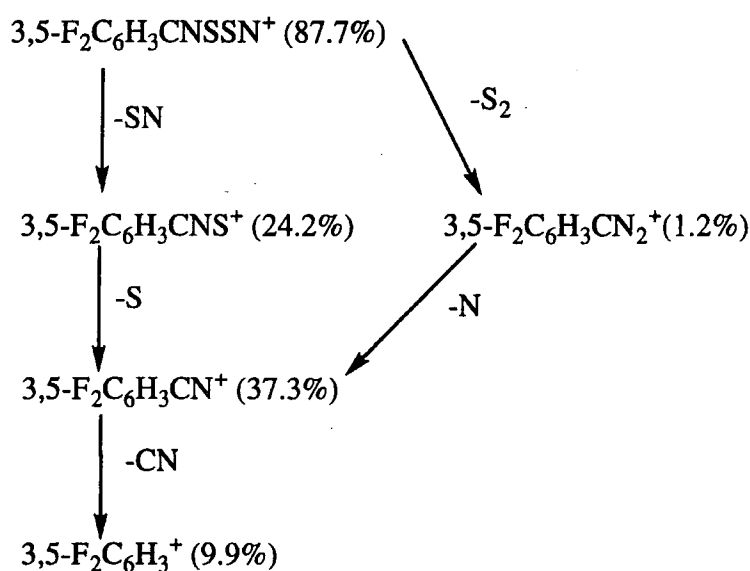
The DSC show that sharp endotherms appear at 101+/-1 °C and 121.7+/-0.5 °C.

3.6.4 Preparation of (3,5-F₂C₆H₃CN₂SSN)₂

The chloride salt was previously prepared by C. Aherne; this was reduced in liquid SO₂ with Zn/Cu couple and subsequently sublimed. The sublimation process produced some yellow material, which could possibly be some starting material, or sulfur. However some grey black crystalline material also appeared, on which analysis was carried out.

The absence of any CN peaks at 2250cm⁻¹ indicated that some degree of substitution had taken place. However the absence of any distinct dithiadiazolyl stretching frequencies between 1126cm⁻¹ and 560cm⁻¹, may indicate that a highly purified dithiadiazolyl may not have been synthesised.

Scheme 3.6.4 Mass spectrum breakdown pattern of impure
(3,5-F₂C₆H₃CN₂SSN)₂



Also present
SN⁺ 24.2%
S₂⁺ 7.9%
S₂N⁺ 100%

The DSC shows a sharp endotherm at 133.7±0.3°C, while an exotherm is observed at 254.8±0.5°C.

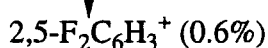
3.6.5 Preparation of (2,5-F₂C₆H₃CN₂SSN)⁺

The chloride salt was previously prepared by C. Aherne, the salt was reduced with Zn/Cu couple under THF overnight. The sublimation process produced black coloured crystalline material.

The absence of the peak at 2250cm⁻¹ indicates that cyclisation has taken place. The peak at 790cm⁻¹ could arise from S-N stretching, while the peaks at 944cm⁻¹ and 1370 cm⁻¹ arise from C-N stretching within the dithiadiazolyl ring.

The mass spectrum breakdown pattern (scheme 3.6.5) outlines the most probable molecular fragments which arise from the electronic ionisation of the dithiadiazolyl.

Scheme 3.6.5 Mass spectrum breakdown pattern of (2,5-F₂C₆H₃CN₂SSN)⁺



Also present

SN⁺ 0.5%

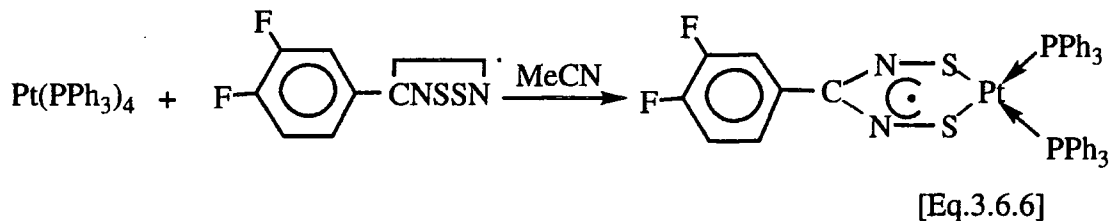
S₂⁺ 0.4%

S₂N⁺ 5.9%

DSC Shows a sharp endotherm (melting) at 105.1±0.2°C, while an exotherm is observed at 228±1°C.

3.6.6 The Reaction of Pt(PPh₃)₄ with (3,4-F₂.C₆H₃.CNSSN)₂

Pt(PPh₃)₄ (0.4g, 0.33mmol) and (3,4-F₂.C₆H₃.CNSSN)₂ (0.07g, 0.32mmol) was allowed to stir in MeCN (ca. 15ml) for 30mins [Eq.3.6.6]. A dark green-blue micro crystalline suspension soon developed. After stirring, the solution was filtered and the precipitate was washed with MeCN (3x5ml); a yield of 46.8% was obtained.



The comparison of its infrared spectrum with the starting dithiadiazoly showed some new peaks. The peak at 1604cm^{-1} increased in intensity and very strong peaks appeared at 1507cm^{-1} and 692cm^{-1} , while the peak at 1740cm^{-1} disappeared.

Excellent elemental analysis was obtained:

Found (%) C 55.11, H 3.76, N 4.29

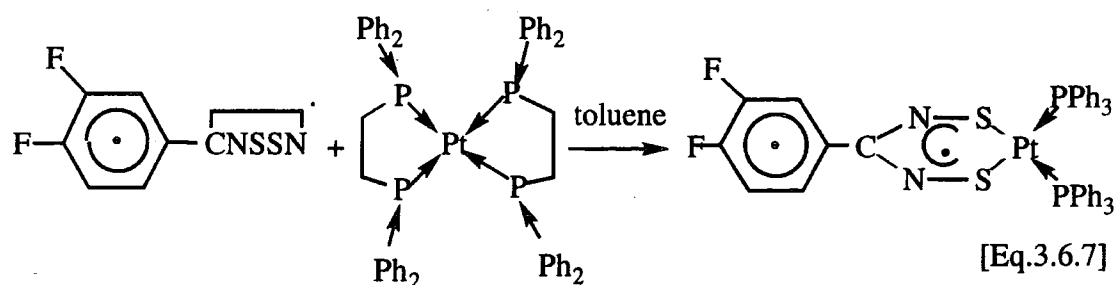
Required (%) C 55.28, H 3.68, N 4.30.

Ultraviolet/visible spectroscopic studies were carried out on the complex. The complex (2mg) was dissolved in dichloromethane (ca.10ml) to give a deep blue solution which eventually turned green on completion of the scan, which was recorded from 400 to 1000nm. The strongest absorbance (682nm , absorbance 3.95) was responsible for the blue solution. Other peaks appeared at 498nm (absorbance 1.5) and 475nm (absorbance 1.7).

The same peaks, at lower intensity, were formed 5min. later. This rapid decrease in peak intensity accounts for the very low extinction coefficient values recorded (cf. Table 2.5, section 2.5).

3.6.7 The Reaction of $\text{Pt}(\text{dppe})_2$ with $(3,4\text{-F}_2\text{C}_6\text{H}_3\text{.CNSSN})_2$

The reaction of $\text{Pt}(\text{dppe})_2$ (0.37g, 0.37mmol) with $(3,4\text{-F}_2\text{C}_6\text{H}_3\text{.CNSSN})_2$ (0.08g, 0.037mmol) in toluene led to the formation of a green coloured micro crystalline precipitate under a green coloured solution. After allowing it to stir (ca. 5hrs) the blue-green solution was filtered and the precipitate washed with toluene. The monometallic platinum complex was formed in 82% yield, [Eq. 3.6.7].



On comparing the infrared spectrum of the complex with that of the infrared of the starting dithiadiazolyl, several new peaks are visible (1376cm^{-1} and 1317cm^{-1} and a weak peak at 2923cm^{-1}). There is a decrease in peak intensity at 721cm^{-1} . The spectrum appear to be very similar to that recorded for the corresponding para chloro phenyl dithiadiazolyl complex. (cf. section 2.3.7).

Elemental analysis figures were as follows:

Found(%) C 49.40, H 3.91, N 2.95.

Required (%) C 48.79, H 3.07, N 3.44.

Ultraviolet/visible spectroscopic studies were carried out on the complex, which was dissolved in dichloromethane. It was then scanned from 200 to 1000nm. The solution appeared as a deep blue colour initially and on completion of the scan it developed a light green colour. The strongest absorbance at 660nm (absorbance 3.75) producing the deep blue colour, was accompanied by a smaller peak at 618nm (absorbance 2.890). All peak intensities were observed to decrease with time. These are very similar to the values recorded for the corresponding chloro complex (662nm, and 622nm).

3.8 References.

1. A.J. Banister and J.M. Rawson, *The Chemistry of Inorganic Ring Systems* ed. R. Steudel, Elsevier, Amsterdam, 1992, p. 323-348.
2. J.M. Rawson, A.J. Banister and I. Lavender, *Adv. in Heterocyclic Chem.*, 1994, **62**, p.137-247.
3. A. Vegas, A. Pérez-Salazar, A.J. Banister and R.G. Hey, *J.Chem. Soc., Dalton Trans.*, 1980, 1812.
4. A.J. Banister, J.A.K. Howard and S.E. Lawrence, *Acta Crystallogr., Sect.C*, manuscript in preparation.
5. C.D. Bryan, A.W. Cordes, R.C. Haddon, R.G. Hicks, D.K. Kennepohl, C.D. Mackinnon, R.T. Oakley, T.T.M. Palstra, A.S. Perel, S.R. Scott, L.F. Schneemeyer and J.V. Waszczak, *J.Am.Chem.Soc.*, 1994, 116,1205.
6. C.D. Bryan, A.W. Cordes, R.M. Fleming, N.A. George, S.H. Glarum, R.C. Haddon, R.T. Oakley, T.T.M. Palstra, A.S. Perel, L.F. Schneemeyer and J.V. Waszczak, *Nature*, 1993, **365**, 821.
7. A.J. Banister, N. Bricklebank, I.B. Gorrell, I. Lavender, J.M. Rawson, W. Clegg, M.R.J. Elsegood, A. McCamley and D.G. Richards in press.
8. H.J. Emelus, J.M. Shreeve and R.D. Varma, *Adv. Inorg. Chem.*, 1989, **33**, p139.
9. E.G. Awere, N. Burford, C. Mailer, J. Passmore, M.J. Schriver, P.S. White, A.J. Banister, H. Oberhammer and L.H. Sutcliffe, *J.Chem.Soc., Chem. Commun.*, 1987, 66.
10. Prepared and isolated as a pure crystalline solid G. Wolmershäuser, M. Schnauber and T. Wilhelm, *J.Chem.Soc., Chem. Commun.*, 1984, 573.
11. C.D. Bryan, A.W. Cordes, R.C. Haddon, S.H. Glarum, R.G. Hicks, D.K. Kennepohl, C.D. Mackinnon, R.T. Oakley, T.T.M. Palstra, A.S. Perel and S.R. Scott, *Chem. Mater.*, 1994, **6**, 508.
12. A.J. Banister, A. Batsanov, J.A.K. Howard, A.S. Partington and J.M. Rawson, unpublished results.
13. A.J. Banister, N. Bricklebank, W. Clegg, M.R.J. Elsegood, C.I. Gregory, I. Lavender, J. Rawson and B.K. Tanner, *J.Chem.Soc., Chem Commun.*, 1995, 697.
14. C.M. Aherne, A.J. Banister, I.B. Gorrell, M.I. Hansford, Z.V. Hauptman, A.W. Luke and J.M. Rawson, *J.Chem.Soc., Dalton Trans.*, 1993, 967.
15. E.A.V. Ebsworth, D.W.H. Rankin and S. Cradock, *Structural Methods in Inorganic Chemistry*, 1987, Blackwell Scientific Publications.

16. J. Rawson, personal communication, University of Durham.
17. A.J. Banister, N.R.M. Smith and R.G. Hey *J.Chem.Soc, Perkin, Trans. I* 1983, 1181.
19. A.W. Cordes, J.D. Goddard, R.T. Oakley and N.P.C. Westwood, *J.Am.Chem.Soc.*, 1989, **111**, 6147-6154.
20. A.J. Banister, N. Bricklebank, C.I. Gregory, I. Lavender, J.M. Rawson, W. Clegg and B.K. Tanner, in preparation.
21. S.E. Lawrence, Ph.D Thesis, University of Durham, 1994.
22. C. Aherne, A.J. Banister, A.Batsanov, N. Bricklebank, W. Clegg, M.R.J. Elsewood, J.A.K. Howard, I. Lavender and J.M. Rawson, unpublished results.
23. H.-U.Höfs, J.M. Bats, R.G. Hartmann, R. Mews, M. Maksic-Eckert M. Oberhammer and G.M. Sheldrick, *Chem. Ber*, 1985,**118**, 3781.
24. A.J. Banister, I.B. Gorrell, S.E. Lawrence, C.E. Lehmann, I. May, G. Tate, A.J. Blake and J.M. Rawson, *J.Chem.Soc., Chem. Commun.*, 1994,1779.
25. A.C Hazell and R.G. Hazell, unpublished work; reported in J.M. Rawson, Ph.D Thesis, University of Durham, 1990, p. 114; and subsequently in the following review articles; A.J. Banister and J.M. Rawson, *Chem. Br.*, 1992, 148; also ref. 1 pg. 323-348.
26. A.W. Cordes, R.C. Haddon, R.G. Hicks, R.T. Oakley, T.T.M. Palstra, *Inorg.Chem.*, 1992, **31**, 1802.
27. J.M. Rawson, A.J. Banister and I. May *Magn. Res. in Chem.*, 1994, **32**, 487-491.
28. A.J. Banister and J.M. Rawson, *Chem. Br.*, 148, 1992.
29. P.D.B. Belluz, A.W. Cordes, E.M. Kristof, S.W. Liblong and R.T. Oakley, *J.Am. Chem. Soc.*, 1989, **111**, 9276.
30. A.W. Cordes, C.D. Bryan, W.M. Davies, R.H. de Laat, S.H. Glarum, J.D. Goddard, R.C. Haddon, R.G. Hicks, D.K. Kennepohl, R.T. Oakley, S.R. Scott and N.P.C Westwood, *J. Am. Chem. Soc.*, 1993, **115**, 7232.
31. K.F. Preston, J.-P. Charland, and L.H. Sutcliffe, *Can. J. Chem*, 1988, **66**, 1299.
32. S.A. Fairhurst, L.H. Sutcliffe, K.F. Preston, A.J. Banister, A.S. Partington, J.M. Rawson, J. Passmore and M.J. Schriver, *Magn., Res. in Chem.*, 1993, **31**, 1027-1030.
33. W.V. Brooks, N. Burford, J. Passmore, M.J. Schriver, and L.H. Sutcliffe, *J.Chem. Soc., Chem. Commun.* 1987, 69.

34. T.G. Hibbert, M.Sc Thesis, University of Durham, 1993.
35. T. Chivers, D.D. Doxose and R.W. Hilts, *Inorg. Chem.* 1993, **32**, 3244-3249.
36. S.C. Nyburg and C.H Faerman, *Acta Cryst.* 1985, **B41**, 274.

CHAPTER 4
EXPERIMENTAL TECHNIQUES.



4.1 General Techniques.

The majority of compounds synthesised in the course of my research are highly moisture sensitive, with an inert atmosphere having to be used. All moisture sensitive material was handled in a pressure regulated Vacuum AtmosphereS HE43-2 glove box fitted with an HE-493 Dri-Train. All the glassware was oven dried overnight at (*ca.* 130°C). All reactions required standard vacuum-line methods and oxygen free nitrogen (BOC white spot, further dried by passage through a P4010 column) as the inert gas.

Reactions requiring liquid sulphur dioxide were carried out on a Monel vacuum line (designed and built by Dr.Z.V. Hauptman, Durham University Chemistry Department). The line was built of stainless steel, with Monel 'Whitney' taps IKS4, (fitted with Teflon compression ferrules), and a Bundenburg pressure gauge.

4.2 Specialised Techniques.

4.2.1 The Closed Extractor

This apparatus (Figure 4.1), which was designed by Dr.Z.V. Hauptman¹ is based on the Soxhlet extraction system. Its closed design enabled extractions involving liquid SO₂ to be carried out. The SO₂(l) was condensed into the bulb, by partial vacuum. The bulb was then heated in a water bath; over a few days the solvent condensed onto the solid present within the cooling jacket.

The bulb, after scoring with a glass knife, was broken in the glove box, the solid product was removed, the glass was cleaned, reassembled and annealed.

4.2.2 The "Dog"

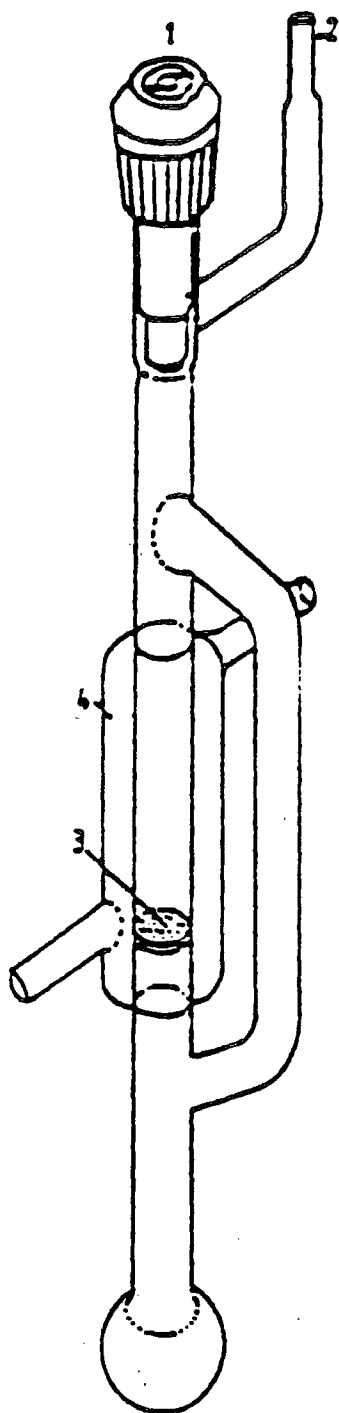
The "dog" is composed of a two-limb reaction vessel connected by a glass sinter,² usually of grade 3 porosity (Figure 4.2). Teflon J. Young taps enable this apparatus to be used for reactions involving liquid SO₂. Connection to the monel vacuum line is by 1/4" tubing, using Swagelok Teflon compression fittings.

Alternatively a glass-adaptor with Swagelok fittings can allow connection to a double-manifold line. After the reaction, the apparatus was taken in the glove-box where the solid material was removed from the bulb as described in 4.2.1.

4.3 Temperature Control.

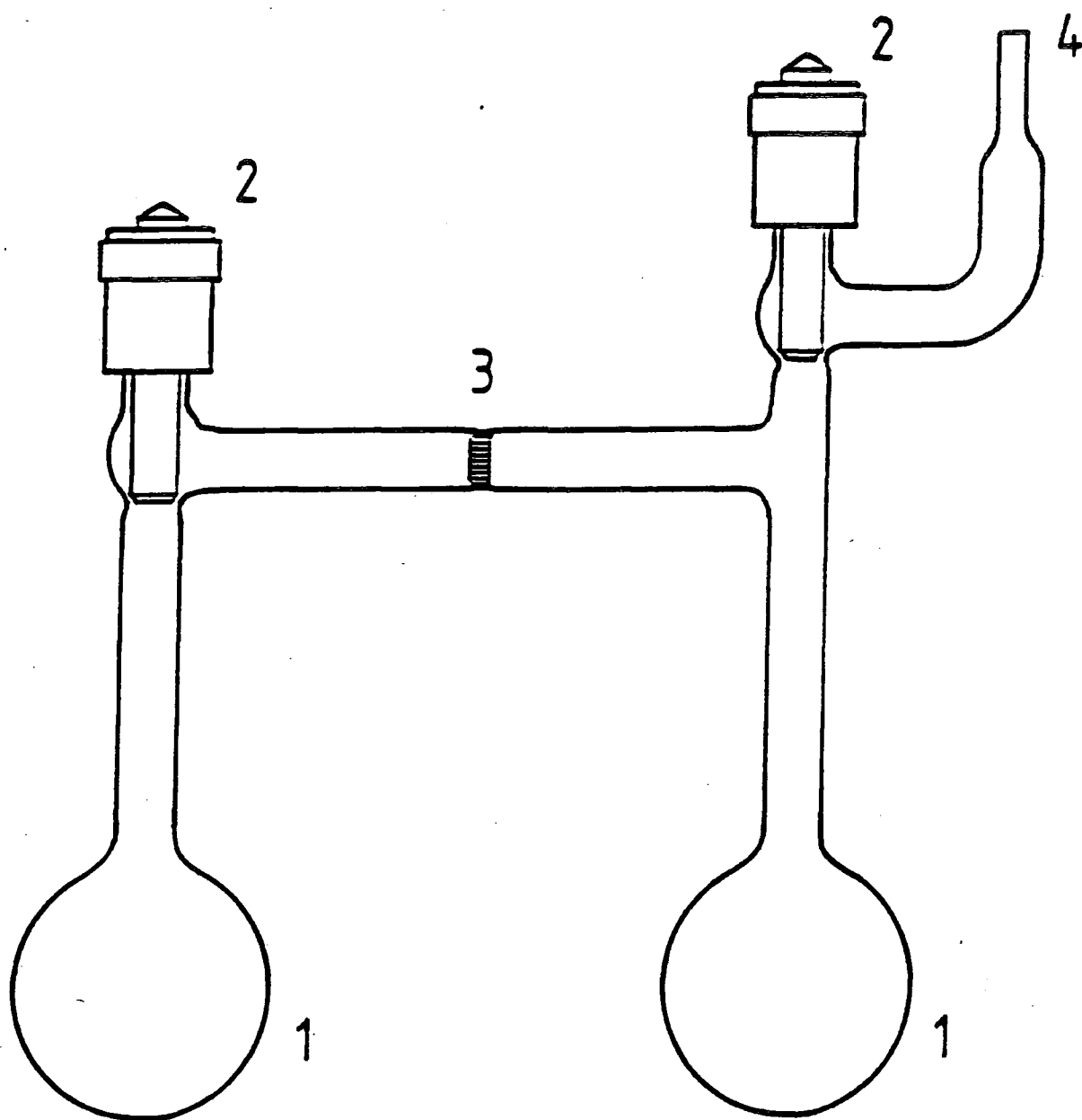
The majority of reactions were carried out at room temperature unless otherwise stated. For low temperature reactions i.e. between -78°C and -40°C, dry-ice/acetone baths were used. For temperatures above 20°C, a water-bath, oil-bath or electrical heating tape was employed.

Figure 4.1 The Closed Extractor



1. J. Young Teflon tap
2. 1/4" Ground glass
3. Glass Sinter(usually porosity grade 3)
4. Cooling jacket

Figure 4.2 The "Dog" or two-bulbed reaction vessel.



1. Reaction bulb
2. J. Young Teflon tap
3. Glass sinter (usually porosity grade 3)
4. 1/4" ground glass

4.4 Analytical Techniques.

4.4.1 Infra red Spectroscopy

All infrared spectra were recorded as Nujol mulls between KBr plates unless otherwise stated. These were recorded using either Perkin-Elmer 577 or 457 grating infrared spectrometers, or Perkin-Elmer FT 1720X or 1600 FTIR spectrometers. For moisture sensitive samples, mulls were made up in the glove box and sealed in brass holders. The Nujol was stored under sodium wire in the glove box.

4.4.2 Differential Scanning Calorimetry (DSC.)

DSC measurements were carried out using a mettler FP80 control unit coupled to a metler FP85 thermal analysis cell interfaced with an opus pc III computer. The DSC program was written by Dr.J.M. Rawson, University of Durham. Samples were cold-sealed aluminium samples pans in the glove box.

4.4.3 Elemental Analysis

Carbon, nitrogen and hydrogen analysis were carried out by Mrs J. Dolstal, and Mr.B. Coult using a Carlo Erba 1106 elemental analyser.

4.4.4 Ultraviolet/visible Spectroscopy

All U.V spectra were recorded on a Unicam UV/Vis spectrophotometer (UV2) connected to an Elonex PC.

4.4.5 Electron Spin Resonance(ESR)

X-band spectra were recorded on a Bruker ER200D-SRC spectrometer. Typical errors are +/-0.002mT for hyperfine coupling and +/-0.005 for g-tensors.

4.4.6 Mass Spectroscopy:

Mass spectra were recorded on a VG analytical 7070E spectrometer using either the electron impact (E.I.) or chemical ionisation (C.I.) technique. They were carried out by Dr.M. Jones and Miss. L.M. Turner, of Durham University Chemistry department.

4.4.7 Nuclear Magnetic Resonance Spectroscopy (NMR):

All n.m.r. spectra were carried out with the help of I. May, department of Chemistry. They were (^{31}P , ^{19}F , ^1H) recorded on a Varian VXR400S spectrometer.

4.5 Chemicals and Solvents.

4.5.1 Purification of Solvents

Acetonitrile (Aldrich HPLC Grade) was dried by refluxing over CaH₂ under a nitrogen atmosphere, followed by distillation into a dry flask. It was then degassed by several freeze-thaw cycles, and stored under nitrogen.

Dichloromethane was dried by distillation from CaH₂ into dry flasks under an atmosphere of nitrogen.

Toluene was dried by refluxing over lump sodium, followed by distillation under an atmosphere of dry nitrogen.

Tetrahydrofuran (THF), was purified (by Mr. B. Hall of the chemistry department) by fractional distillation from sodium under an atmosphere of dry nitrogen; it was stored over dry sodium wire.

Diethyl ether (Aldrich Na Dried GPR Grade). This was further purified by placing some sodium wire into the flask and leaving overnight in a fume cupboard.

Sulphur dioxide (BDH GPR Grade). This was dried by standing over P₄O₁₀ for one week, followed by distillation onto CaH₂ at least 24 hrs before use. It was vacuum transferred at -78 °C onto respective solutes which were in a "dog" or a closed extractor.

4.6 Single X-Ray Structure Determination.

The structure of both the (2,3-F₂.C₆H₃.CNSSN)₂ and (2,5-F₂.C₆H₃.CNSSN) dithiadiazolyls were determined on a Rigaker AFC6S four-circle diffractometer with a graphite-monochromator using Cu-K α radiation, and cryostream³ open-flow N₂ gas cryostat (T=150K). The crystal structure of Pt₃[PPh₃]₄[3,4-F₂.C₆H₃.CNSSN]₂ was resolved on a Siemens SMART CCD detector with a graphite-monochromator using Mo-K α radiation ($\lambda = 0.71073 \text{ \AA}$) the programs SHELX⁴ and SHELXL were used to solve and refine the structures.

4.7 References.

1. A.J. Banister, M.I. Hansford, and Z.V Hauptman *J. Chem. Soc., Dalton Trans.*, 1984, 1377.
2. A.J. Banister, M.I. Hansford, Z.V. Hauptman, A.W. Luke, S.T. Wait, W. Clegg and K.A. Jørgensen, *J.Chem.Soc., Dalton Trans.*, 1990, 2793.
3. J.Cosier and A.U. Glazer, *J.Appl. Cryst.*, 1986, **19**, 105.
4. SHELXS-Program for crystal structure determination, G.M Sheldrick, University of Göttingen, 1986.

APPENDIX I

ADDITIONAL CRYSTALLOGRAPHIC DATA.

Table 3.3(a)i Anisotropic displacement parameters ($A^2 \times 10^3$) for (a). The anisotropic displacement factor exponent takes the form: $-2\pi^2 [h^2 a^{*2} U_{11} + \dots + 2hka^*b^*U_{12}]$

	U11	U22	U33	U23	U13	U12
Pt(1)	31(1)	23(1)	24(1)	0(1)	10(1)	0(1)
Pt(2)	31(1)	23(1)	25(1)	-1(1)	10(1)	0(1)
S(1D)	36(1)	23(1)	21(1)	-2(1)	10(1)	-1(1)
S(2D)	30(1)	25(1)	25(1)	1(1)	10(1)	-2(1)
P(2)	31(1)	24(1)	26(1)	0(1)	10(1)	0(1)
P(1)	32(1)	26(1)	25(1)	-1(1)	9(1)	3(1)
N(2D)	31(4)	30(4)	29(4)	-5(3)	14(3)	-4(3)
C(126)	39(6)	37(5)	35(5)	0(4)	12(4)	1(4)
N(1D)	31(4)	24(4)	33(4)	-1(3)	17(3)	4(3)
C(111)	34(5)	22(4)	28(5)	-1(4)	10(4)	-2(4)
C(112)	36(5)	33(5)	44(6)	1(4)	12(5)	2(4)
C(113)	35(6)	36(6)	62(7)	9(5)	15(5)	6(4)
C(114)	32(5)	46(6)	62(7)	18(6)	11(5)	8(5)
C(115)	35(6)	60(7)	38(6)	20(5)	11(5)	9(5)
C(116)	39(5)	33(5)	36(5)	7(4)	15(4)	2(4)
C(121)	34(5)	31(5)	26(5)	-2(4)	16(4)	2(4)
C(122)	42(6)	29(5)	36(5)	1(4)	18(4)	4(4)
C(123)	59(7)	30(5)	39(6)	4(4)	16(5)	6(5)
C(124)	44(6)	39(6)	49(6)	5(5)	14(5)	-14(5)
C(125)	44(6)	39(6)	47(6)	9(5)	9(5)	-7(5)
C(131)	43(6)	25(5)	23(4)	-6(4)	8(4)	2(4)
C(132)	31(5)	27(4)	31(5)	1(4)	14(4)	0(4)
C(133)	41(6)	42(6)	36(5)	-4(5)	17(5)	-10(5)
C(134)	47(6)	33(5)	41(6)	-4(4)	19(5)	0(5)
C(135)	43(6)	28(5)	34(5)	3(4)	13(4)	1(4)
C(136)	33(5)	35(5)	35(5)	6(4)	14(4)	6(4)
C(210)	44(6)	29(5)	31(5)	2(4)	13(4)	-4(4)
C(211)	42(6)	34(5)	45(6)	-2(5)	22(5)	5(4)
C(212)	61(7)	39(6)	34(5)	1(4)	24(5)	0(5)
C(213)	55(6)	22(5)	29(5)	3(4)	10(4)	3(4)
C(214)	38(5)	24(4)	30(5)	-2(4)	12(4)	0(4)
C(211)	43(5)	22(4)	28(5)	-1(4)	12(4)	-2(4)
C(221)	33(5)	29(5)	23(4)	3(4)	7(4)	-1(4)
C(222)	40(6)	33(5)	42(6)	-3(4)	15(5)	-3(4)
C(223)	40(6)	41(6)	54(7)	-6(5)	8(5)	-8(5)
C(224)	31(5)	51(6)	44(6)	8(5)	11(5)	4(5)
C(225)	37(6)	37(6)	61(7)	16(5)	17(5)	4(5)
C(226)	37(5)	34(5)	39(5)	7(4)	12(4)	0(4)
C(231)	24(4)	30(5)	25(4)	-1(4)	5(4)	-5(4)
C(232)	37(5)	31(5)	31(5)	-5(4)	16(4)	7(4)
C(233)	42(6)	53(7)	37(6)	-6(5)	16(5)	2(5)
C(234)	49(6)	26(5)	40(6)	-7(4)	12(5)	6(4)
C(235)	43(6)	24(5)	29(5)	-1(4)	0(4)	-1(4)
C(236)	36(5)	31(5)	35(5)	-1(4)	16(4)	0(4)
C(1D)	39(5)	25(4)	31(5)	-3(4)	16(4)	5(4)
C(2D)	43(6)	29(5)	33(5)	7(4)	17(4)	9(4)
C(3D)	38(6)	45(6)	30(5)	9(4)	12(4)	12(5)
C(4D)	31(5)	49(6)	54(7)	10(5)	19(5)	7(5)
C(5D)	53(7)	48(6)	37(6)	15(5)	30(5)	21(5)
C(6D)	68(8)	42(6)	48(7)	8(5)	34(6)	11(6)

C(7D)	59(7)	30(5)	29(5)	-2(4)	20(5)	11(5)
F(2)	60(4)	77(5)	50(4)	15(3)	36(3)	19(4)
F(1)	57(5)	84(6)	73(5)	7(4)	26(4)	0(4)
C1(1S)	83(3)	91(3)	50(2)	-5(2)	14(2)	-10(2)
C1(2S)	56(2)	110(3)	73(2)	20(2)	31(2)	27(2)
C1(3S)	100(3)	74(2)	93(3)	-25(2)	49(2)	-20(2)
C(1S)	48(7)	58(7)	48(7)	2(6)	18(5)	7(6)
C1(4S)	48(2)	80(2)	53(2)	-13(2)	17(1)	-17(2)
C1(5S)	54(2)	66(2)	52(2)	-10(2)	19(1)	-12(2)
C1(6S)	60(2)	72(2)	71(2)	9(2)	18(2)	17(2)
C(2S)	45(6)	53(7)	44(6)	-4(5)	20(5)	1(5)

Table 3.3(a)ii Hydrogen co-ordinates ($\times 10^4$) and isotropic displacement parameters ($\text{\AA}^2 \times 10^3$) for (a).

	x	y	z	U(eq)
H(12A)	1550(8)	273(5)	6911(6)	80
H(11A)	2468(8)	1765(5)	7752(7)	80
H(11B)	1122(8)	2432(5)	6933(7)	80
H(11C)	595(8)	2393(5)	5522(7)	80
H(11D)	1309(8)	1618(6)	4919(7)	80
H(11E)	2602(8)	902(5)	5729(6)	80
H(12B)	4460(8)	-536(4)	7759(6)	80
H(12C)	3681(9)	-1551(5)	7631(6)	80
H(12D)	1849(9)	-1649(5)	7137(7)	80
H(12E)	770(9)	-736(5)	6802(7)	80
H(13A)	4219(7)	983(4)	6016(5)	80
H(13B)	5709(8)	785(5)	5695(6)	80
H(13C)	7252(9)	349(5)	6671(6)	80
H(13D)	7273(8)	123(5)	7974(6)	80
H(13E)	5773(7)	301(5)	8299(6)	80
H(21A)	7122(8)	1800(5)	8311(6)	80
H(21B)	7398(8)	2006(5)	7093(6)	80
H(21C)	6014(9)	2427(5)	5959(6)	80
H(21D)	4383(9)	2637(4)	6055(6)	80
H(21E)	4073(8)	2409(4)	7247(5)	80
H(22A)	6933(8)	2859(5)	9732(6)	80
H(22B)	8594(9)	2781(5)	10801(7)	80
H(22C)	9263(8)	1793(5)	11338(7)	80
H(22D)	8349(8)	861(5)	10764(7)	80
H(22E)	6670(8)	920(5)	9720(6)	80
H(23A)	3703(8)	2276(5)	9460(6)	80
H(23B)	2971(9)	3239(5)	9679(6)	80
H(23C)	3537(9)	4214(5)	9322(6)	80
H(23D)	4805(8)	4230(4)	8705(6)	80
H(23E)	5575(8)	3269(4)	8520(6)	80
H(3DA)	8809(8)	-275(5)	9753(6)	80
H(6DA)	7644(10)	-1572(6)	7410(7)	80
H(7DA)	6676(9)	-1546(5)	8292(6)	80
H(1SA)	10929(9)	966(6)	8986(7)	80
H(2SA)	8552(9)	4970(6)	9626(7)	80

Table 3.3(b)i Anisotropic displacement parameters ($\text{\AA}^2 \times 10^3$) for (b). The anisotropic displacement factor exponent takes the form: $-2\pi^2 [h^2 a^{*2} U_{11} + \dots + 2hka^* b^* U_{12}]$

	U11	U22	U33	U23	U13	U12
S(1A)	40(1)	25(1)	22(1)	4(1)	-2(1)	0(1)
S(2A)	41(1)	20(1)	30(1)	5(1)	-4(1)	-1(1)
N(3A)	32(4)	26(3)	25(3)	6(3)	-1(3)	-5(3)
N(5A)	38(4)	23(3)	15(3)	2(2)	-4(3)	-1(3)
C(1A)	31(4)	17(3)	12(3)	-6(2)	0(3)	-5(3)
C(2A)	38(5)	21(4)	12(3)	-7(3)	-2(3)	-4(3)
C(3A)	33(4)	19(4)	22(4)	3(3)	3(3)	3(3)
C(4A)	42(5)	21(4)	21(4)	0(3)	-5(3)	2(3)
C(5A)	46(5)	26(4)	24(4)	4(3)	-3(4)	3(4)
C(6A)	33(4)	21(4)	29(4)	1(3)	-2(3)	-3(3)
C(7A)	28(4)	23(4)	17(3)	2(3)	6(3)	-2(3)
F(2A)	73(4)	27(2)	20(2)	-7(2)	-6(2)	8(2)
F(3A)	65(4)	21(2)	30(2)	-1(2)	2(2)	9(2)
S(1B)	42(1)	28(1)	23(1)	-2(1)	0(1)	-2(1)
S(2B)	38(1)	22(1)	28(1)	-1(1)	-5(1)	6(1)
N(3B)	34(4)	28(3)	24(3)	9(3)	-1(3)	9(3)
N(5B)	36(4)	31(4)	18(3)	4(3)	0(3)	5(3)
C(1B)	27(4)	22(4)	22(4)	1(3)	-7(3)	-3(3)
C(2B)	30(4)	20(4)	16(3)	8(3)	-3(3)	-6(3)
C(3B)	27(4)	21(4)	18(3)	3(3)	-4(3)	-2(3)
C(4B)	27(4)	26(4)	20(3)	-1(3)	-1(3)	-8(3)
C(5B)	37(5)	22(4)	18(3)	0(3)	0(3)	-6(3)
C(6B)	27(4)	24(4)	25(4)	10(3)	-4(3)	-2(3)
C(7B)	28(4)	28(4)	21(4)	4(3)	-5(3)	3(3)
F(2B)	63(3)	25(2)	19(2)	4(2)	-10(2)	2(2)
F(3B)	58(3)	18(2)	26(2)	5(2)	1(2)	4(2)

Table 3.3(b)ii Hydrogen co-ordinates ($\times 10^4$) and isotropic displacement parameters ($\text{\AA}^2 \times 10^3$) for (b).

	x	y	z	U(eq)
H(4A)	7695(13)	-755(9)	5825(5)	34
H(5A)	6829(14)	1869(9)	6173(6)	40
H(6A)	6227(13)	3646(9)	4932(6)	33
H(4B)	2706(12)	-736(9)	-870(5)	29
H(5B)	1702(12)	1909(8)	-1186(5)	31
H(6B)	1262(12)	3658(9)	58(5)	31

Table 3.3(c)i Anisotropic displacement parameters ($\text{\AA}^2 \times 10^3$) for (c). The anisotropic displacement factor exponent takes the form: $-2\pi^2 [h^2 a^2 U_{11} + \dots + 2hka^* b^* U_{12}]$

	U11	U22	U33	U23	U13	U12
S(1)	48(1)	28(1)	118(3)	9(1)	42(2)	4(1)
S(2)	63(2)	23(1)	84(2)	13(1)	40(2)	8(1)
N(3)	54(4)	25(3)	45(4)	8(3)	26(4)	7(3)
N(5)	44(4)	27(3)	72(5)	13(4)	21(4)	3(3)
C(1)	50(4)	26(3)	14(4)	4(3)	7(3)	7(3)
C(2)	65(6)	39(4)	31(5)	3(4)	-1(5)	21(4)
C(3)	112(9)	34(4)	29(5)	-4(4)	-14(6)	11(5)
C(4)	91(8)	57(6)	31(6)	9(5)	-10(6)	-17(6)
C(5)	44(5)	65(6)	25(5)	6(4)	-4(4)	-2(4)
C(6)	49(5)	31(4)	31(5)	19(4)	-2(4)	-3(3)
C(7)	39(4)	30(4)	36(5)	6(4)	18(4)	7(3)
F(2)	37(4)	44(4)	51(5)	-7(4)	7(4)	4(3)
F(5)	36(4)	64(5)	69(5)	-8(5)	12(4)	4(3)
F(3)	143(20)	43(9)	89(15)	-32(10)	-28(14)	17(11)
F(6)	47(8)	30(7)	68(12)	5(7)	21(8)	2(6)

Table 3.3(c)ii Hydrogen co-ordinates ($\times 10^4$) and isotropic displacement parameters ($\text{\AA}^2 \times 10^3$) for (c).

	x	y	z	U(eq)
H(2)	7524(4)	5801(4)	5281(25)	54
H(3)	8196(5)	6631(4)	6006(28)	70
H(4)	9287(5)	6468(5)	4853(29)	72
H(5)	9633(4)	5480(5)	2701(23)	54
H(6)	8911(4)	4665(3)	2286(24)	44

APPENDIX II

COLLOQUIA, LECTURES AND SEMINARS FROM INVITED SPEAKERS.

1994-1995 (August 1-July 31)

- October 5 Prof.N.L. Owen, Brigham Young University, Utah, USA
Determining Molecular Structure-the INADEQUATE NMR way
- October 19* Prof.N. Bartlett, University of California
Some Aspects of Ag(II) and Ag(III) Chemistry
- November 2 Dr.P.G. Edwards, University of Wales, Cardiff
The Manipulation of Electronic and Structural Diversity in Metal Complexes-New Ligands
- November 3* Prof.B.F.G. Johnson, Edinburgh University
Arene-metal Clusters
- November 9* Dr.G. Hogarth, University College, London
New Vistas in Metal-imido Chemistry
- November 10 Dr.M. Block, Zeneca Pharmaceuticals, Macclesfield
Large-scale Manufacture of ZD 1542, a Thromboxane Antagonist Synthase Inhibitor
- November 16 Prof.M. Page, University of Huddersfield
Four-membered Rings and β -Lactamase
- November 23 Dr.J.M.J. Williams, University of Loughborough
New Approaches to Asymmetric Catalysis
- December 7 Prof.D. Briggs, ICI and University of Durham
Surface Mass Spectrometry
- January 11 Prof.D. Parsons, University of Reading
Applications of Tandem Reactions in Organic Synthesis
- January 18 Dr.G. Rumbles, Imperial College, London
Real or Imaginary Third Order Non-Linear Optical Materials

- January 25 Dr.D.A Roberts, Zeneca Pharmaceuticals
The Design and Synthesis of Inhibitors of the
Renin-angiotension System.
- February 1* Dr.T. Cosgrave, Bristol University
Polymers do it at Interfaces
- February 8 Dr.D. O'Hare, Oxford University
Synthesis and Solid State Properties of Poly-, Oligo- and
Multidecker Metallocenes
- February 22 Prof.E. Schaumann, University of Clausthal
Silicon- and Sulfur-mediated Ring-opening Reactions of
Epoxide
- March 1 Dr.M. Rosseinsky, Oxford University
Fullerene Intercalation Chemistry
- March 22* Dr.M. Taylor, University of Auckland, New Zealand
Structural Methods in Main-Group Chemistry
- April 26 Dr.M. Schroder, University of Edinburgh
Redox-active Macrocyclic Complexes: Rings, Stacks and Liquid
Crystals
- May 3 Prof.E.W. Randall, Queen Mary and Westfield College
New Perspectives in NMR Imaging
- May 4 Prof.A.J. Kresge, University of Toronto
The Ingold Lecture Reactive Intermediates: Carboxylic-acid
Enols and Other Unstable Species

* indicates Lectures attended by the author.

